

AALBORG UNIVERSITY

Modelling and Control of Wind Turbines, Solar PVs and Electric Vehicles in Residential Grids



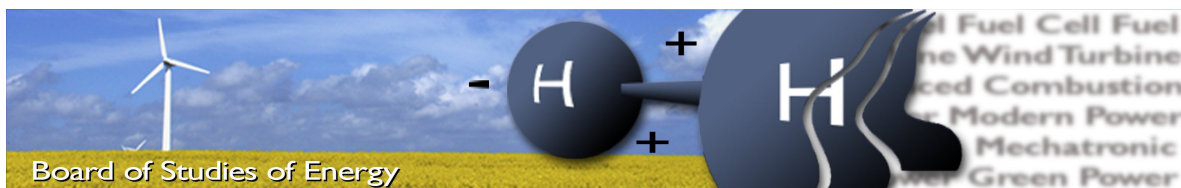
AALBORG UNIVERSITET

Department of Energy Technology
EPSH-1030

Master Student: NICOLAE BĂDULESCU



July 31, 2016



Title: Modelling and Control of Wind Turbines, Solar PVs and Electric Vehicles in Residential Grids
Semester: 10th
Semester theme: Master Thesis
Project period: 1.02.2016 to 1.08.2014
ECTS: 30
Supervisor: Weihao Hu and Chi Su
Project group: EPSH4 - 1030

Bădulescu Nicolae

SYNOPSIS:

The recent energy policies imply that by 2050, Denmark should become independent from conventional fuels. The need for a clean and environmental friendly transportation systems requires a high integration level of electric vehicles. The main focus of this thesis consists in the determination of the maximum allowable wind power production, photovoltaic generation and electric vehicle charging for a typical distribution system, under various scenarios. First, a benchmark of a distribution grid is validated, in order to perform a steady-state analysis when renewable sources are integrated. The simulations are performed for both winter and summer scenarios. By gradually increasing the renewable quota, the maximum penetration level is determined by using a trial and error strategy, until the grid reaches the operational limit. Finally, five different EV charging strategies are implemented, by plugging-in the vehicles during peak-load hours and during the night.

Copies: 4
Pages, total: 65
Appendix: -

By signing this document, each member of the group confirms that all group members have participated in the project work, and thereby all members are collectively liable for the contents of the report. Furthermore, all group members confirm that the report does not include plagiarism.

Preface

This report has been written by group EPSH4-1030, during the 4th semester of the 'Electrical Power Systems and High Voltage Engineering' Master program at the Department of Energy Technology at Aalborg University. The focus of this project is to investigate the impact of different integration levels for renewable energy sources and electric vehicles on a typical distribution grid.

Reading Guide

This project will contain references, illustrations, tables and equations. The literature references will be referred to according to the IEEE citation method, the sources will be shown as [number]. This citation refers to the bibliography at the end of the report, which contains further information about the source. Books are listed with author, year, title, edition and publisher; Websites are listed with author, title, date and URL. Figures, tables and equation will be referred to by a chapter and a number [chapter, number], furthermore a word or an abbreviation indicating what is being referred to. The words/abbreviation are Figure for illustrations and Table for tables. If no reference is given on a figure it means that the figure was created by the project group.

Software

The following software has been used during the project:

- LaTeX is used to write the report.
- Matlab is used for coding scripts and plotting.
- DigSilent is used for steady-state power flow simulations.

List of symbols

Table 1: List of symbols used in this report

Symbol	Unit	Name
B_{ik}	$[\Omega^{-1}]$	Imaginary component of the bus admittance matrix
C_p	[-]	Wind turbine power coefficient
f	[Hz]	Frequency
G	$[W/m^2]$	Solar irradiation
G_{ik}	$[\Omega^{-1}]$	Real component of the bus admittance matrix
I	[A]	Current
P	[W]	Active power
P_{STC}	[W]	Peak power of PV panel
Q	[VAr]	Reactive power
R	[m]	Wind turbine radius
R, r	$[\Omega]$	Resistance
S	[VA]	Apparent power
t	$[\text{°C}]$	Temperature
U_i	[-]	Harmonic number
V	[V]	Voltage
v	[m/s]	wind speeds
x	$[\Omega]$	Reactance
Y_{nn}	[-]	Bus admittance matrix
y	$[\Omega^{-1}]$	Admittance
z	$[\Omega]$	Impedance
δ	$[\text{°}]$	Voltage angle
ρ	$[kg/m^3]$	Air density

Table 2: List of abbreviations used in this report.

Abbreviation	Name
AC	Alternating Current
BSS	Battery Switch Stations
BEV	Battery Electric Vehicle
CHP	Combined Heat and Power plant
CT	Current Transformer
DC	Direct Current
DG	Distributed Generation
DPL	DIgSILENT Programming Language
EMT	Electro Magnetic Transients
EU	European Union
EV	Electric Vehicle(s)
FCS	Fast Charging Station(s)
GHG	Green House Gases
GUI	Graphical User Interface
HP	Heat Pump(s)
ICE	Internal Combustion Engine
LV	Low Voltage
MV	Medium Voltage
OHL	Overhead Line
PF	Power Factor
PV	Photovoltaic panel
RMS	Root Mean Square
RES	Renewable Energy Source
SOC	State Of Charge
THD	Total Harmonic Distortion
TSO	Transmission System Operator
UGC	Underground Cable
VT	Voltage Transformer
VUF	Voltage Unbalance Factor
WT	Wind Turbine(s)

List of Figures

1.1	Installed power generation capacity (in [MW]) and the share of renewables [1]	1
1.2	Wind power capacity and share of domestic supply in Denmark [2]	2
1.3	The energy policy for Denmark until 2050 [3]	2
1.4	Primary energy production in Denmark [2]	2
1.5	Grid topologies used in the Danish distribution system [4]	4
1.6	Illustration of a Danish Smart Grid design [5]	6
1.7	Estimated new vehicles share based on the driving technology for a 20 year period (left). Vehicle share distribution based on the vehicles powertrain technology (right) [6]	8
1.8	Adjustments in the annual energy production resulted after the implementation of the EVs fleet [6]	8
1.9	Changes in the total CO2 emissions when implementing electric vehicles [6]	9
1.10	Electric vehicle penetration level in the three LV residential grids investigated [7] . .	9
1.11	Voltage profile (a) and Voltage unbalance factor (b) during one winter day at node 613 [8]	10
1.12	Voltage profile (a) and Voltage unbalance factor (b) during one winter day at node 613, by using the 'dumb charge' strategy [8]	10
1.13	Voltage profiles for three critical feeders (left) and loading profile for three highly congested lines (right) for the uncontrolled charging strategy [9]	11
1.14	Voltage profiles for three critical feeders (left) and loading profile for three highly congested lines (right) for the smart charging strategy [9]	11
1.15	The load factor for the 250 kVA distribution transformer [9]	11
1.16	Installed power plant capacity to cover FCS (left) and BSS (right) in Europe by 2020 [10]	12
1.17	Supply of the load demand from BSS with RES integration in Germany by 2020 [10]	12
3.1	IEEE 13 Bus Test System [11]	17
3.2	Single line diagram of a simple power system	19
3.3	Bus admittance diagram for the power system presented in Figure 3.2	19
3.4	Single line diagram with specified and unknown variables for the power system in Figure 3.2	20
3.5	<i>PowerFactory</i> Main Window - illustration for a LV electricity grid	22
3.6	<i>PowerFactory</i> Individual block for a typical electric load	23
3.7	The IEEE 13 bus distribution system implemented in <i>PowerFactory</i> software	24
3.8	Result comparison between the IEEE distribution system and the model implemented in <i>PowerFactory</i>	26
4.1	Consumption profile at each household for January and July cases	28
4.2	Voltage profiles during one regular week with no RES generation	29
4.3	Transformer loading (a) and Infeed active power (b) with no RES generation	30
4.4	Line loading factors for Line 1 and Line 5 during the winter and summer scenario .	31
4.5	Solar irradiation and wind speed profile during one year with respect to [12]	32
4.6	Solar irradiation vs. PV module output power (a) and Wind speed vs. WT output power (b)	33
4.7	Renewable generation profiles for each WT and PV module for one week	33

4.8	Voltage profiles during one normal week with even distributed RES	35
4.9	Transformer loading (a) and Infeed active power (b) for evenly distributed RES . . .	36
4.10	Cable loading for summer and winter case with even distributed RES	37
4.11	Voltage profiles for renewables connected close to the transformer	38
4.12	Transformer loading (a) and Infeed power (b) for RES close to transformer	38
4.13	Cable loading for summer and winter case for RES close to transformer	39
4.14	Voltage profiles for renewables connected close to the transformer	40
4.15	Transformer and cable loading for RES at the end of the feeder	41
5.1	Probability plot for EV regarding the availability for charge during an average weekday [13]	44
5.2	Results for the power flow analysis during the January case, with regards to the voltage fluctuations at the weakest busbar (a), the infeed power from the system (b) and the power consumed during the dumb charge (c)	46
5.3	Results for the power flow analysis during the January case, with regards to the transformer and cable loadings (a) and the power consumed during the dumb charge (b)	46
5.4	Results for the power flow analysis during the July case, with regards to the voltage fluctuations at the weakest busbar (a), the infeed power from the system (b) and the power consumed during the dumb charge (c)	47
5.5	Results for the power flow analysis during the July case, with regards to the transformer and cable loadings (above) and the power consumed during the dumb charge (bellow)	48
5.6	Results for the power flow analysis during the January case, with regards to the voltage fluctuations at the weakest busbar (a), the infeed power from the system (b) and the power consumed during the night charge (c)	49
5.7	Results for the power flow analysis during the January case, with regards to the transformer and cable loadings (a) and the power consumed among night charge (b)	49
5.8	Results for the power flow analysis during the July case - voltage fluctuations at the weakest bar (a), the infeed power from the system (b) and the power consumed for the night charge (c)	50
5.9	Results for the power flow analysis for the July case, with in regard with the transformer and cable loadings (a) and the power consumed during night charge (b)	50
5.10	Results for the load flow analysis among the January case, with regards to the voltage fluctuations at the weakest busbar (a), the infeed power from the external grid (b) and the power consumed during the night charge (c)	51
5.11	Results for the load flow analysis during the January case, with regards to the transformer and cable loadings (a) and the power consumed among night charge (b)	52
5.12	Results for the load flow analysis during the July case, with regards to the voltage fluctuations at the weakest busbar (a), the infeed power from the system (b) and the power consumed during the night charge (c)	52
5.13	Results for the load flow analysis during the July case, with regards to the transformer and cable loadings (a) and the power consumed among night charge (b)	53
5.14	Results for the load flow analysis during the January case, with regards to the voltage fluctuations at the weakest busbar (a), the infeed power from the system (b) and the power consumed during the night charge (c)	54

5.15	Results for the load flow analysis during the January case, with regards to the transformer and cable loadings (a) and the power consumed among night charge (b)	54
5.16	Results for the load flow analysis during the January case, with regards to the voltage fluctuations at the weakest busbar (a), the infeed power from the system (b) and the power consumed during the night charge (c)	55
5.17	Results for the load flow analysis during the January case, with regards to the transformer and cable loadings (a) and the total power consumed among the morning charge (b)	56
5.18	Results of the load flow analysis for the January case, with regards to the voltage fluctuations at the weakest busbars (a), (b), (c) and the infeed power form the system (d)	57
5.19	Results of the power flow analysis for the January case, for the transformer and cable loadings (a) and the power demand for EV charging (b)	57
5.20	Results of the load flow analysis for the July case, with regards to the voltage fluctuations at the weakest busbars (a), (b), (c) and the infeed power form the system (d)	58
5.21	Results of the power flow analysis for the July case, for the transformer and cable loadings (a) and the power demand for EV charging (b)	59

Table of contents

List of Figures	vii
Chapter 1 Introduction	1
1.1 Background and motivation	1
1.2 The Danish distribution system	3
1.3 Assessment of Electric Vehicle Technology	6
1.4 State of the art review regarding the integration of RES and EVs in distribution grids	7
1.5 Outline of the Thesis	13
Chapter 2 Problem statement	15
2.1 Problem Statement	15
2.2 Project limitations	16
2.3 Methodology	16
Chapter 3 Description of the distribution test system	17
3.1 IEEE 13 bus distribution system	17
3.2 Description of Load Flow Method	18
3.3 DIgSILENT Power Factory modelling	21
3.4 IEEE 13 bus distribution system validation	23
Chapter 4 RES integration and power flow analysis	27
4.1 Overview on the household consumption profiles	27
4.2 Power flow analysis on the distribution grid without any RES connected	28
4.3 Generation profiles for the PV modules and wind turbine	32
4.4 Maximum renewable sources penetration level	33
4.5 Load flow analysis with evenly distributed renewable sources	34
4.6 Power flow analysis with RES connected close to the transformer	37
4.7 Load flow analysis for RES connected at the far away buses	39
4.8 Chapter summary	41
Chapter 5 Power flow analysis with regards to EV integration	43
5.1 Outline of electric vehicle modeling	43
5.2 Dumb charge strategy for the EVs between 17:00-19:00	45
5.3 EV night charge between 00:00-2:00	48
5.4 EV night charge during 02:00-04:00	51
5.5 EV morning charge between 04:00-06:00	53
5.6 Distributed charging of EVs between 00:00 to 06:00	56
5.7 Summary of charging strategies	59
Chapter 6 Conclusions and Future work	61
6.1 Conclusions	61
6.2 Future Work	62
Bibliography	63

Introduction 1

The following chapter aims to introduce some basic concepts regarding Renewable Energy Sources (RES) and their integration in the actual Danish power system. The following chapter is motivated by the recent technologies that have been developed with regards to Electric Vehicles (EV). The state of the art is presented with regards to the impact of RES and EVs on Danish distribution grids. The importance of studies concerning the integration of renewables and electric vehicles is emphasized by the present tendency to integrate renewable energy sources in the distribution system and the increasing influence of transportation based on electric engines.

1.1 Background and motivation

The number of renewable energy sources that are being integrated in the actual power system is increasing. Many of the RES are represented by Photovoltaic (PV) or wind power generating plants. These types of renewables are being connected at both Medium Voltage (MV) and Low Voltage (LV) levels. At European level, during 2014 a total of 21.3 GW of renewable power capacity was installed, according to [1]. The total quota of new renewable installed capacity was 79.1 % for 2014. The share of the new renewable power capacity installations for the European Union (EU) during the last years is being presented in Figure 1.1.

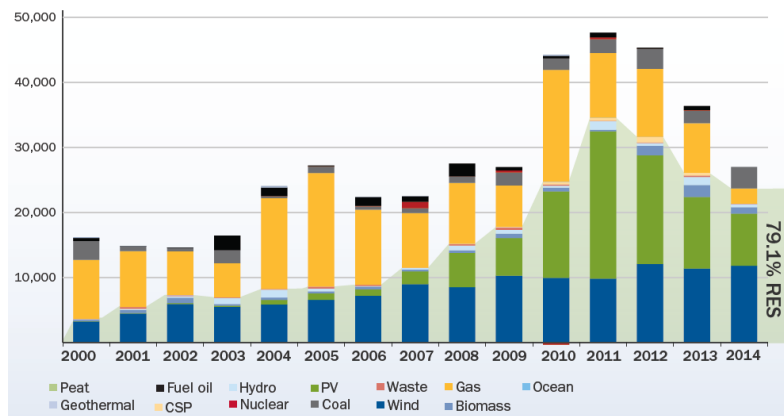


Figure 1.1: Installed power generation capacity (in [MW]) and the share of renewables [1]

In Figure 1.1, it can be seen that the predominant new RES installed in Europe during the past years are represented by PV panels and wind turbines (WT). In the case of wind turbines, it can be observed that during each year, the share of the new installations is increasing in a steady way. Regarding the photovoltaic technology, since 2011 the share has been decreasing with approximately 60 %. Although there has been a decrease in the installed power generating capacity since 2011, the share of the renewables has been increasing constantly. This will lead to a more sustainable and clean energy system, having a positive impact on the environment. According to the annual report [2] by the end of 2014, the total onshore installed capacity for wind power in Denmark was 3574 MW. Regarding the offshore capacity, numbers show that the total installed power represented 1271 MW. Figure 1.2 presents the wind power capacity and the share of domestic electricity supply in Denmark during the past years.

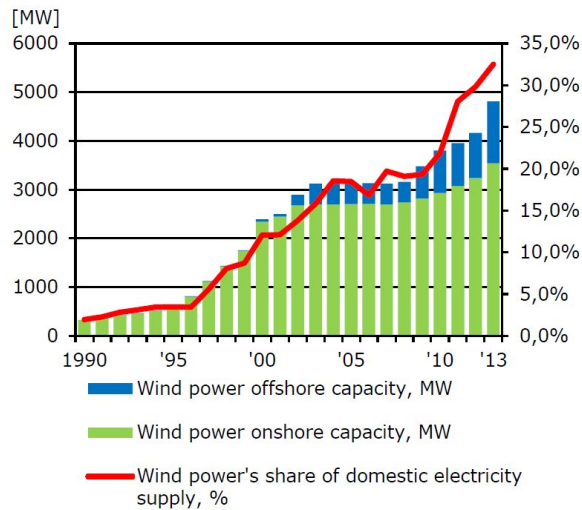


Figure 1.2: Wind power capacity and share of domestic supply in Denmark [2]

From Figure 1.2 it can be observed that the number of wind power plants is expected to increase in the following years. Most of the wind power plants are integrated at a distribution level, as discussed in [14].

The ambitious energy strategy set by the Danish government, is to achieve full independency from conventional power generating installations until the year 2050. In order to achieve this major goal, the penetration level of RES should increase and new energy strategies and policies need to be implemented. According to [3], the key milestones needed to implement this ambitious strategy are presented in Figure 1.3.

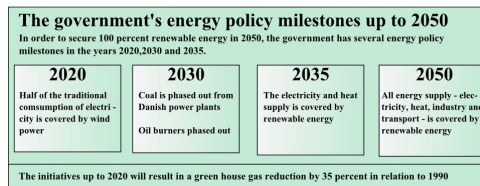


Figure 1.3: The energy policy for Denmark until 2050 [3]

In order to reduce the CO2 emissions and keep up with the energy strategy imposed, the Danish power system is gradually changing from conventional centralized large power generating plants (based on fossil fuels), to distributed generation (DG) power plants, based on renewables [2], [3].

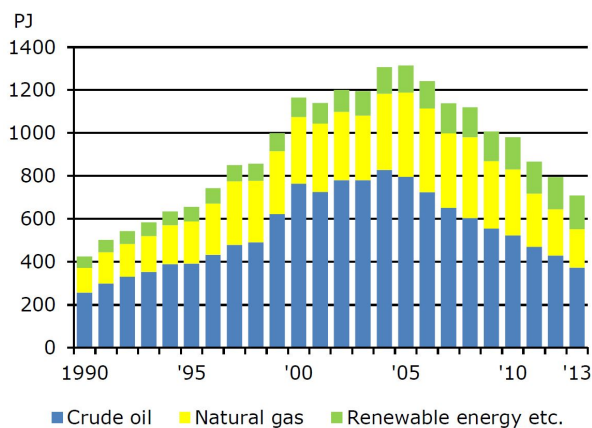


Figure 1.4: Primary energy production in Denmark [2]

In Figure 1.4, the fluctuation of the primary energy production in Denmark is being presented, for the past years. It can be observed that the energy production based on conventional fuels has been decreasing over the last years. This is a consequence of the fact that the power system has been integrating more renewables while limiting the energy produced by traditional power plants, by decommissioning them.

In order to achieve the goals presented in Figure 1.3, The Danish Ministry of Climate, Energy and Buildings has published the Smart Grid Strategy [15]. This strategy aims to integrate a smart grid design, which includes a continuous exploitation of the wind and solar energy as soon as it is produced. This can be done by powering heat pumps and electric vehicles or by storing the excess energy. By implementing a smart grid design, it is expected that the transition to RES to be cheaper (contributing to smaller electricity prices) and also, it can offer new services and products for the consumers. Another initiative is to motivate the consumers to use more energy in the off-peak hours and to provide the right framework, in order to manage the emerging increase in solar and wind energy [15].

The number of electric vehicles registered in Denmark is expected to increase in the coming years. This fact comes in accordance with the current tendencies regarding cleaner and sustainable transportation systems. According to the Danish Electric Vehicle Association, in Denmark the number of EV registered by the end of 2015 was close to 8000 units [16]. Between January 2014 and January 2016, the number of EV registered in Denmark has increased more than four times [16]. This large number of EV can be motivated by the increasing interest regarding a more environmental friendly transportation. Also this comes in hand with the expectations regarding the electric vehicles market for the Northern Europe. It is anticipated that by 2020 the share of EV to represent approximately 15 % [6].

In summary there are numerous reasons for investigating the impact of integrating electric vehicles and renewables in residential grids. The most significant are the following:

- The present energy strategies imposed by the Danish government.
- The current tendencies to shift from large generation plants to small distributed generation plants.
- The increasing number of renewables integrated at low and medium voltage levels.
- The expanding share of electric vehicles in Denmark.

1.2 The Danish distribution system

The following section represents a short overview of the actual Danish distribution system. According to the Transmission System Operator (TSO) 'Energinet.dk', the power system is separated into two levels, based on the voltage [17]. The Transmission level is composed out of networks having voltages from 400 kV to 60 kV. The Distribution system includes networks from 60 kV down to 0.4 kV.

Most of the end-use consumers are connected at a distribution level (0.4 kV). The energy is provided at 0.4 kV level from the upper voltage networks (60 and 6 kV) [18]. Due to the increase level of distributed generation, more than 40 % of the generating capacity is connected at 60 kV or lower voltage levels. These DG sources are mostly composed of renewables, especially wind turbines, photovoltaics and local combined heat and power (CHP) plants [18]. The lengths of the underground cable (UGC) and overhead lines (OHL) present in the Danish distribution system are presented in Table 1.1.

Table 1.1: Length of cables and overhead lines in the Danish distribution system [18]

Voltage level	UGC [km]	OHL [km]
60-30 kV	2957	5757
20-6 kV	57097	5215
0.4 kV	90462	6054
Total length	151588	22261

1.2.1 Grid topologies

The distribution grids can present different architectural topologies. Based on these topologies the distribution grids can benefit in several ways such as cost, simplicity, supply reliability or robustness. Three of the most common topologies used in the distribution system are illustrated in Figure 1.5.

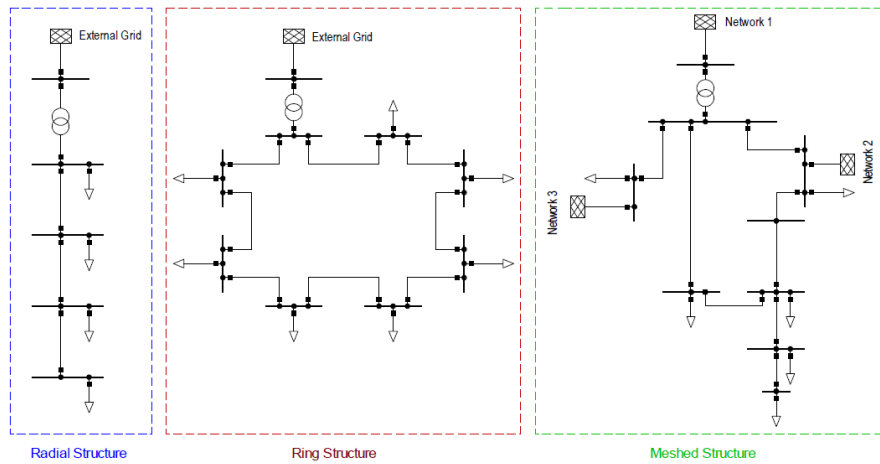


Figure 1.5: Grid topologies used in the Danish distribution system [4]

As presented in Figure 1.5, the three main distribution grid topologies are represented by the following structures:

- **Radial Structure** - This type of feeder is represented by a number of busses connected between each one of them by a single line. It is mainly used in rural areas or in places where the distances between the consumers are high. This type of distribution system can provide a simple and cost efficient solution. The drawback of such a topology is represented by the reduced supply reliability. In case of a fault, the consumers connected after the fault location will not be provided with electricity.
- **Ring Structure** - The structure of this type of feeder offers the possibility to increase the supply reliability. Each busbar is connected with two other different buses. By using such a topology, in case of a fault the demand for electricity is not compromised for any of the consumers deserved. The biggest disadvantage of such a structure is represented by the increased cost due to the oversizing of the power lines needed to supply the required load in case of a fault.
- **Meshed Structure** - This type of feeders presents the best technical advantages (but the poorest economic advantages), due to its interconnections with buses and other feeders and/or networks. The architecture of such structures is more complex compared to the previous cases. Due to the numerous connections between other busses, feeders

and networks, this type of topology is considered to present the highest level of supply reliability.

1.2.2 Grid Codes

For an electric grid to operate properly under normal conditions, several technical specifications need to be followed. These specifications are known as grid codes. They consist of several guidelines that plant operators, grid owners and grid operators need to satisfy under both normal and fault operating conditions. In Denmark, the grid codes concerning the power system are elaborated by 'Energitsynet', which is the Danish Energy Regulatory Authority and 'Energinet.dk'.

In Denmark, the grid codes follow the European Standard EN 50160 [19] regarding voltage quality. In [19], the standard presets a full analysis of the grid code regulations for European countries. The main grid codes concerning the supply voltage for distribution networks are presented in Table 1.2

Table 1.2: Requirements regarding power quality of supply voltage in distribution networks [19]

Parameter of supply voltage	Limits
Frequency	LV and MV : 50 Hz nominal (49.5-50.2 Hz)
Voltage magnitude	LV and MV : $\pm 10\%$ and $\pm 5\%$
Harmonics	LV:THD $\leq 8\%$ (for each harmonic) MV:THD $\leq 5\%$ (for each harmonic)
Long interruptions	LV and MV : 48h/year

The total harmonic distortion factor THD can be determined by using the following equation:

$$THD = \sqrt{\frac{\sum_{h=2}^{40} (U_h^2)}{U_1^2}} \quad (1.1)$$

where, U_h represents the individual harmonic and U_1 represents the fundamental voltage.

1.2.3 Smart Grid design in Denmark

The concept of 'Smart Grid' has been widely debated during the past years. A proper definition is given by "The European Technology Platform", which can be found in [5]. According to this paper, a Smart Grid is represented by an electrical network which can integrate in an intelligent way the behavior and performance of all the users connected, in order to ensure sustainable, economical and secure electricity supplies.

From Figure 1.6 it can be observed that a typical Smart Grid design requires a certain degree of communication between its components. If operating in an intelligent manner, according to [5], the advantages of operating a Smart Grid are the following:

- An improved system stability which can ensure a higher supply security.
- An increased number of options to establish the power balance in a more efficient manner.
- Reduced time of fixing the faults in the power grid.
- Increased energy savings and reduced electricity prices for consumers who utilize EV and heat pumps (HP) intelligently.
- An increase in the integration level of renewables through the flexibility offered by EV and HP.

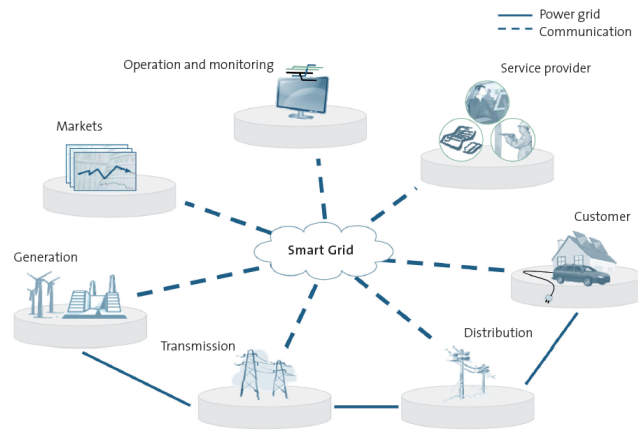


Figure 1.6: Illustration of a Danish Smart Grid design [5]

1.3 Assessment of Electric Vehicle Technology

In the following section, an overview regarding EVs will be presented. The main advantages that can be attributed to an electrified transportation system are related to their sustainable and nonpolluting relationship with the environment. For the past century conventional vehicles, based on internal combustion have been the most used transportation systems. The main drawback of this type of transportation is represented by the huge quantities of greenhouse gases (GHG) resulted from burning conventional fuel, thus polluting the environment. In terms of efficiency, an internal combustion engine (ICE) does not present the same performance as an electric motor, due to fact that energy is wasted through the exhaust gases resulted and the transmission system.

Electric vehicles operate by using the electricity stored in batteries to convert it into momentum by using an electric motor. The direct connection of the motor to the drive system implies less losses and a high efficiency. The batteries can be recharged by using electricity from the grid and by intelligent energy recuperation based on a regenerative braking system [20]. By using an electric vehicle, the emissions of GHG and air pollutants can be considered as being zero.

1.3.1 Battery technology

The battery pack represents one of the most important components of an electric vehicle. The batteries installed in an EV have to store the required electrical energy needed for propulsion. The average driving range for an EV is considered to be around 150 km [20]. With the development of new technologies regarding batteries, it is expected that the range of EV to increase in the future. According to [20], the key parameters for batteries consist of:

- **The energy storage capacity (kWh)** - determines the range of an electric vehicle. The current technology enables storage capacities between 30-50 kWh.
- **The peak power (kW)** - represents the maximum power that the battery can deliver. It relies on the range, the mass of the vehicle and the driving style.
- **The life time (years)** - can be split between the calendar life time and the number of charging cycles. For a conventional EV battery the average expected life time is assumed to be around 10-15 years and a number of full charging cycles of 3-5000.
- **The cost of the battery pack (DKK/kWh)** - represents the most important economical aspect which determines the total price of an EV. The total cost of a battery pack increases with the extended electric range.

- **Recharging time (h)** - is considered as an important aspect which affects also the life time of the battery pack. The recharging of the battery can lead to power losses up to 8%, due to the power electronics involved in the electrical recharging circuit.

Advantages for electric vehicles

By using electric vehicles as transportation, several benefits can be gained. Some of the most important ones are the following:

- **No requirement for fossil fuels** - this represents a huge advantage due to the fact that EVs do not pose a conventional engine, thus there is no requirement for a fuel tank. Also with the fluctuating prices of gas, an EV can be a suitable solution for long term transportation.
- **No GHG emissions** - because of their electric propulsion system, EVs can be considered as being a 100% environmental friendly. Because they run on clean energy sources, EVs contribute to a more sustainable and green climate.
- **Reduced maintenance costs** - the powertrain used for propulsion implies that electrical vehicles require less maintenance than conventional vehicles. This is due to the fact that the only parts that require service are represented by the battery, the electrical motor and the electronics.
- **Reduced noise pollution** - the operating principle of the electric motor leads to less noise generated due to the moving parts, hence ensuring a more comfortable and smoother driving experience.
- **Increased energy efficiency** - the overall performance of a transportation system is given by the required energy used to cover the desired distance. According to [20], EVs are more efficient up to 2-5 times than conventional vehicles based on ICE.
- **Usage of excess wind energy** - in periods of excess electricity generation based on wind production, it is recommended that EVs should recharge. This will lead to a more efficient usage of electricity during the outside peak load hours [20]. Also EVs might help by improving the flexibility in power systems, if the recharging process is made in an intelligent manner, by taking into consideration several aspects such as the available energy in the grid, the electricity prices and the displacement of the electricity production [20].

1.4 State of the art review regarding the integration of RES and EVs in distribution grids

The increasing number of RES and EVs that are integrated in the current power system push the need to develop and implement intelligent strategies that will ensure cleaner and more sustainable energy systems. The purpose of this section is to present some of the main studies that have been done so far with regards to the scope of this project. Also some new concepts will be introduced in this section, in order to ensure a better understanding of the scope of this report.

The effects of EVs integration on power systems is presented in [6]. In this paper, an analysis is performed to highlight how a large-scale implementation of PHEVs and BEVs (Battery Electric Vehicles) can influence the power system of Denmark, Finland, Germany, Norway and Sweden. The assumed quota of integrated EVs is represented in Figure 1.7.

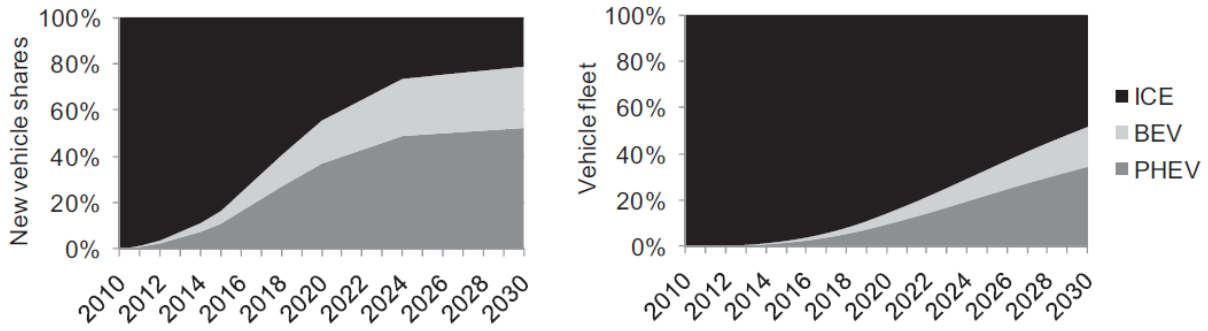


Figure 1.7: Estimated new vehicles share based on the driving technology for a 20 year period (left). Vehicle share distribution based on the vehicles powertrain technology (right) [6]

By analyzing Figure 1.7, it can be seen that the interest in EVs is expected to increase a lot in the future. The integration share for the years 2015, 2020, 2025 and 2030 is expected to reach 2.5%, 15%, 34% and 53% respectively. The analysis performed in [6], reveal that the effects in electricity generation will change significantly, due to the implementation of the increasing EVs fleet. The results obtained are being highlighted in Figure 1.8.

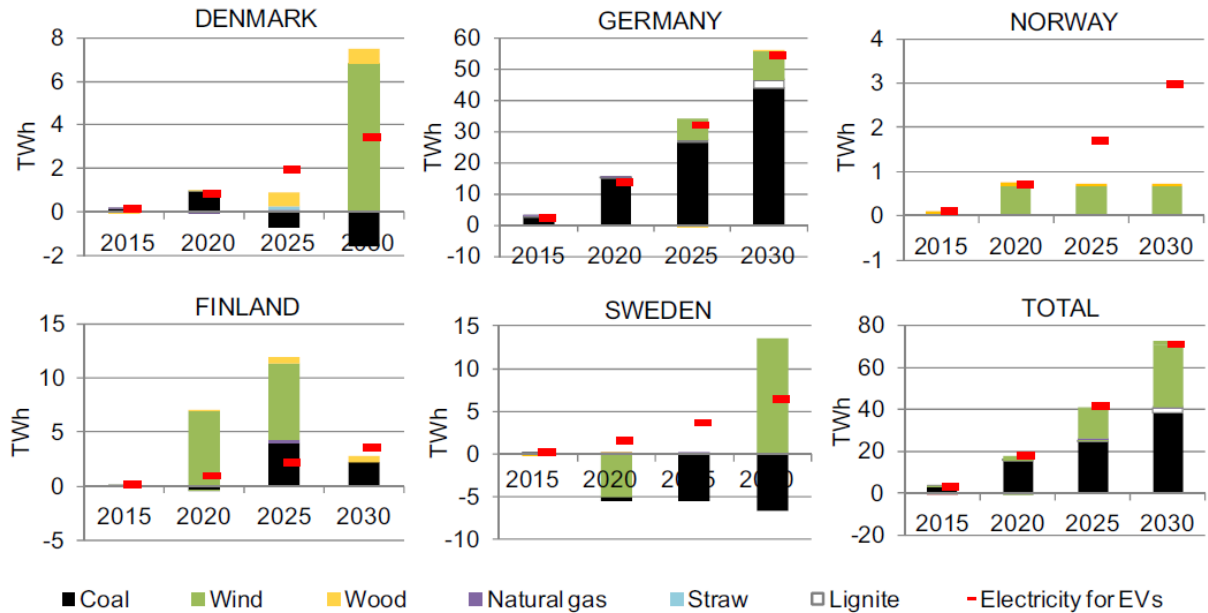


Figure 1.8: Adjustments in the annual energy production resulted after the implementation of the EVs fleet [6]

The illustration in Figure 1.8 highlights that the changes in the energy generation differ for each of the five countries, depending on their own energy strategies imposed. In the first part of the 20 year period, coal is expected to represent the dominant energy source to power the EVs. As the penetration level of renewables is expected to increase, starting with 2025, wind power will represent the dominant energy source for the electric vehicles. The effects on the CO₂ emissions are expected to change drastically if a huge number of EVs are integrated. For the five European countries analyzed in [6], the effects on the carbon dioxide emissions are presented in Figure 1.9.

The total reductions in carbon dioxide emissions are significant due to the integration of electric vehicle, especially from 2025 to 2030. This is mainly due to the fact that in this period renewables will provide almost all the electricity needed to power the EV fleet.

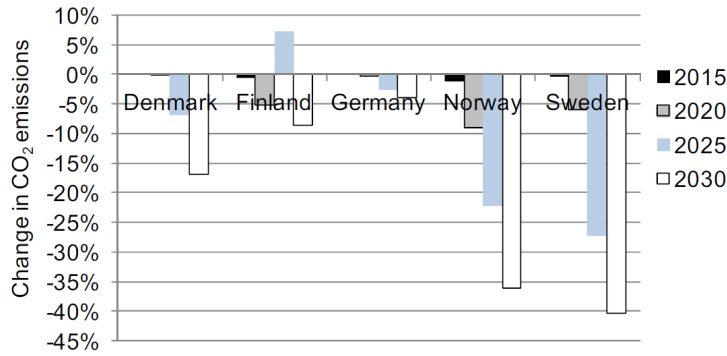


Figure 1.9: Changes in the total CO2 emissions when implementing electric vehicles [6]

The case study presented in [7], analyzes how the integration of electric vehicles in low voltage distribution grids will affect their operation. In this paper, three detailed models of Danish distribution grids are being evaluated, when the increasing amount of EV loads is varied from 0 to 40%. The purpose is to investigate the level of EV integration in LV residential grids, without overcoming the standard and technical operating limits of the grid [7]. A steady-state analysis is performed for the three modeled grids for different simulation scenarios, by taking into consideration the daily load profiles for each residential consumer. In order to assess the maximum penetration level of EV in the distribution grids, the minimum (4 am) and peak demand (5 pm) are taken into consideration. An average EV load absorbs approximately 0.3 kW (2500 kWh/ year or around 8 kWh for daily charging). This will lead to an increase of the transformer load factor by 20% [7].

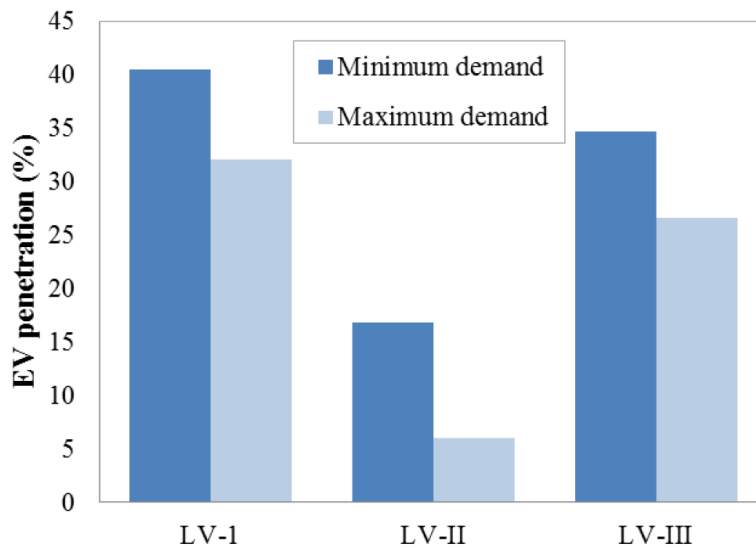


Figure 1.10: Electric vehicle penetration level in the three LV residential grids investigated [7]

The results presented in Figure 1.10 reveal that the first and third residential grids present the highest level for integrating EV, during maximum and minimum demand periods. This is due to their reduced transformer load factor in these intervals. They can be considered as being strong grids. In consequence, the second residential grid presents the lowest integration level of EV due to the increased loading of the transformer. In [7], a strategy to increase the allowable number of EV for the second residential grid is represented by the reinforcement of the grid. If this method is applied, the EV penetration level can increase with up to 20% (during peak-load hours) and 50% for minimum demand interval. The investigation performed in [7], reveals that the average transformer loading factor is found to be around 20%, thus proving that there is potential for EV if charged using intelligent strategies, during hours of excess generation based

on wind power. During the winter days the EV penetration level can reach up to 40%. This number is expected to increase during summer days, due to smaller residential loads.

The investigation presented in [8], focuses on an approach regarding how the charging strategies for EVs can reduce the load imbalances and to support the voltage levels. The paper aims to implement a charging strategy which can enable to select the phase used for charging the EV. Measurements of the phase-to-neutral voltage are made for each of the three phases, in the charging station. The EV will use the phase with the highest voltage for charging. This charging strategy is applied for a residential LV grid in which EVs are integrated. In [8], two different consumption profiles were taken into consideration: load profile during one day in the winter and during the summer. The results for the winter scenario, are presented in Figure 1.11.

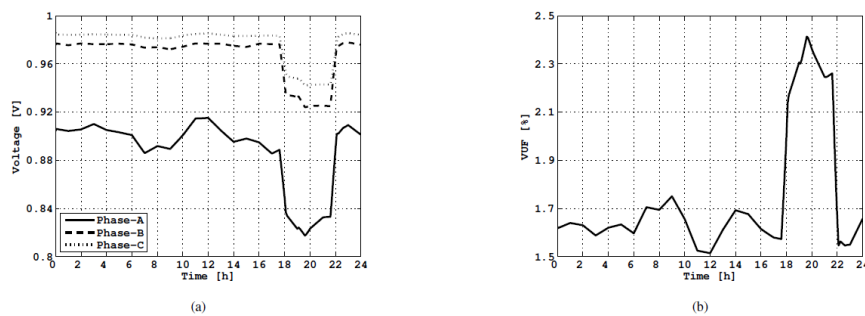


Figure 1.11: Voltage profile (a) and Voltage unbalance factor (b) during one winter day at node 613 [8]

By investigating Figure 1.11, it can be observed that the highest voltage imbalances appear during the peak consumption, especially on Phase A. This leads to an increase in the Voltage Unbalance Factor (VUF). The IEEE [21] 1159 Standard implies that a VUF higher than 2% results in an unbalanced operating condition of the grid. Hence, the residential grid is unbalanced during the peak load hours. By using the 'dumb charging' profile (presented in [8]), the energy consumed by recharging the EVs fleet is equally distributed among the three phases. This leads to a total decrease of the VUF during the peak consumption. The results are being presented in Figure 1.12

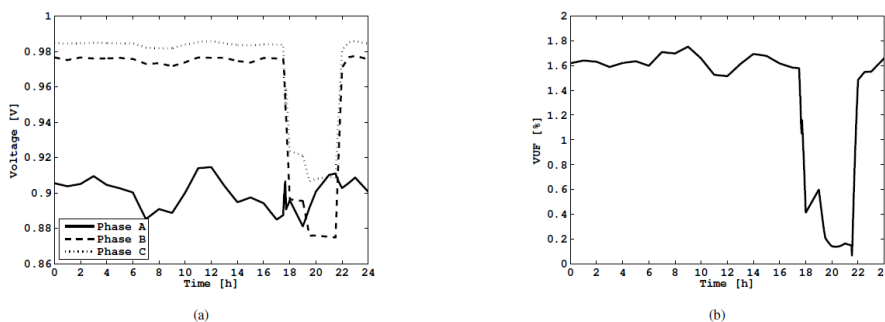


Figure 1.12: Voltage profile (a) and Voltage unbalance factor (b) during one winter day at node 613, by using the 'dumb charge' strategy [8]

By implementing the 'dumb charge' strategy, the electric vehicles are able to reduce the total voltage unbalances, thus improving the quality of the energy, as it can be seen in [8].

In [9], an analysis regarding several key power distribution parameters, by integrating EVs is being performed. The charging strategies used for the EVs are the dumb/uncontrolled charging mode and the smart charging mode. The result of using these two charging strategies when ranging the EV integration level from 0 to 50% is presented in Figure 1.13 and Figure 1.14.

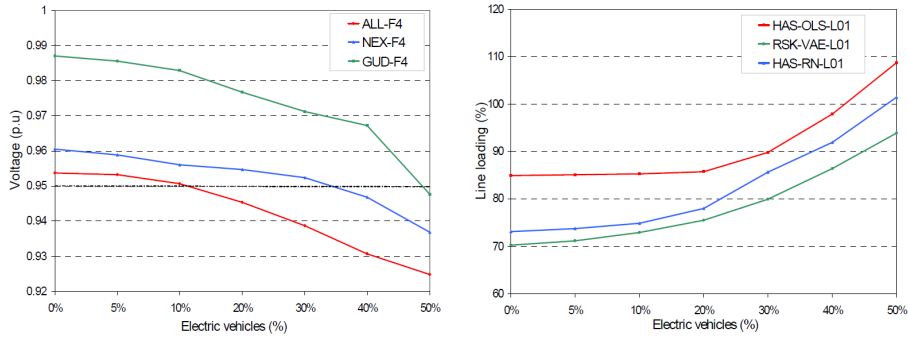


Figure 1.13: Voltage profiles for three critical feeders (left) and loading profile for three highly congested lines (right) for the uncontrolled charging strategy [9]

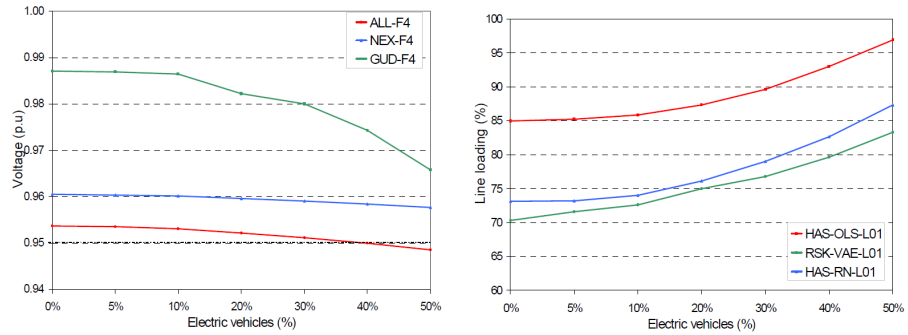


Figure 1.14: Voltage profiles for three critical feeders (left) and loading profile for three highly congested lines (right) for the smart charging strategy [9]

A comparison between Figure 1.13 and Figure 1.14, highlights that the smart charging strategy does not exceed the voltage operation limits of the grid for an EV penetration level of less than 40%. Also, the line loadings are within the admissible range if the smart charging mode is implemented.

Figure 1.15 presents the load factor of the distribution transformer used in [9], when implementing the two charging strategies. It can be observed that in the case of the smart charging mode, the load factor is reduced with approximately 2.5% if the EV number is constant. The results presented in [9], highlight that an intelligent charging strategy is more efficient for integrating more electric vehicles in a typical distribution system. The allowed number of EVs that can be integrated depends both on the charging strategies and also on the operating limits of the grid parameters.

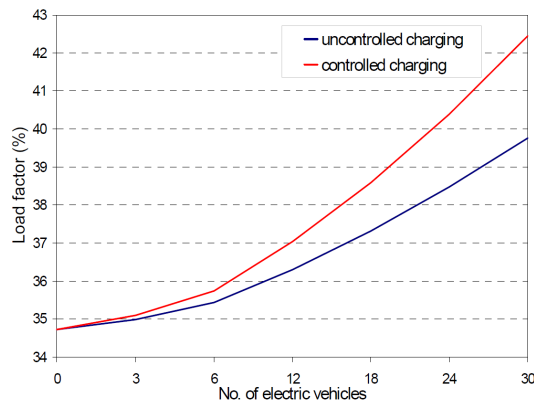


Figure 1.15: The load factor for the 250 kVA distribution transformer [9]

The analysis performed in [10], presents the integration potential of RES in order to fulfill the demand for electricity used for charging BEVs. The range technologies investigated include

Battery Switching Stations (BSS) and Fast Charging Stations (FCC). The average energy usage of a BEVs is approximately 14.8 kWh/100 km and by the year 2020, the average driving cycle is expected to be around 150 km/day [10]. In order to cover the demand for energy, renewables represent an important aspect. Figure 1.16 presents a comparison of the installed plant capacities to supply the BEVs fleet by 2020.

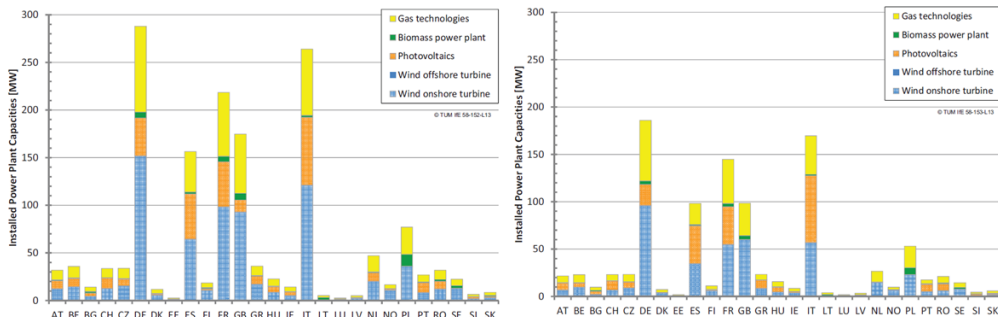


Figure 1.16: Installed power plant capacity to cover FCS (left) and BSS (right) in Europe by 2020 [10]

In Figure 1.16, it can be observed that renewables will present a huge potential by the year 2020, as primary energy sources for BEVs. Wind power, gas technologies and photovoltaics represent the dominant RES used for charging the EVs fleet by 2020, by using both battery switch and fast charging stations.

Figure 1.17 highlights the load curve during a spring week in Germany for BSS (2020). Wind and solar based energy technologies are predominant in this case. It can be observed that during the peak hours, BSS step in and decrease the demand peak. The switched batteries are charged again during extra-generation periods due to the renewables. The conclusions presented in [10], reveal that EVs and fast charging stations are presenting a huge potential for the integration of renewable energy sources and may be considered as an effective transportation system in the future.

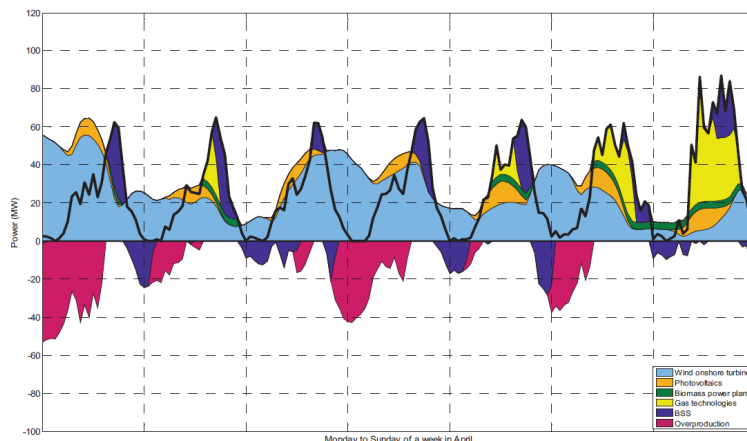


Figure 1.17: Supply of the load demand from BSS with RES integration in Germany by 2020 [10]

Summary

The articles presented in this section, highlight that in the following decades, the number of EVs is expected to increase drastically. Also, in the following years, the quota of renewable power will raise as well. It has been shown that electric vehicles represent sizable loads in distribution grids and their integration level depends on the interval of the day, in which they are charging. The

following master thesis focuses on investigating how different integration levels of renewables and EVs affects the grid parameters. Another focus is represented on the determination of the maximum penetration for both renewables and electric vehicles, by considering the grid limitations.

1.5 Outline of the Thesis

The structure of the report consists of different chapters. They are summarized as following:

Chapter 1 - Introduction: In this chapter the background information with regards to the topic is presented. An analysis with regards to the Danish distribution system is presented, as well as a short assessment of battery electric vehicles (BEV). The state of the art is outlined with regards to the impact of electric vehicles on Danish distribution systems and the integration of renewables as a primary energy source for BEVs.

Chapter 2 - Problem Statement: The focus of this chapter is to present the problem statement of the thesis together with the specific objectives required to solve the initial problems. The delimitation of the project scope is highlighted as well as the chosen methodology.

Chapter 3 - Description of the distribution test system: In this chapter, the chosen distribution grid is modeled and validated against the IEEE13 bus model. A basic overview regarding the load flow calculation method is presented. The Digsilent *PowerFactory* software interface is displayed and the results of the validated distribution grid modeled in this software are being highlighted.

Chapter 4 - RES integration and power flow analysis: This chapter focuses on the results obtained by applying the load flow analysis on the distribution grid. Starting with the households load profiles for two distinct cases (January and July), the voltage fluctuations and grid loading factors are explored. Three different placements of the renewable generation will be studied in order to determine the maximum penetration level for each case. This is necessary as a favorable renewable distribution will ensure a high EV integration level.

Chapter 5 - Power flow analysis with regards to EV integration: In this chapter, the results of the power flow analysis when integrating the EV fleet are presented. Five different charging strategies are investigated with regards to the time interval in which the electric vehicles are plugged in for charging.

Chapter 6 - Conclusions: This chapter highlights the main conclusions of this project. Also the potential future work is thoroughly discussed in this chapter.

Problem statement 2

This chapter focuses on the presentation of the problem statement of this thesis in regards with the specific objectives listed to solve the initial problem. The delimitation of the project scope is presented in concordance with the selected methodology.

2.1 Problem Statement

The focus of this master thesis is to perform a technical analysis regarding the integration of renewable energy sources and electric vehicles in a typical distribution network. The aim is to investigate the impact of distributed renewable generation and different charging strategies for electric vehicles in association with the electrical parameters of a distribution network. The latest energy policies in Denmark present a huge emphasize as the penetration level for solar and wind based energy is expected to increase in the future. The fluctuating character of renewable energy influences the operation of electrical grids as technical issues may emerge. These problems relate to the power quality (harmonics, frequency and voltage variations), small time and seasonal power fluctuations, energy storage systems and optimal placement of renewables. On the other hand, the need for a cleaner and environmental friendly transportation system will include the development of an increasing fleet of electric vehicles. They represent electric loads, in the range of approximately 3-11 kW. The charging strategies impose the use of energy in the peak and off-peak hours of the day. Large power variations (caused by RES and EVs) are challenging for distribution grids because issues such as managing voltage limits, grid congestions and power quality may arise.

The aim of the present master thesis is represented by the modelling and control of different units in medium and low voltage distribution grids. Hence, an investigation needs to be performed, for different scenarios which include different penetration levels of photovoltaic panels, small size wind turbines and electric vehicles.

Objectives

The main scope of this project is to determine the effects of different units (represented by PV panels, wind turbines and electric vehicles) under various penetration levels and operation scenarios on a distribution grid. In order to realize this, the following objectives need to be considered:

- Modelling and control of different units in a distribution grid.
- Identify voltage rise problem in the distribution networks with high penetration of wind and solar power.
- The main objective is represented by the estimation of the maximum allowable amount of wind power and PV production, and EV charging per household on typical public distribution grids under various scenarios.
- Evaluate the impact of different charging strategies for electric vehicle on the distribution grid.

2.2 Project limitations

The limitations considered in this project are the following:

- The power flow analysis will include only steady-state simulations for the different scenarios investigated in this project.
- The steady-state analysis will be performed under balanced conditions for both power and voltage.
- The generation and load units will be represented as aggregates connected at different bus bars in the distribution grid.
- The electric vehicles will be modelled in the simulations only as active power consumers, where as the households represent electrical loads with a power factor (PF) of 0.9.
- The photovoltaic panels used in this study will be considered to generate only active power.
- The investigation performed in this project will not include studies concerning the harmonics present in the distribution grid. All simulations will be considered for the fundamental harmonic of 50 Hz.
- In the following study, the cost analysis regarding the installation of the wind and solar based energy systems will not be included.

2.3 Methodology

The primary tool used in this project is represented by DIgSILENT Power Factory 15.2. The steady state analysis performed for the distribution network, has been accomplished by using in this software power flow simulations. The load flow simulations are based on the Newton-Raphson calculation method. By using the DPL (DIgSILENT Programming Language) the load flow simulations are implemented, by taking into consideration the grid components. Lastly, Matlab/Simulink software is utilized to generate the input data and to analyze the output data from the simulation scenarios performed in DIgSILENT.

The applied methodology for solving the initial problem is summarized as following:

- First, an investigation is performed in order to obtain the consumption and generation profile for the units modelled. Based on the available data, the load profile for the Danish households is being generated. The solar irradiation and wind speed profiles for one year represent the key parameters required to obtain the energy generation profile from the renewables. In order to determine the load profiles for the integrated electric vehicles, the driving patterns are analyzed with regards to distances, time periods and charging cycles.
- The distribution grid implemented in Power Factory software is represented by the IEEE 13 bus test system, found in [11]. The load flow simulation results are compared against the numbers found in [11] in order to validate the modelled electricity grid.
- Simulations will be conducted on the validated model of the distribution system. The steady-state investigation will include load flow simulations in which varying penetration levels for renewables and electric vehicles are taken into consideration. Also different strategies will be implemented for the charging of the electric vehicles.
- A thorough analysis is performed on the simulation results obtained under varying scenarios, in order to determine the maximum allowable renewable generation and EV charging per household. The impact of high penetration of wind and solar power on different grid parameters will be investigated.

Description of the distribution test system 3

In this chapter, the IEEE 13 bus distribution system is presented. Also the load flow calculus method is being highlighted with regards to the basic mathematics used. A minimal overview on the DIGSILENT PowerFactory software is being revealed in order to offer an outline of the main tool which will be used for the investigation performed in this project. The last section of this chapter focuses on the validation of the IEEE 13 bus system against the PowerFactory model, as this is required to obtain a benchmark for the residential grid which is aimed to be investigated.

3.1 IEEE 13 bus distribution system

In this section, the test distribution system is presented. The chosen system for this project is represented by the IEEE 13 Bus Distribution System [11]. This test system will represent the base model of the residential distribution grid which is aimed to be investigated in this project. The IEEE 13 bus test feeder serves as a standard circuit, often used for power distribution analysis. The operating voltage of the system is 4.16 kV. The grid is composed out of a voltage regulator, a HV/MV and a MV/LV power transformer, overhead lines, underground cables and shunt capacitors. The loads connected at the nodes of the test system are represented by unbalanced active and reactive loads. These loads are both spot and distributed.

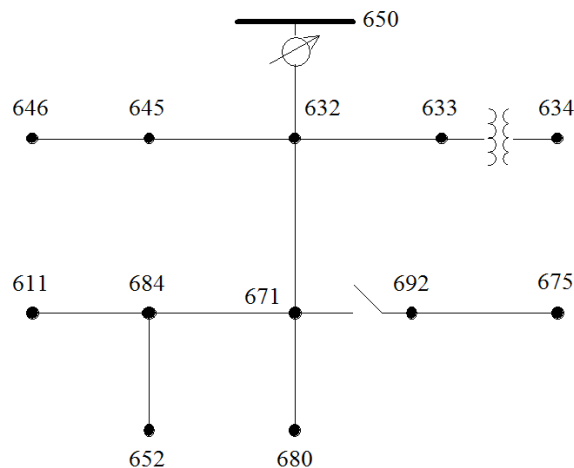


Figure 3.1: IEEE 13 Bus Test System [11]

In Figure 3.1, an illustration of the distribution test system is presented. Between nodes 650 and 632, a voltage regulator is introduced in order to maintain a constant voltage level. The MV/LV (4.16/0.48 kV) power transformer is added between nodes 633 and 634 and a line switch is added between node 671 and 692.

The components of the distribution test system are highlighted in Table 3.1.

Table 3.1: Configuration of the 13 bus test feeder

Node A	Node B	Length [feet]	Component
632	645	500	OHL
632	633	500	OHL
633	644	0	4.16/0.48 kV Trafo
645	632	300	OHL
650	632	2000	OHL
684	652	800	UGC
632	671	2000	OHL
671	684	300	OHL
671	680	1000	OHL
671	692	0	Line Switch
684	611	300	OHL
692	675	500	UGC

3.2 Description of Load Flow Method

The following section aims to present the basic principles of load flow studies. In power systems engineering the load flow analysis is used to determine the operating status of the interconnected components. A more detailed definition of the load flow formulation is given in [22] and [23]. The power flow study represents a numerical analysis focusing on determining the power flow between associate nodes of an electrical system. The components attached to these nodes can be represented by units which inject (generators) and consume power (loads) [23]. This method is widely used in transmission and distribution system, focusing on various alternative current (AC) parameters, such as voltage, active and reactive power, active and reactive current and voltage angles.

The system under analysis is considered to be operating under balanced conditions, thus the single line diagram can be used for calculation. The electrical grid is composed out of nodes and branches with specified impedance in the per unit system [22]. The network equations are formulated. The model problem is appropriate for determining the magnitude and phase voltage for each bus bar, as well as the injected or consumed active and reactive power. Load flow calculation is used during the planning and design stages as well as during different operational conditions of a power system [24].

The bus admittance matrix

The following subsection is aiming to introduce the node admittance matrix. This matrix is used in power engineering in order to describe a power system with N buses. The size of the admittance matrix is represented by a square matrix composed of N by N elements. In order to calculate the voltage magnitude and angles at each node, this matrix is used [22].

In Figure 3.2, an example of a single line diagram for a simple power system is highlighted. The exemplified power system is composed out of 4 nodes and branches.

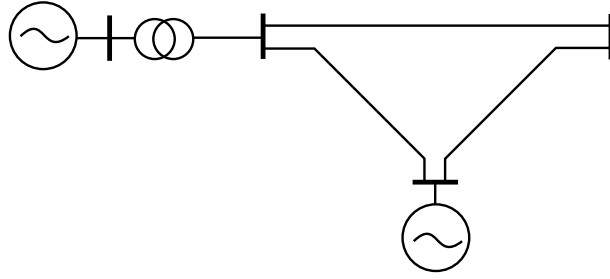


Figure 3.2: Single line diagram of a simple power system

Starting from the power system presented in Figure 3.2, the bus admittance matrix Y_{nn} is composed for the given system. In Figure Figure 3.3, the nodal admittance matrix is represented.

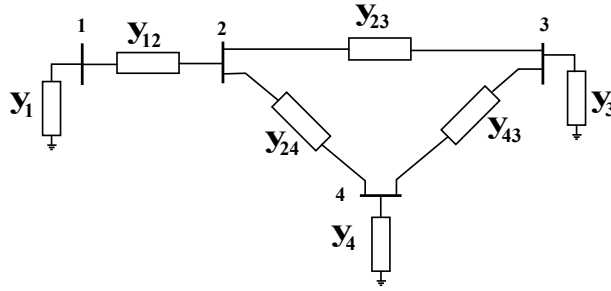


Figure 3.3: Bus admittance diagram for the power system presented in Figure 3.2

After the bus admittance diagram is being drawn, the admittance matrix can be constructed. For the admittance diagram presented in Figure 3.3, the bus admittance matrix is represented in by:

$$Y_{nn} = \begin{bmatrix} Y_{11} & Y_{12} & Y_{13} & Y_{14} \\ Y_{21} & Y_{22} & Y_{23} & Y_{24} \\ Y_{31} & Y_{32} & Y_{33} & Y_{34} \\ Y_{41} & Y_{42} & Y_{43} & Y_{44} \end{bmatrix}$$

The Y_{nn} matrix diagonal elements $Y_{11}, Y_{22}, \dots, Y_{nn}$ represent the *self-admittances* at each node. They are equal to the sum of the admittances connected directly to each specific node. The other admittances represent the *mutual admittances* located between the two distinct branches [22]. The *self-admittances* terms can be determined by using the following equation:

$$Y_{ij} = y_i + \sum_{k=1, k \neq i}^N y_{ik}, \quad \text{if } i = j \quad (3.1)$$

The *mutual admittances* terms can be determined by using the following equation:

$$Y_{ij} = -y_{ij}, \quad \text{if } i \neq j \quad (3.2)$$

In Equation 3.1 and Equation 3.2, the admittance y_{ij} is determined by using:

$$y_{ij} = \frac{1}{z_{ij}} = \frac{1}{r_{ij} + jx_{ij}} \quad (3.3)$$

where, y_{ij} is the admittance between nodes i and j (in $[\Omega^{-1}]$), z represents the impedance between busbars i and j (in $[\Omega]$), r stands for the resistance between i and j (in $[\Omega]$) and x is the inductance among nodes i and j (in $[\Omega]$).

The admittance matrix is symmetric along the leading diagonal. In an ordinary power system, each bus bar is connected to only several nodes. As a result, the bus admittance matrix is sparse, with most of the elements equal to 0 [23].

3.2.1 Load flow equations

In order to perform the load flow analysis on a power system, several parameters need to be taken into consideration. These parameters are represented by: the active power P , the reactive power Q , the voltage magnitude $|V|$ and the voltage angle δ (which is determined based on the reference voltage angle). Each bus bar connected in a power system can be categorized as being one of the following:

- **Load bus** - considered as consumption nodes. In a conventional power system there are no generating plants connected at this type of bus. They represent approximately 85% of the total number of nodes in a power system.
- **Voltage controlled bus** - also named *PV bus*, at which the power generation is connected. The value of the voltage magnitude is maintained at a constant level for as long as the reactive power is kept between the limits ($Q_{min} < Q_{required} < Q_{max}$). If this condition is violated, the bus is considered as being a load bus (*PQ*).
- **Slack bus** - this bus represents the connection with the external grid. This bus is considered as being the reference bus to which the voltage phase angles for all the nodes are relative to. In a power system there is only one node of this type. Another distinction is that this bus is used to balance the power in order to maintain the voltage constant.

Table 3.2 presents the load flow bus types in accordance with the specified and unknown variables.

Table 3.2: Load flow bus types and parameters [25]

Bus type	Specified variables	Unknown variables
PQ/Load Bus	P, Q	$ V , \delta$
PV Bus	$P, V $	Q, δ
Slack Bus	$ V , \delta$	P, Q

For the power system highlighted in Figure 3.2, the single line diagram, as well as the power circulation is presented in Figure 3.4. In this figure, the known and unknown variables needed to determine the power flow are being represented.

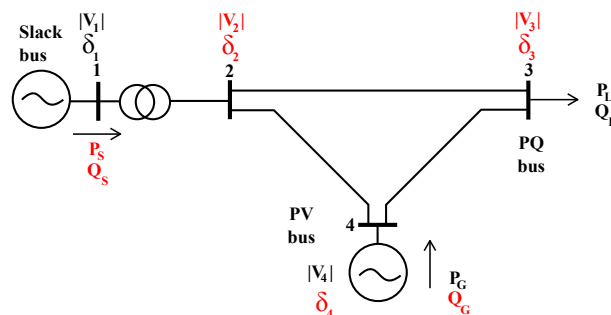


Figure 3.4: Single line diagram with specified and unknown variables for the power system in Figure 3.2

After the determination of each bus type and variable for it, the load flow analysis is used to determine the voltage magnitude and angle for each bus bar. For a power system with N buses and R generators, the number of unknowns are equal to $2(N-1)-(R-1)$ [26]. The equations used represent power balance equations. They can be written to determine the active and reactive

power for each bus bar. The active power balance equation is:

$$P_i = \sum_{k=1}^N |V_i||V_k|(G_{ik}\cos\theta_{ik} + B_{ik}\sin\theta_{ik}) \quad (3.4)$$

where P_i represents the net injected power at the bus, G_{ik} is the real component of the element in the nodal admittance matrix Y_{nn} , B_{ik} represents the imaginary part of the element corresponding to the Y_{nn} bus and θ_{ik} is the voltage angle between buses i and k .

The reactive power balance equation is represented by the following:

$$Q_i = \sum_{k=1}^N |V_i||V_k|(G_{ik}\sin\theta_{ik} - B_{ik}\cos\theta_{ik}) \quad (3.5)$$

where Q_i represents the reactive power injected at the bus i .

In some examples, the power flow equations represented in Equation 3.4 and Equation 3.5 can be solved analytically if the number of nodes interconnected in the power system is small. For more complex power systems, it is necessary to implement the usage of iterative methods. These solutions are based on numerical complex computations, and can be found in [22] and [23]. The methods are the following:

- **The Newthton-Raphson iteration method**
- **The Gauss-Siedel iteration method**
- **The Fast-decoupled load-flow method**

3.3 DIgSILENT Power Factory modelling

The DIgSILENT (DIgital SIMuLation of Electrical NeTworks) *PowerFactory* software is a computer-aided simulation tool used for the analysis of transmission, distribution and industrial power systems. This software has been designed as an advanced integrated graphical user software package devoted to electrical power systems and control analysis. The DIgSILENT tool represents a graphical single-line interface, suited to provide a comprehensive analysis regarding the planning and operation optimisation of power systems [27].

DIgSILENT PowerFactory software represents a strong simulation tool, incorporating a large number of simulation functions, defined thoroughly in [27]. These simulation functions include some of the following:

- Load Flow Analysis (for 1-, 2-, and 3-phase AC or DC networks)
- Short-Circuit Analysis (for 1-,2-, and 3-phase AC grids)
- Harmonic Analysis
- RMS Simulation (time-domain simulation for stability analysis)
- EMT Simulation (time-domain simulation of electromagnetic transients)
- Protection Analysis

3.3.1 General Design of PowerFactory

The *PowerFactory* software has been designed as a graphical environment interface. The data is introduced by depicting the electrical network elements, after which the assigned data to these items is being edited by the use of dialog boxes. *PowerFactory* utilizes a hierarchical, object-oriented database. The data input represents power system Elements, Single Line Graphics, Study Cases, system Operation Scenarios, etc., and are gathered as individual objects in an inside hierarchical set of folders [27].

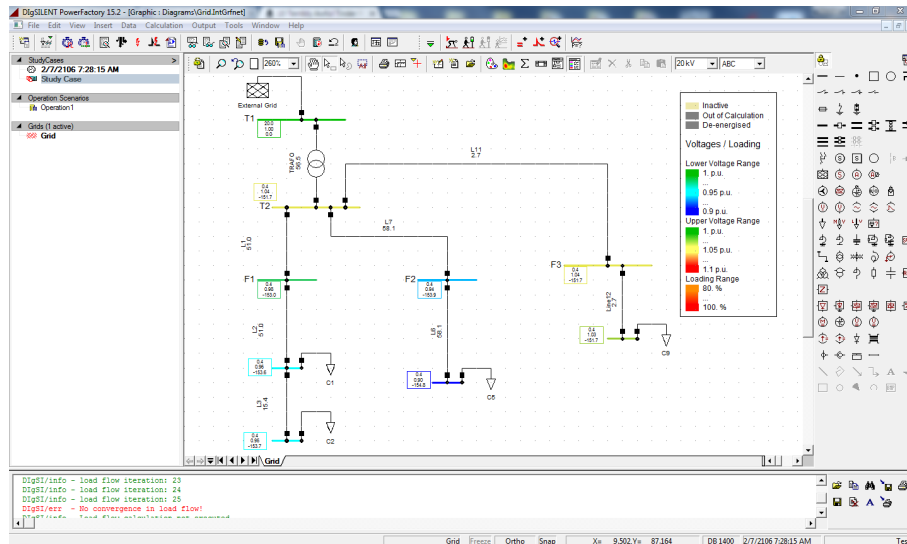


Figure 3.5: *PowerFactory* Main Window - illustration for a LV electricity grid

In Figure 3.5, an illustration for the *PowerFactory* Graphical User Interface (GUI), is presented. In this figure, a project containing a LV electricity network is active. The interactive GUI presents an easy method to model the power system components.

PowerFactory is utilized to model and simulate power systems by using standardized materials and components. The "Global Library" option contains an expanded range of pre-defined models for different grid components, such as standard system components (conductors, electrical generators and motors, transformers, etc.); standard control system frames; standard current and voltage transformers (CT and VT), fuses and relay models; pre-defined model templates (battery systems with frequency control, different wind turbine topologies and photovoltaic systems). The software offers the possibility for the user to create its own power system components by the use of the "Equipment Type Library". Hence, the electrical parameters of the components may be input individually.

3.3.2 Grid components modelling in *PowerFactory*

In *PowerFactory* software each component of the grid can be modelled individual. The use of singular blocks allows the input of different parameters (physical, mechanical or electrical) regarding the element which is aimed to be modelled. In this project, the units aimed to be modelled are represented by the following:

- Household electrical loads
- Photovoltaic panels
- Small-scale wind turbines
- Distribution power transformers
- Distribution power lines (OHL and UGC)
- Electric vehicles (modelled as simple electrical loads)

Depending on the network component which is aimed to be modelled, the individual blocks grants the option of inserting the required parameters, in order to perform the chosen power system analysis.

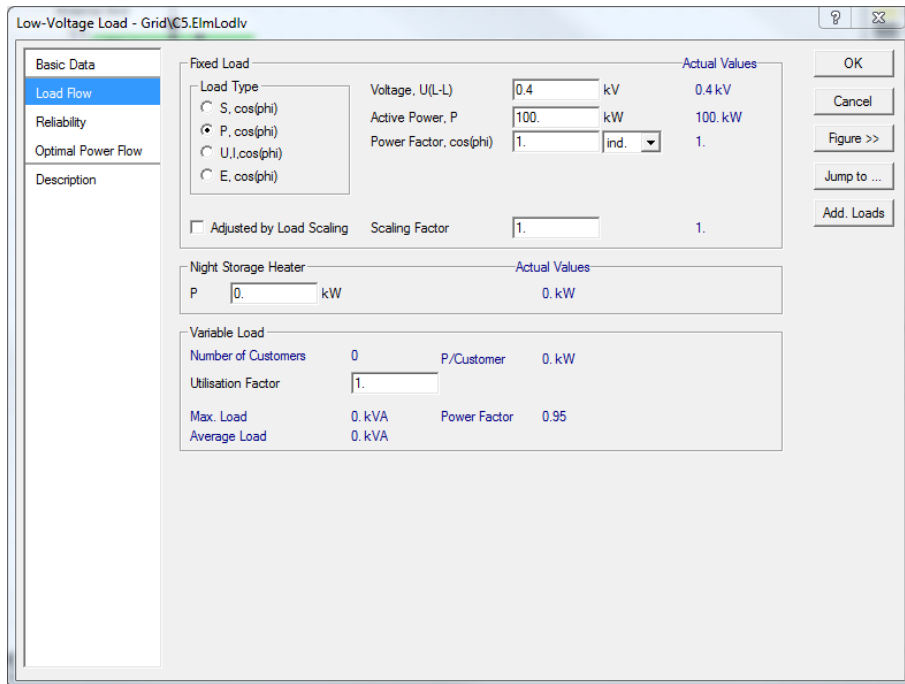


Figure 3.6: *PowerFactory* Individual block for a typical electric load

In Figure 3.6, the block for a general electrical load is illustrated. It can be observed that depending on the simulation function chosen, the parameters are inserted. For the case of the load flow analysis, the load is considered as being fixed. After the load type is determined, the electrical parameters (such as voltage, active/reactive power, power factor, etc.) can be introduced. The input data for the blocks depends on the different grid element modelled.

3.4 IEEE 13 bus distribution system validation

This section focuses on the validation of the IEEE 13 bus test system [11] against DlgSILENT *PowerFactory* software. This is necessary in order to create a benchmark model of the distribution grid which is aimed to be investigated. Starting from this validated model, the renewables and EVs loads will be connected into different configurations (by varying the penetration levels at different nodes of the network), by taking into consideration also the household electrical consumption.

In order to reduce the complexity model of the distribution system implemented in *PowerFactory* software, the voltage regulator between nodes 650 and 632 is not being modeled. The result of such a thing is represented by the impossibility of regulating independently the voltage per each phase. The voltage adjustment is being performed by the usage of tap changers of the power transformer. For a better control of the voltage level, the LV side of the power transformer is selected to operate the tap changers.

The distribution model presented in Figure 3.1 is modeled by using the *PowerFactory* software. An illustration of the IEEE 13 bus test system implemented is represented in Figure 3.7.

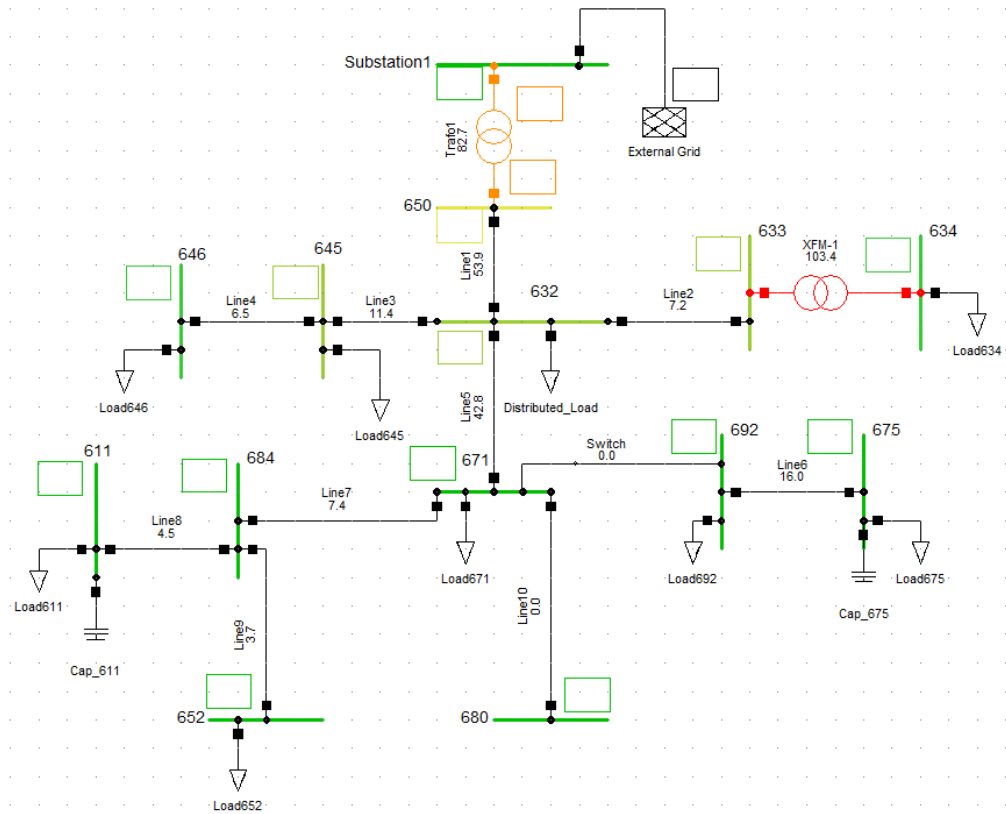


Figure 3.7: The IEEE 13 bus distribution system implemented in *PowerFactory* software

The load flow analysis is implemented on the distribution system modeled. This analysis is being performed for the same unbalanced conditions regarding the active and reactive power as the ones presented in [11]. The results of the power flow method are being presented for each phase, the following tables.

Table 3.3: Voltage profiles (in per unit and angles) for **Phase A** at each node of the distribution system modelled in *PowerFactory* (PF) against the IEEE 13 bus model

Node	PF V_A (pu)	IEEE V_A (pu)	Diff [%]	PF δ_A	IEEE δ_A	Diff [°]
650	1.07	1.06	0.94	0.3	0	0.3
632	1.02	1.02	0	-2.1	-2.5	0.4
645	-	-	-	-	-	-
646	-	-	-	-	-	-
633	1.02	1.02	0	-2.2	-2.5	0.3
634	1.05	0.99	6	-3.2	-3.2	0
671	0.99	0.99	0	-3.9	-5.3	1.4
684	0.99	0.99	0	-4	-5.3	1.3
611	-	-	-	-	-	-
652	0.98	0.98	0	-4.1	-5.2	1.1
692	0.99	0.99	0	-3.9	-5.3	1.4
675	0.99	0.98	1.02	-4.2	-5.5	1.3
680	0.99	0.99	0	-3.9	-5.3	1.4

Table 3.4: Voltage profiles (in per unit and angles) for **Phase B** at each node of the distribution system modelled in *PowerFactory* (PF) against the IEEE 13 bus model

Node	PF V_B (pu)	IEEE V_B (pu)	Diff [%]	PF δ_B	IEEE δ_B	Diff [°]
650	1.06	1.05	0.94	-120	-120.1	0.1
632	1.03	1.04	0.94	-122.4	-121.7	0.5
645	1.03	1.03	0	-122.6	-121.9	0.7
646	1.02	1.03	0.94	-122.7	-122	0.7
633	1.03	1.04	0.94	-122.4	-121.8	0.5
634	1.02	1.02	0	-120.5	-122.2	1.7
671	1.01	1.05	3.8	-123.9	-122.3	1.6
684	-	-	-	-	-	-
611	-	-	-	-	-	-
652	-	-	-	-	-	-
692	0.99	0.99	0	-123.9	-122.4	1.5
675	1.01	1.05	3.8	-123.9	-122.5	1.4
680	1.01	1.05	3.8	-123.9	-122.4	1.5

Table 3.5: Voltage profiles (in per unit and angles) for **Phase C** at each node of the distribution system modelled in *PowerFactory* (PF) against the IEEE 13 bus model

Node	PF V_C (pu)	IEEE V_C (pu)	Diff [%]	PF δ_C	IEEE δ_C	Diff [°]
650	1.06	1.06	0	119.3	120.1	0.7
632	1.02	1.02	0	117.1	117.8	0.7
645	1.01	1.01	0	117.2	117.9	0.8
646	1.01	1.01	0	117.3	117.9	0.6
633	1.02	1.02	0	117.1	117.8	0.7
634	0.98	0.99	0.94	115.3	117.3	2
671	1.01	0.98	2.97	114.9	116.0	1.1
684	1.00	0.98	2.97	114.9	115.9	1
611	1.00	0.97	4.11	114.8	115.7	0.9
652	-	-	-	-	-	-
692	1.00	0.98	2.97	115.0	116.0	1
675	1.00	0.98	2.97	114.8	116.0	1.2
680	1.01	0.98	2.97	114.9	116.0	1.1

A thorough analysis on Table 3.3, Table 3.4 and Table 3.5 reveal that the results obtained in *PowerFactory* are comparable to the ones presented in [11]. Regarding the voltage in p.u. values, it can be observed that the maximum difference is represented by 6 %, for phase A, at node 634. Also, in terms of the voltage angle, the results obtained when the load flow is applied for the implemented model in DIGSILENT, can be considered as being comparable with the IEEE distribution model. The maximum voltage angle deviation between the two models is represent by an angle of 1.7°, for phase B, at node 634. This is due to the fact that the voltage regulator is not modelled in *PowerFactory* software.

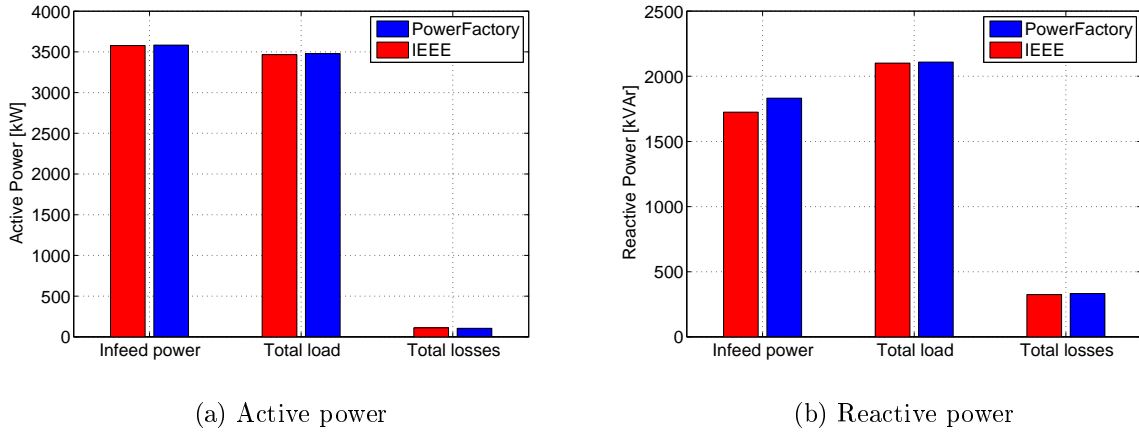


Figure 3.8: Result comparison between the IEEE distribution system and the model implemented in *PowerFactory*

In Figure 3.8a, the active power results obtained for the distribution system modelled in *PowerFactory* are compared against the IEEE distribution test system. It can be observed that two models present almost no difference, regarding the infeed active power and total losses. Regarding the total active load, the difference between the two models is represented by 0.4%. This low difference can be considered as admissible, hence the two models can be comparable.

The illustration presented in Figure 3.8b highlights the results between the *PowerFactory* and IEEE model regarding the reactive power. The difference between the values of the total reactive losses and load for the two distribution systems can be considered as being irrelevant. When it comes to the reactive infeed power, the distribution grid modelled in *PowerFactory* consumes 6% more reactive power. This is due to the fact that the voltage regulator is not modelled. As a consequence, the value for the infeed reactive power is higher, when compared to the IEEE distribution model.

The results presented in this section validate the distribution grid modelled in *PowerFactory* against the IEEE 13 bus system [11]. The results presented regarding the voltage profiles for each node and the active and reactive power flow can be considered as being equivalent for both models. As a consequence, the validated model of the grid will be considered as being the benchmark distribution grid aimed to be investigated in this project. In the next chapter, the modelled distribution grid will be adapted, as renewables will be integrated, by taking into consideration different penetration levels. These scenarios will include power flow calculus by ranging the penetration level of both renewable sources and also electric vehicle loads.

RES integration and power flow analysis 4

The next chapter aims to present the results of the investigation performed on the distribution grid. Starting from the households load profiles for two distinct cases, the voltage fluctuations and grid loading factors are explored. Three different placements of the renewable generation will be studied in order to determine the maximum penetration level for each case. This is necessary as a favorable renewable distribution will ensure a high EV integration level.

4.1 Overview on the household consumption profiles

The following section focuses on the consumption profile for a residential household in Denmark. The household loads are modelled as aggregates, connected at each busbar. The load flow analysis is being performed for the same distribution grid, as presented in Chapter 3, in Figure 3.1, during a one week time interval, by using an one hour time step. In the simulation scenarios, all distribution lines are modeled as underground cable systems. The total number of households modeled in the simulation scenarios is being highlighted in Table 4.1.

Table 4.1: Total number of households connected at each bus for the distribution grid

Node	Number of households	Node	Number of households
611	70	652	42
632	37	671	37
633	56	675	53
634	56	680	42
645	68	684	42
646	70	692	42
650	42	-	-

The simulation scenarios aimed to be investigated in this chapter, follow two distinct cases for each household: **January case** - one normal week in January, when the consumption is highest and **July case** - one regular week in July, during which the electricity demand is at the very less. Each household load modelled in the simulations, present the same profile. The residential consumption is taken from [28], in which the consumers present no electrical heating system. The daily load profile for a typical house in Denmark is dependent on the month of the year and the type of day (normal working day or weekend day). The results presented in [29], reveal that some correction factors need to be applied in order to accurately model the load of the grid (depending on the month of the year). In this project, the base consumption is considered to be in July. By applying Equation 4.1 the consumption for January can be found (if considering the same load scaling factor as in [29]) with regards to each household, for an hourly time step.

$$P_{Household,January} = k_1 \cdot P_{Household,July} \quad (4.1)$$

where, $P_{Household,January}$ represents the active power consumption, in [kW] for each house in January, k_1 represents the load scaling factor for January (from [29] $k=1.75$) and $P_{Household,July}$ is the active power consumption in July. The load profiles modeled for each consumer are presented in Figure 4.1.

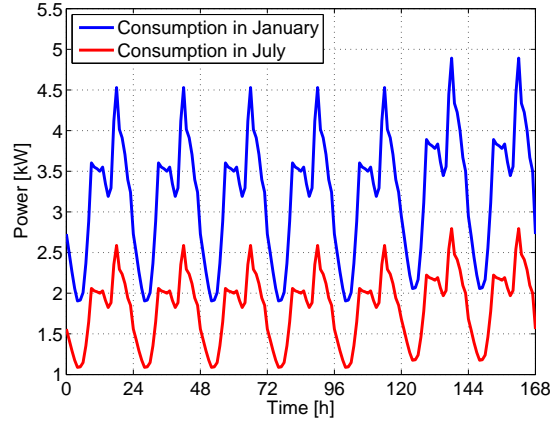


Figure 4.1: Consumption profile at each household for January and July cases

In the simulation scenarios performed in this chapter, the aggregated households connected at the buses are considered as electrical loads having a power factor of 0.9. Due to the fact that the consumers are modeled as aggregates connected at 4.16 kV, a correction factor of 1.05 is imposed, by the use of Equation 4.2. This value has been chosen arbitrary to model the voltage step down (from 4.16 to 0.48 kV) distribution power losses.

$$P_{bus,i} = n \cdot P_{load} \cdot k_2 \quad (4.2)$$

where $P_{bus,i}$ is the total consumed power at bus i (in [kW]), n represents the total number of household connected at the bus, k_2 stands for the aggregate correction factor (considered as 1.05) and P_{load} is the electrical demand of one house (in [kW]).

4.2 Power flow analysis on the distribution grid without any RES connected

In this section the load flow analysis is being performed for the distribution grid highlighted in Figure 3.1. The number of household loads connected at each node is presented in Table 4.1; each house has the same consumption profile as the one presented in Figure 4.1. The power flow analysis is implemented on an hourly basis for one week, by taking into consideration two consumption scenarios (January and July cases). The load flow method will be applied, by maintaining the tap changer on the distribution transformer set to position 5. This is required in order to observe the voltage deviations at each busbar, during a week.

The power flow method is implemented by taking into consideration three different operational parameters of the distribution grid:

- **Voltage profile** - in Per Unit [p.u.] for the closest and the farthest nodes of the distribution grid, in regards with the placement of the distribution transformer. This is necessary in order to observe the voltage fluctuations for the scenarios investigated.
- **The Transformer loading factor** - in percentage [%], necessary to study the power flow from the external grid to the distribution network and to determine the maximum loading hours.

- **The line loading factor** - in percentage [%], needed to examine the operational limits of the distribution power lines. The distribution system [11] does not give any information regarding the current ratings for the cables. Due to this, the selected ampacity for the each cable in the distribution system is given by a NYFGY 3x300 SM 3.6/6 kV IEC Standard Cable, found in the *PowerFactory* Library. The value of the current rating is equal to **0.517 [kA]**.

4.2.1 Voltage profiles

In this subsection, the voltage profiles are presented with regards to the two different scenarios. The analysis focuses on studying the voltage fluctuations at the closest and farthest away nodes from the distribution transformer. The voltage profiles for each busbar are dependent on the voltage drops between the reference node and each individual bus. The voltage drop can be estimated by using Equation 4.3.

$$\Delta V = V_{tr} - \sum Z_{ij} \cdot I_{ij} \quad (4.3)$$

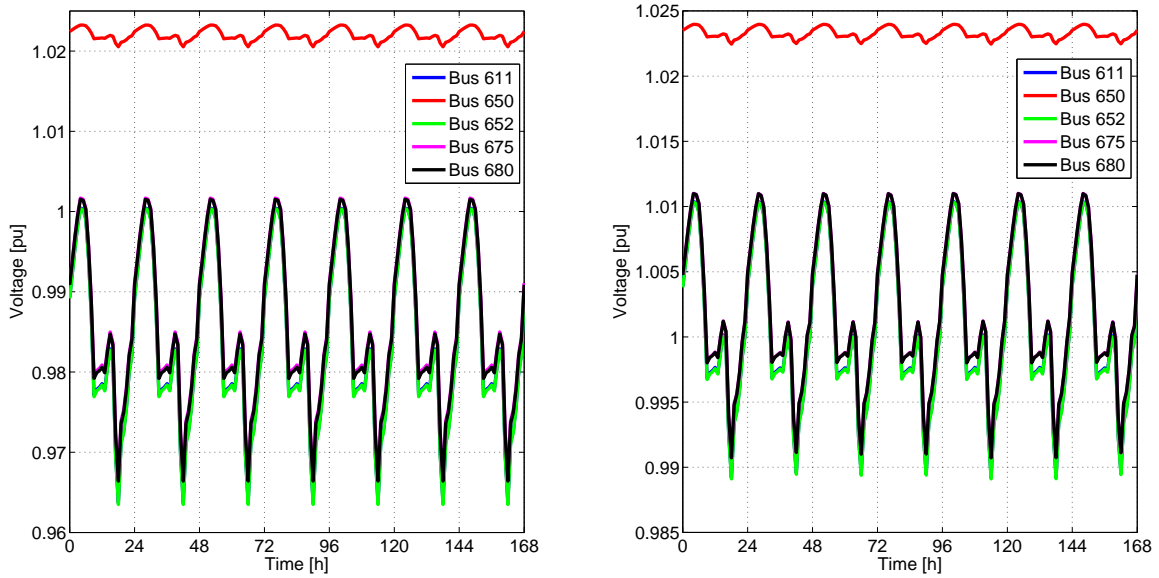
where, V_{tr} represents the voltage measured at the secondary side of the distribution transformer (reference voltage), Z_{ij} is the line impedance between nodes i and j and I_{ij} stands for the line current from bus i to j . In Equation 4.4 an example is given for the estimation of the voltage drop at node 646.

$$\Delta V_{646} = V_{tr} - Z_{650-632} \cdot I_{650-632} + Z_{632-645} \cdot I_{632-645} + Z_{645-646} \cdot I_{645-646} \quad (4.4)$$

By knowing the estimated voltage drop at each busbar, the voltage profile (in p.u.) can be determined for an hourly basis during the entire week. This can be done by using Equation 4.5.

$$V_{i[p.u]} = \frac{V_i}{V_{tr}} = \frac{V_{tr} - \Delta V_i}{V_{tr}} \quad (4.5)$$

where, V_i represents the voltage at node i , V_{tr} stands for the reference voltage and ΔV_i is the voltage drop on bus i . In this project all of these values are represented by the line to line (L-L) voltages, and are taken in [kV].



(a) January

(b) July

Figure 4.2: Voltage profiles during one regular week with no RES generation

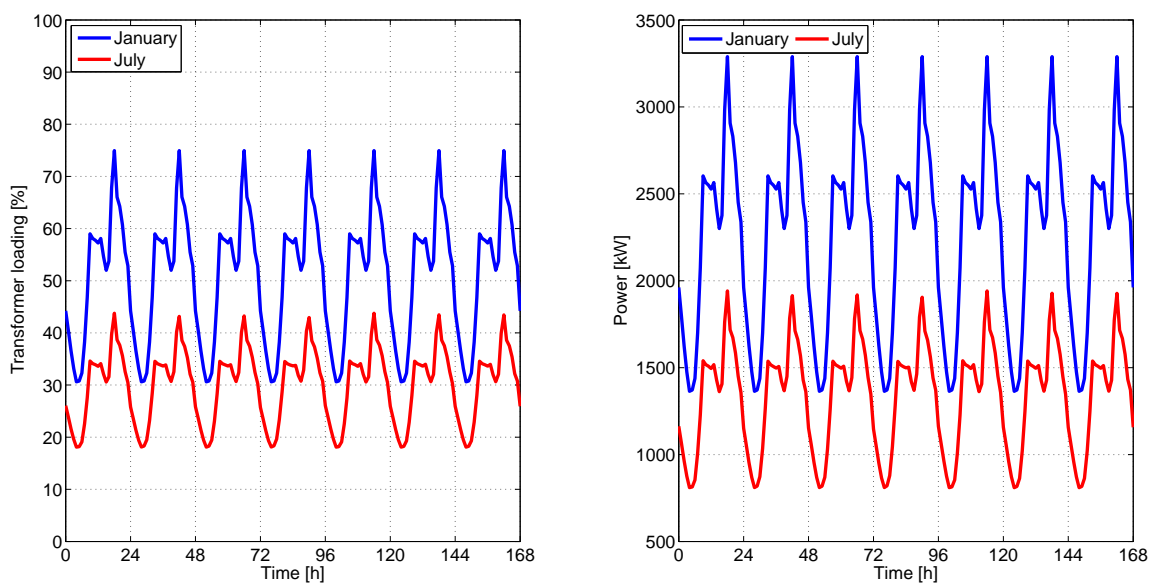
The examination of Figure 4.2 reveals that the voltage profile at node 650 (the reference bus) can be considered as being constant for both scenarios. The voltages at the far away nodes (611, 652, 676 and 680) fluctuate during the week for both winter and summer scenario. For the winter case, shown in Figure 4.2a, it can be observed that the voltages at the far away buses present one major spike, during the low-demand hours (2 a.m. - 7 a.m.). During this, the power consumption at each node is lower, compared with the peak-load hours. This leads to an increase of the voltage values, as in any distribution system, the voltages at the nodes increase as the overall power demand is decreased. During the peak-load hours, it can be observed that the inverse appears. The voltage value is decreasing as the load at each node starts to raise. It can be seen that during the peak consumption hour for each day (19 p.m.), the lowest voltage in the grid reaches 0.964 p.u. at node 652. For the summer case, highlighted in Figure 4.2b, it can be observed that the voltages present the same profile as in the winter case, but the values are higher. This is due to the lower power consumption in this week. During the peak hour of each day, the lowest voltage occurs at bus 652 (0.989 p.u.). For both cases, during the whole week, the voltages at the far away buses are maintained within the admissible limits of 0.95 - 1.05 p.u.

4.2.2 Transformer loading factor

The loading factor of the transformer represents a key factor in any distribution grid. This is dependent with the total power flowing from the external grid to the household loads. A high loading factor will lead to a significant decrease regarding the lifetime of a power transformer. Other effects of a high load factor are related to the premature aging of the insulation, the increase of the active power losses, etc. The transformer loading factor can be determined by using Equation 4.6.

$$Tr_{lf} = \frac{S_t}{S_n} \cdot 100 \quad (4.6)$$

where, Tr_{lf} stands for the transformer loading (in [%]), S_t represents the power flowing through the transformer at a given time (in [MVA]) and S_n is the nominal power of the distribution transformer (the one used in the simulations has a nominal power of 5 [MVA]).



(a) Transformer loading factor

(b) Infeed active power

Figure 4.3: Transformer loading (a) and Infeed active power (b) with no RES generation

The loading factor for the distribution transformer used is presented in Figure 4.3. A close comparison of the two loading factor profiles presented, highlights that during the winter the power flowing through the transformer is significantly higher, compared to the summer case. It can be observed that, the maximum loading occurs during the winter, in the peak-load hours, when it reaches approximately 75%. Regarding the summer profile, the maximum loading reaches the value of 44%, during the same hours. The individual household consumption profiles (shown in Figure 4.1) and the infeed power from the external power system (observed in Figure 4.3b), backup the transformer loading profile, as it can be seen that the loading factor increases with the rising of the overall load and vice-versa.

4.2.3 Distribution lines loading factors

The most loaded lines in the distribution grid presented in Figure 3.1, are represented by Line 1 (from node bus 650 to 632) and Line 5 (from node 632 to 671). Due to this, the results presented in this subsection are focused only on these two cable systems. The rest of the cables used in the distribution grid, present loading factors significantly lower, thus the cable loading for these will not be shown. The cable loading factor can be determined if Equation 4.7 is used.

$$Cable \quad l_f = \frac{I_t}{I_{rated}} \cdot 100 \quad (4.7)$$

where, I_t represents the load current for the cable at a given time (in [kA]) and I_{rated} stands for the ampacity of the cable, also in [kA]. The cable loading factor is in [%].

For the two different cases investigated, the cable loading factors are represented in Figure 4.4.

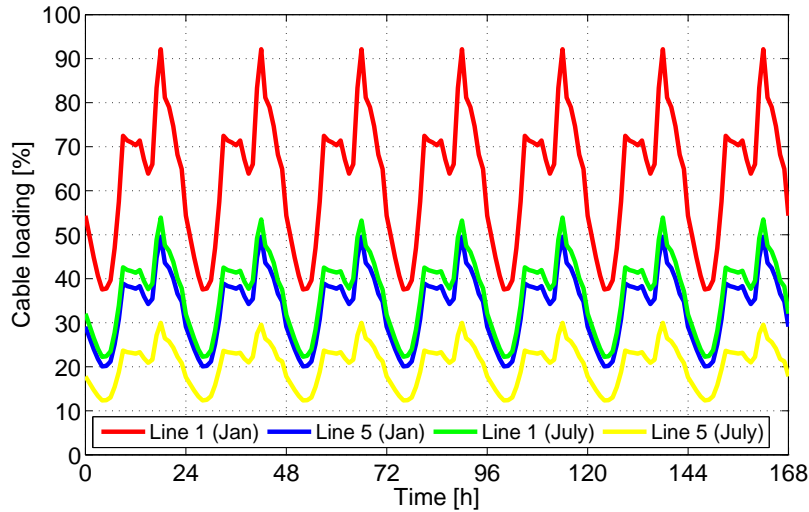


Figure 4.4: Line loading factors for Line 1 and Line 5 during the winter and summer scenario

The results presented in Figure 4.4 show that the most congested cable is the one connecting busbars 650 and 632 (Line 1). During the week in January, the highest loading factor occurs in the peak-load hours, reaching a value of 92%. The loading factor regarding Line 1 during the summer scenario is less (approximately 53%), due to the less demand for electricity in this period. In regards with Line 5, it can be noticed that the loading follows the same profile, but the maximum loading reaches 50% (in January), respectively 30% (in the summer).

The results displayed in this section highlight that the grid parameters (after the load flow calculus is applied) with regards to the case when no RES are connected, are within the admissible limits. The voltage fluctuations are maintained within the permissible values (the

maximum and minimum deviations are 0.965 and 1.01 pu) and also the loading factor for the distribution transformer and power lines are kept within the operational limits.

4.3 Generation profiles for the PV modules and wind turbine

This section provides information about the generation profile for the renewable sources modeled in this project. The renewable generation is based on the weather profile given by [12], for the region of Copenhagen, Denmark with regards to the monthly average values for wind speed and solar irradiation. The profile for these two parameters are generated by using a stochastic model over a one year time interval, (for a 5 minutes time step) and are represented in Figure 4.5.

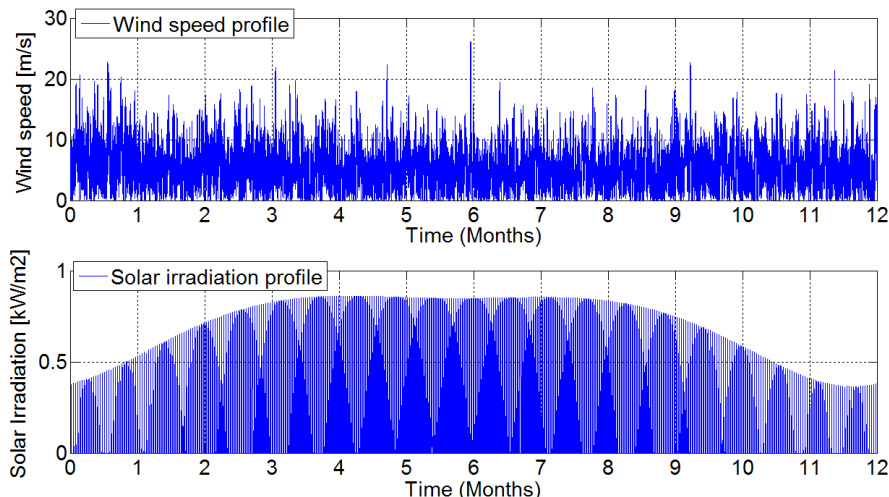


Figure 4.5: Solar irradiation and wind speed profile during one year with respect to [12]

In Figure 4.5 the wind speed and solar irradiation profiles are highlighted over a one year interval, starting from January. The solar irradiation profile can be divided into two different periods: the high irradiation interval, between March and August and the low irradiation duration, between September and February (with the mention that the minimal irradiation occurs during December and January).

The power generation of the wind turbines is determined by using look-up tables in Matlab/Simulink software, in which the input parameter represents the wind speed and the output parameter represents the generated power, by taking into consideration the wind speed versus power output ($v - P$) curve. The same principle is applied for the PV system with the mentioning that for this, the input parameter is represented by the solar irradiation. The renewable sources modeled in this report are represented by a *Polaris P - 15 50 kW* wind turbine, and a PV module composed of 20 *Mitsubishi Electric PV - MLE265HD* (each individual PV panel has 0.265 kWp) with a total output power of 5.3 kWp.

The output power for the WT and PV panel presented in Figure 4.6, are determined as functions of the wind speed and solar irradiation. The power generation is dependent on these parameters, as shown in Equation 4.8 and Equation 4.9.

$$P_{PV} = \frac{G}{1000} \cdot P_{STC} \cdot [1 + \alpha (t - t_0)] \quad (4.8)$$

where G represents the solar irradiation, P_{STC} represents the peak power of the panel, t stands for the ambient temperature, t_0 is the standard temperature, α represents the temperature coefficient of the PV panel ($0.0056/^\circ C$).

$$P_{WT} = \frac{1}{2} \cdot \rho \cdot \pi \cdot R^2 \cdot v^3 \cdot C_p \quad (4.9)$$

where ρ is the air density, R represents the radius of the wind turbine, v is the wind speed, C_p stands for the wind turbine power coefficient.

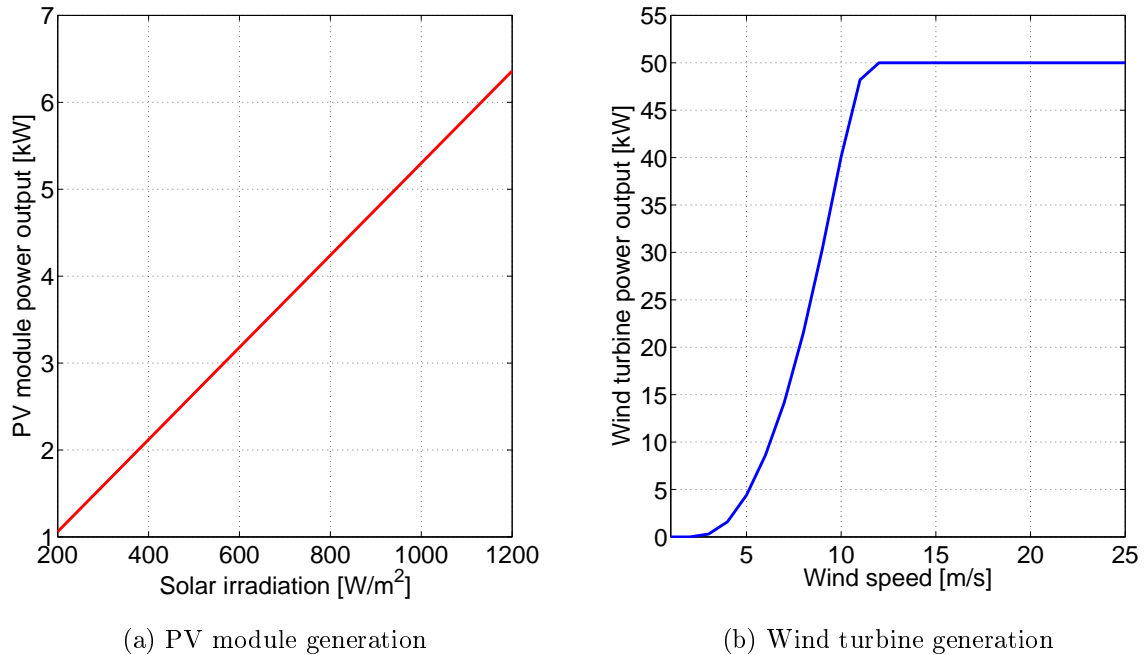


Figure 4.6: Solar irradiation vs. PV module output power (a) and Wind speed vs. WT output power (b)

The generation profiles for the renewable sources used in the load flow analysis in Sections 4.5, 4.6 and 4.7 are outlined in Figure 4.7, for both winter and summer scenario.

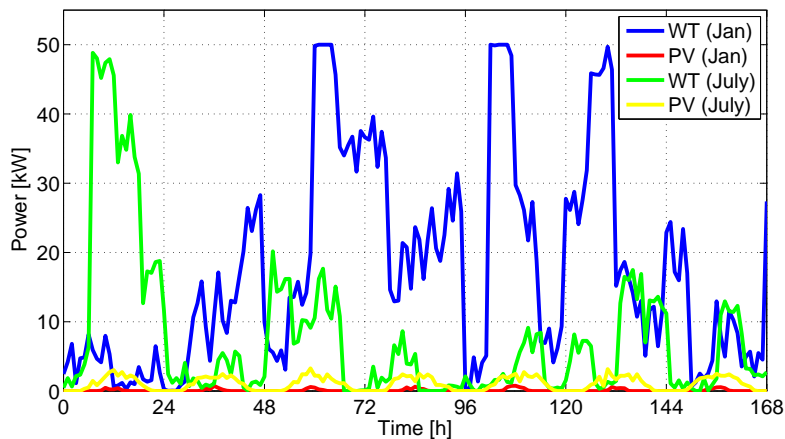


Figure 4.7: Renewable generation profiles for each WT and PV module for one week

4.4 Maximum renewable sources penetration level

The renewable penetration level in distribution grids presents a huge emphasis, due to their fluctuating generation profile. In order to determine the maximum penetration level for residential grids, the most important concern is the safe and steady operation of the grid with the interconnected renewables. In this paper, the renewable allowed limit is given by investigating three main criteria: maximum voltage fluctuations at the grid nodes, the cables current limits and the maximum transformer loading factor. According to [28] and [30], the PV and wind

power penetration level are explained as:

$$PV_{Penetration} = \frac{\text{Peak Power of Panels}}{\text{Peak Consumption of Grid}} \quad (4.10)$$

$$WT_{Penetration} = \frac{P_{wind}}{P_{sync} + P_{wind} + P_{import}} \quad (4.11)$$

where, P_{wind} represents the total wind power in the system, P_{sync} stands for the total power generation from synchronous generators (in this project it is equal to 0 - no generators are connected to the buses) and P_{import} is the peak power from the interconnection/external grid.

In this project, the maximum penetration level is determined by using the above equations and by imposing the following grid operation limitations, for both January and July cases:

- The voltage at each node needs to be maintained between $0.95 < V_i < 1.05$ (in p.u.),
- The transformer loading factor cannot overcome the maximum operational limit ($Tr_{lf} < 100$ [%])
- The cable loading factor is required to be lower than the admissible limit ($Cable_{lf} < 100$ [%])

In this report, the maximum penetration level has been determined by gradually increasing the renewable quota for both wind and solar, until reaching the grid limitations (by considering the restraints above). Three different scenarios are considered, as in [28], by placing the renewables in an evenly distribution, close to the distribution transformer and at the end of the feeder. The results regarding the maximum penetration level for each scenario are being highlighted in the following sections, with regards to the winter and summer cases.

4.5 Load flow analysis with evenly distributed renewable sources

The results for the power flow analysis on the grid with evenly distributed RES are being presented in this section. By using Equation 4.10 and Equation 4.11 the maximum number of integrated renewable sources has been found as:

- The limit number of PV modules is equal to 1183 (all the nodes have a number of 105 PV modules connected, which generate power at a P.F. of 1)
- The maximum number of WT is equal to 45 (nodes 632, 633, 634, 645, 646 and 650 have 4 *Polaris P-15* WT connected and each of the rest of the nodes include 3 such WT). All wind turbines generate power at a P.F. of 1.

The maximum penetration level is given by the following equations:

$$PV_{max} = \frac{N \cdot n \cdot PV_{out}}{P_{load\ max}} = \frac{13 \cdot 91 \cdot 5.3}{3643} = 172\% \quad (4.12)$$

where, N stands for the number of buses in the system, n represents the total number of PV modules connected at each bus, PV_{out} is the maximum output power of each PV module (5.3 [kVA], if taking into consideration the P.F. of 1) and $P_{load\ max}$ is the maximum load of the grid (of 3643 [kVA], during the peak-hour in January; this value is taken from the output data from DIGSILENT software).

$$WT_{max} = \frac{m \cdot WT_{out}}{m \cdot WT_{out} + P_{load\ max}} = \frac{45 \cdot 50}{45 \cdot 50 + 3643} = 39.4\% \quad (4.13)$$

where m represents the total number of wind turbines, WT_{out} is the maximum output power of a WT (50 [kVA], by considering the P.F. of 1).

4.5.1 Voltage profiles

In this subsection, the voltage fluctuations at the far away and the reference nodes are being highlighted, for the case of maximum renewable penetration for both wind and solar power. They are presented in Figure 4.8.

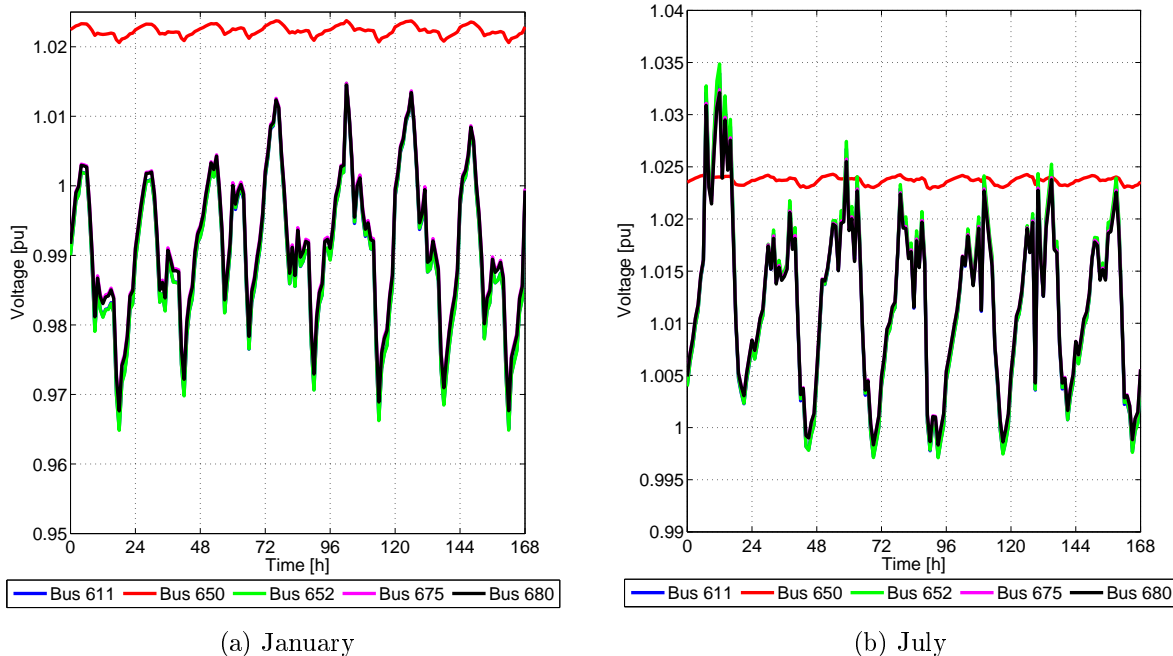


Figure 4.8: Voltage profiles during one normal week with even distributed RES

For the January case, highlighted in Figure 4.8a, it can be observed that the voltages for the far away buses are lower than the reference during the whole week. It can be observed that the voltages arise above 1.01 p.u. in several "off-peak hours", in the week. This is due to the fact that the wind turbines are modeled only as active power generators, and in these intervals there is an overproduction in active power. Compared with the case of no RES generation (Section 4.2), it can be seen that the fluctuations in the voltages are more present. This is due to the intermittence of the renewable generation, mostly from wind turbines. If the wind generation from Figure 4.7 is studied, it can be seen that the voltage spikes in the winter scenario, occur during the hours in which there is low demand for power and the WT are close to generate the ratted power. The lowest voltage in this case is almost 0.965 p.u. in the peak-load hour of the last day of the week (hour 162), during which the renewable generation is low. In the summer case, highlighted in Figure 4.8b, it can be observed that the voltage at the farthest buses is above 1 p.u. in most hours of the week. This is due to the less energy consumption and the fact that in the summer the renewable generation is higher, due to the installed PV systems (as it can be seen in Figure 4.7). The high voltage values in the first day, are due to the excess production in wind and solar power. It can be observed that each day during the midday hours, the voltage fluctuates between 1.01 - 1.02 p.u. (in some hours it exceeds the reference voltage - node 650). If the voltage profiles are compared with the infeed active power, in Figure 4.9b, it can be seen that in July, the peak voltages occur during the hours in which there is an overproduction in energy, hence the voltage values at each busbar is increasing. The voltage profiles presented in both cases, highlight that although the fluctuations are high due to the renewable sources integrated, they are still maintained within the allowable limits, especially during the summer case.

4.5.2 Transformer loading factor

For the case of even renewable distribution, the transformer loading is determined as in Equation 4.6. A close analysis of Figure 4.9a reveals that the transformer loading depends on the infeed active power from the system, shown in Figure 4.9b. It can be seen that during the winter scenario, the transformer is loaded mostly due to the active power consumption from the external power system (expected, as less renewable energy is available in this interval). The highest loading during January reaches approximately 72%, during the peak-load hours. Regarding the summer case, the loading of the transformer is given mainly from the reverse power flow (due to extra renewable generation) from the distribution grid, back in to the external power system. It can be seen that the maximum loading occurs during the first day (13:00) when the extra energy from renewables reaches its maximum. In this case, the transformer loading reaches the maximum value of 84%, as it can be seen in the figure.

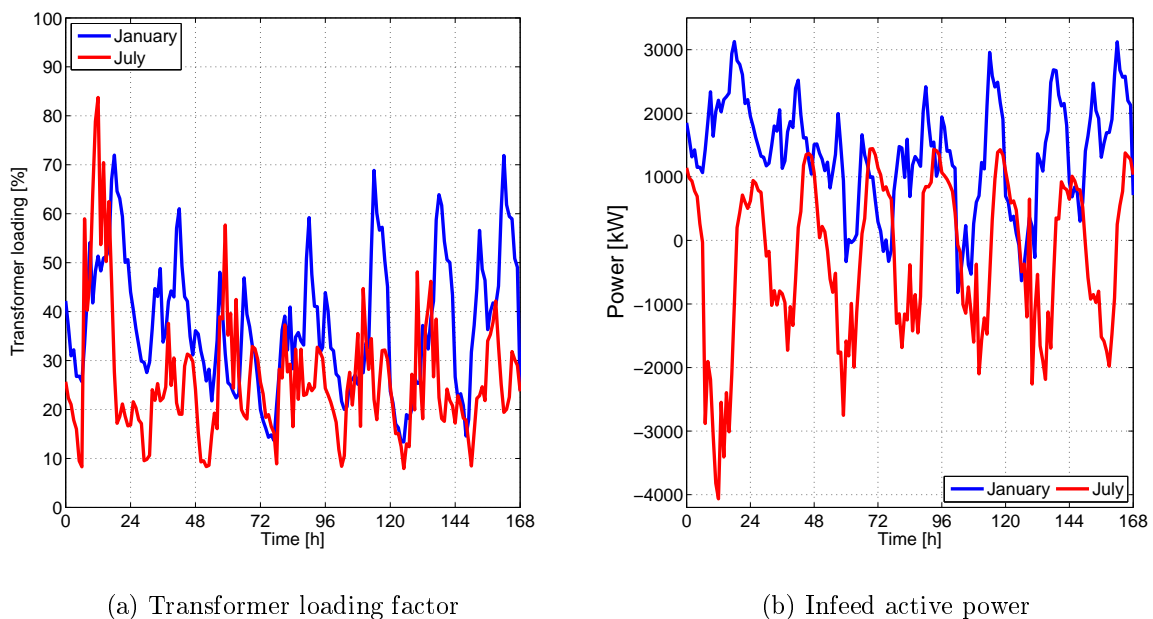


Figure 4.9: Transformer loading (a) and Infeed active power (b) for evenly distributed RES

4.5.3 Cable loading factors

In Figure 4.10, the loading factors for the most congested lines are presented. They are determined by using Equation 4.7. In the winter case, it can be seen that the line loadings follow almost the same profile as the transformer loading. The maximum loading occurs during the peak-load hours, reaching approximately 88% and 48% (for Line 5). Regarding the summer case, the cable loadings are higher, especially in the midday hours (mostly due to the increased renewable generation). During this case, the cable limit is reached, thus one of the three conditions (presented in Section 4.4) is violated, thus the maximum penetration level is reached for both wind and solar production. The maximum loading for the cable reaches 99.89%, in the same interval (hour 13) in which the reverse power flow is the highest. It can be observed also that the highest loading for the cable system of Line 5 is 56%, during the summer.

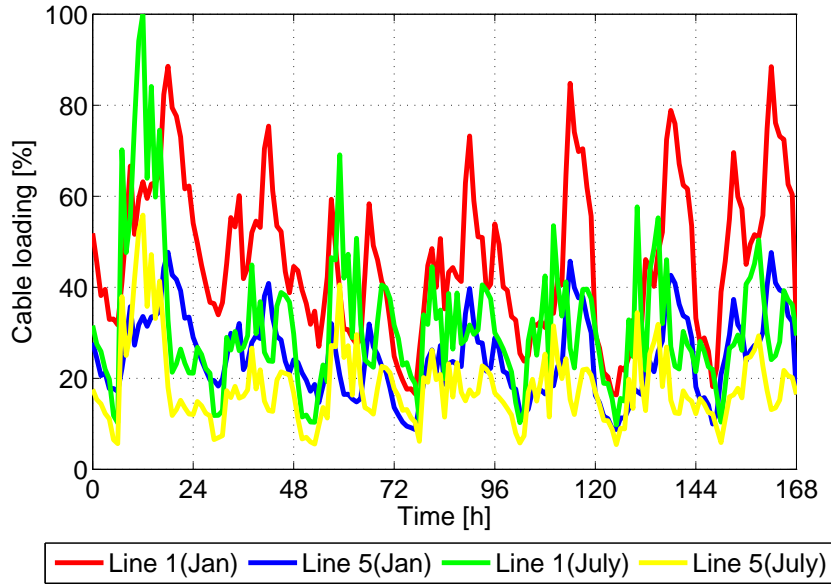


Figure 4.10: Cable loading for summer and winter case with even distributed RES

By performing simulations on the distribution grid, when the RES are connected in an even manner, the maximum penetration level of wind and solar power generation has been determined. This is done by reaching the maximum loading for the cable connecting the LV side of the distribution transformer to the rest of the grid. For both cases, it has been shown that the voltage deviations at the end buses, the loading of the transformer and the second most congested cable are within the admissible limits.

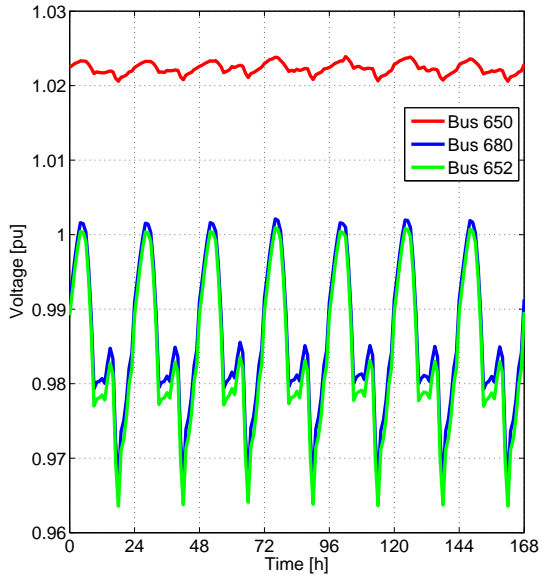
4.6 Power flow analysis with RES connected close to the transformer

In this section, it is considered that all renewable generation is connected close to the low voltage side of the distribution transformer. Hence, all RES are connected at bus 650. The penetration level is increased gradually, until the maximum level is reached (by considering the grid limits - maximum voltage deviations and loading for the transformer and lines). For this scenario, the penetration level limits is found as:

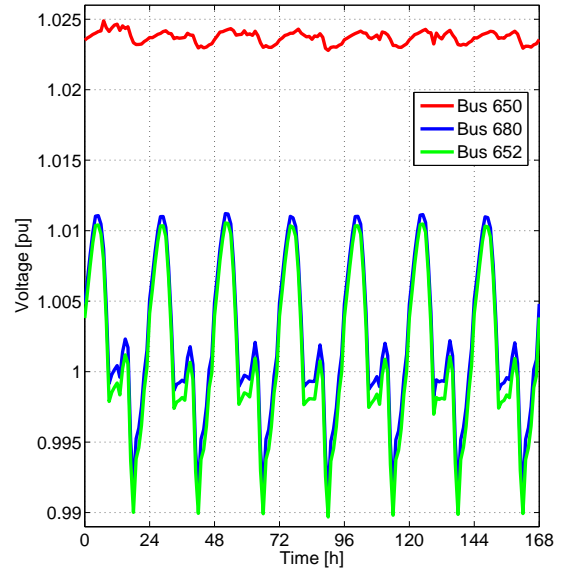
- $PV_{max} = 176\%$, determined by using Equation 4.12, where a number of 1210 of PV modules are connected at node 650 (each of the PV panels generate power at a P.F. of 1).
- $WT_{max} = 45.1\%$, determined by using Equation 4.13, where a total number of 60 wind turbines are coupled at node 650 (each of them generating power at a P.F. of 1).

4.6.1 Voltage profiles

Due to the fact that all renewable generation is located near the distribution transformer, only the voltage fluctuations at the farthest away bus will be investigated (node 680, located at 1.52 [km]). Also, by looking at Figure 4.2 and Figure 4.8, it can be observed that the lowest voltage occurs at node 652 for both summer and winter cases. Hence the voltage profile at this bus will be investigated. For the two cases, the voltage profiles is presented with regards to the reference, in Figure 4.11.



(a) January

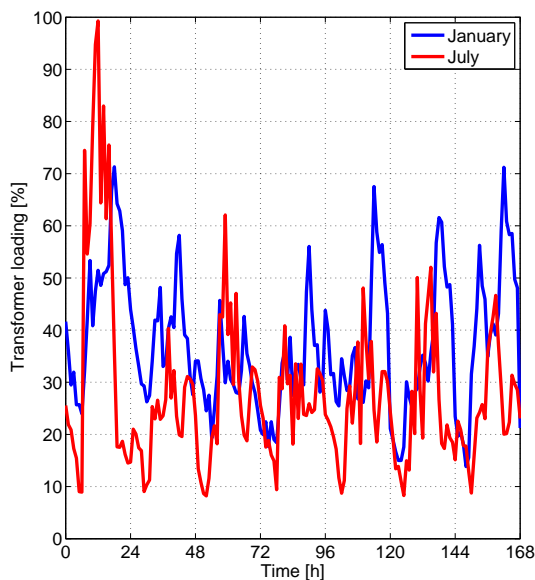


(b) July

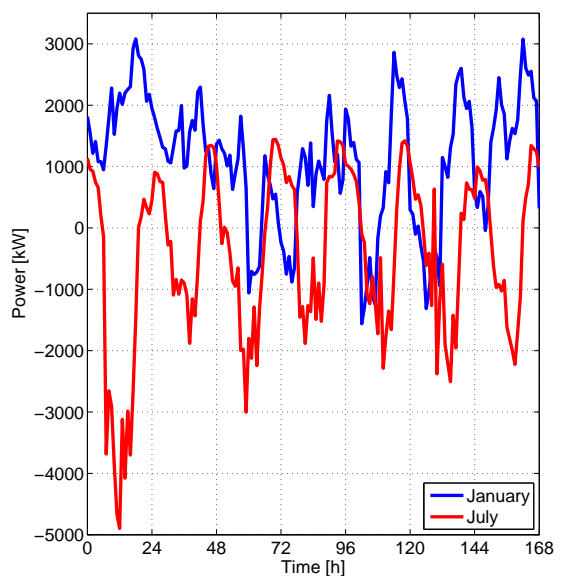
Figure 4.11: Voltage profiles for renewables connected close to the transformer

The voltage fluctuations at nodes 652 and 680, present the same profiles as the ones presented in Section 4.2.1, for both winter and summer scenarios. A thorough explanation for the fluctuations is given in the same section. For the case of RES connected close to the distribution transformer, the only difference is given by the source of power. In this case the renewables represent the generation facility covering the residential power demand. As shown previously, during summer days the RES generation is higher than in the winter, mostly due to the PV generation.

4.6.2 Transformer loading factor



(a) Transformer loading



(b) Infeed power

Figure 4.12: Transformer loading (a) and Infeed power (b) for RES close to transformer

For this scenario, the results regarding the transformer loading are shown in Figure 4.12a. Compared to the case of even distributed RES, it can be seen that the loading presents increased values, due to the raising level of renewable penetration. This is expected, as the power losses

in the grid are lower if the RES are connected close to the transformer. It can be seen that the transformer loading reaches the admissible limit, in the first day of the week at 13:00 (when the renewable generation is the maximum as shown in Figure 4.12b). This is due to the inverse power flow which from node 650 to the exterior power system. By reaching the transformer power flow limit, the maximum penetration has been determined for this scenario, by considering the restrictions imposed in Section 4.4.

4.6.3 Cable loading profiles

The cable loading for the most congested lines (Line 1 and Line 5) are highlighted in Figure 4.13. The loading factors for these two lines are comparable with the ones presented in Figure 4.4 (the case when no renewable sources are connected at neither node). This is due to the fact that, the only the difference concerns the source of energy (in this case, most of the demand is covered by renewables during the whole week), while the overall load for winter and summer is unchanged, leading to the same cable loadings. A more thorough explanation of these profiles is given in subsection 4.2.3.

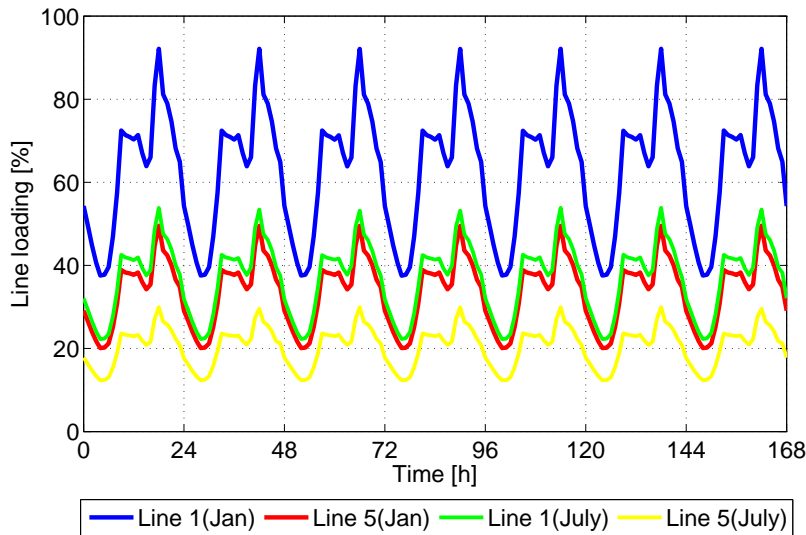


Figure 4.13: Cable loading for summer and winter case for RES close to transformer

In the case of RES connected close to the transformer, it has been show that the penetration level for both the PV and WT systems has increased with 4%, respectively 5.7%. Also, the voltage fluctuations at the far away nodes and the line loadings are the same as in Section 4.2. The placement of the renewables only affect the loading of the transformer, as the renewable penetration level increases, allowing more power to flow to the external grid than the case of even DG.

4.7 Load flow analysis for RES connected at the far away buses

This section aims to highlight the load flow results when the renewables are connected at the end of the feeder. By gradually increasing the number of PV modules and wind turbines, the maximum penetration level has been determined (in the same manner as in Sections 4.5 and 4.6) as being equal to:

- $PV_{max} = 139\%$, determined by using Equation 4.12, where each of the nodes 611, 652, 675 and 680 present a number of 230 PV modules (each of the PV panels generate power at a P.F. of 1).

- $WT_{max} = 36.6\%$, resulted by using Equation 4.13, where 10 wind turbines are coupled at each of the nodes 611, 652, 675 and 680 (all WT are generating power at a P.F. of 1).

4.7.1 Voltage profiles

The voltage fluctuations at the far away nodes are presented in Figure 4.14. For the winter case shown in Figure 4.14a, it can be seen that the voltages at the far away buses present the highest values compared to all scenarios investigated in this chapter. The reason is represented by the active power production by the renewable sources connected at the investigated nodes. It can be observed that the voltages in this case are closing to the value of the reference voltage, at bus 650. For this scenario, the high voltage values are attributed to the high number of renewables connected at the nodes. Regarding the summer case, it can be seen that the voltages present also the highest values (in p.u.) compared to all scenarios investigate. It can be seen that the highest value occurs at bus 652 (1.041 p.u.), during the midday hours (13:00) of the first day. This interval overlaps the time period in which the renewable production is highest (exceeding the consumption, hence the voltage is highest). The high voltage values shown in Figure 4.15b are expected, if considering the high renewable penetration level at these nodes during the July case.

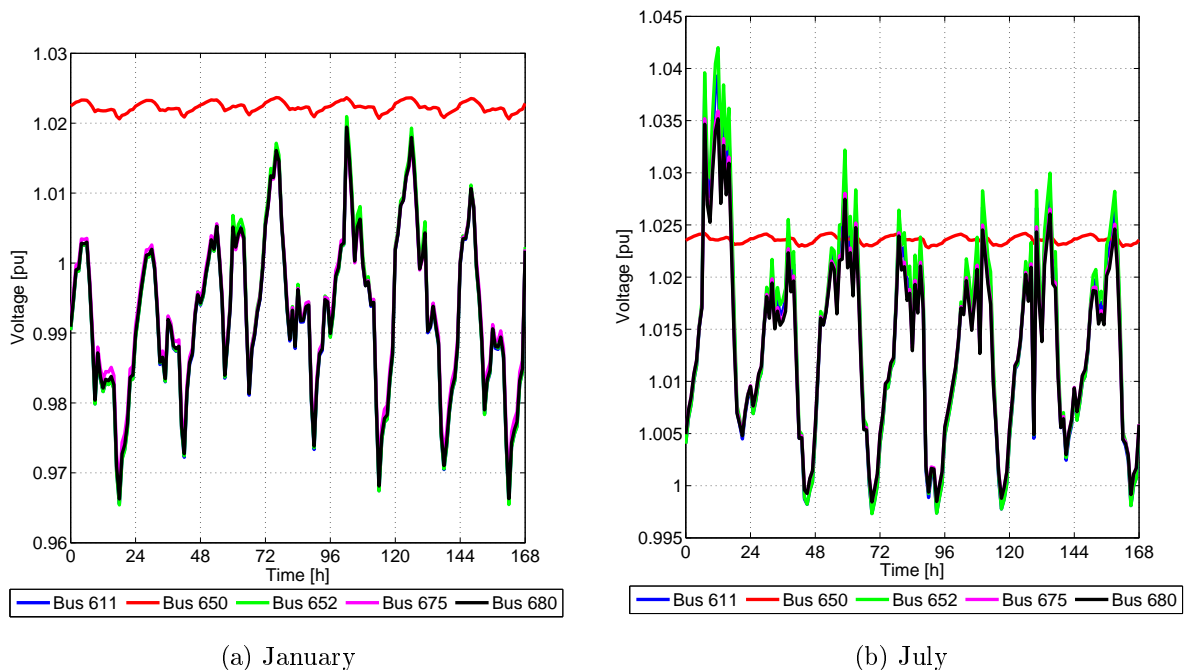
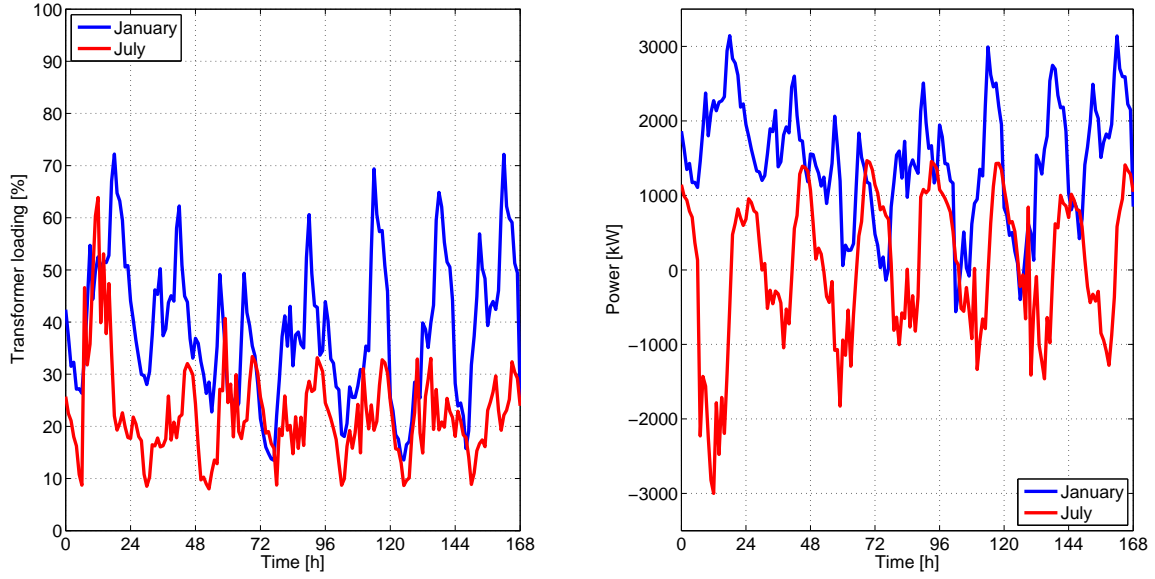


Figure 4.14: Voltage profiles for renewables connected close to the transformer

Although the voltages fluctuations present huge differences for both winter and summer cases, they are still maintained between the maximum admissible limits (0.95 - 1.05 p.u.), as it can be observed in the Figure 4.14.

4.7.2 Transformer loading factor

The transformer loading profile, highlighted in Figure 4.15a reveals that, the maximum loading occurs in the winter case, when it reaches almost 72%. In this scenario, most of the power flowing through the transformer comes from the external grid, as it can be observed in Figure 4.15b. Regarding the summer case, the maximum loading is among the value of approx 64%. For this case, this loading factor is due to the active power which is flowing up level, to the external grid, the renewable sources installed at the far away nodes can fully cover the load and a case of over generation occurs.



(a) Transformer loading

(b) Infeed power

Figure 4.15: Transformer and cable loading for RES at the end of the feeder

4.7.3 Cable loading factor

Regarding the cable loadings, it can be seen from Figure 4.15a, that when the RES are placed at the end of the feeder, Line 5 is the most congested (in the summer case). The reason for this is represented by the placement of the RES at the end of the feeder, as in July they exceed the demand, hence the power is flowing back to the external grid. The line reaches the admissible limit in the first day of the week during noon (13:00), when the renewable generation is maximum. Line 5 connects nodes 671 and 632 (as in Figure 3.1), and through node 671, the farthest nodes are interconnected. In the winter case, it can be observed that Line 1 (connecting buses 632 and 650) is the most loaded, during the peak-load hours. This is expected, as in this scenario, the load demand is higher than in the summer and also, the renewable generation is very low (as shown in Figure 4.7).

4.8 Chapter summary

The purpose of this section is to give an overview on the results obtained (with regards to the maximum renewable penetration level, voltage fluctuations, transformer and cable loadings) for the scenarios investigated in this chapter, by considering both the January and July case. Another scope of this chapter is to determine which is the best configuration of the RES, in order to integrate a high quota of electric vehicles. These results of each section are presented in Table 4.2. In the table, the results are presented for each of the three cases tested, with regards to the maximum penetration level for both wind and solar power generation.

Table 4.2: Overview on maximum RES penetration level and grid parameters

Case	PV_{max} [%]	WT_{max} [%]	V_{max} [pu]	V_{min} [pu]	Tr_{lf} [%]	$Cable_{lf}$ [%]
I	-	-	1.011	0.964	75.1	92.2
II	172	39.4	1.035	0.965	84.2	99.89
III	176	45.1	1.011	0.963	99.3	92.2
IV	139.8	36.6	1.042	0.965	72.2	99.7

where, I stands for no RES integrated (Section 4.2), II represents the case of evenly distributed renewable generation (Section 4.5), III is the scenario in which the RES are placed close to the transformer (Section 4.6) and IV covers the case in which the renewables are located at the end of the feeder (Section 4.7).

The numbers presented in the above table show that different placement of renewable sources affect the grid parameters in a distinctive manner. The most high renewable penetration is given by placing them close to the transformer, but this case presents highest transformer loading. By analyzing the case of even RES distribution, it can be seen that the transformer loading does not exceed 84.2%, but still the maximum loading for the cables reaches almost 100%. This is mostly due to the reverse power flow (due to high RES generation). If this scenario is applied and the EVs are integrated at each busbar (by varying the penetration level), the electric load will be located close to the power generation, hence the line loadings are expected to drop. As a result the power losses in the system are expected to decrease as well, if the renewable sources are placed in this configuration. In the following chapter, an analysis on the same distribution grid will be performed (by considering an even distribution of the RES), by ranging the penetration level of EVs in order to estimate the maximum number of renewable sources and EV per household.

Power flow analysis with regards to EV integration

5

This chapter presents the results of the load flow calculus, regarding different charging strategies when the maximum penetration level for the EVs is reached. The power flow is performed by using a 'trial and error' strategy, until the grid operation limit is reached. The first subsection of the chapter analyses the driving patterns and the average energy consumption of an electric vehicle per day. For the simulations in this chapter, the renewables will be placed in an evenly distribution, as in Section 4.5.

5.1 Outline of electric vehicle modeling

In this section, the energy consumption for each EV is highlighted, with regards to the available information. The analysis is performed by taking into consideration the parameters which influence the electric vehicle modeling (average driving distance, battery capacity, energy consumption/km and the probability of the EVs to be stationed home). According to [31], the daily average distance covered by an EV in Denmark is around 43 km. In this project it will be considered that each of the electric vehicles drives a total of 45 km/day. In [6] and [20], the average battery size of an EV is between the range of 30 to 50 kWh. For the simulation scenarios implemented in this chapter, the battery capacity for all EVs will be chosen as 40 kWh. The energy consumption per km driven will be considered as 200 Wh/km, as given in [6], [20] and [31]. The efficiency of the EV charging is considered to be 0.9, as highlighted in [32].

The daily energy consumption required to charge each EV can be determined by using:

$$E_{daily} = D \cdot E_{km} = 45 \cdot 0.2 = 9 \quad [kWh] \quad (5.1)$$

where, D represents the average distance traveled (considered as 45 km/day) and E_{km} stands for the energy consumption per km (taken as 0.2 kWh/km).

By knowing the daily required energy that needs to be stored in the battery, the daily energy consumed from the grid, by each EV is calculated as:

$$E_{grid} = \frac{E_{daily} \cdot k}{C_{eff}} = \frac{9 \cdot 1.05}{0.9} = 10.5 \quad [kWh] \quad (5.2)$$

where, k is a correction factor imposed due to the aggregate modeling of EV (this factor is taken into consideration as in the simulations the vehicles are modeled as loads connected to the 4.16 kV level; this 'aggregate correction factor' is imposed as in Section 4.2 in order to consider the voltage step down from 4.16 to 0.48 kV, distribution power losses) and C_{eff} represents the efficiency of the energy charging, considered as 0.9 in this project.

Because a one hour time step is imposed in the load flow calculus, the EV load modeling is made by using the following equation:

$$P_{grid}(h) = \frac{E_{grid}}{t} \quad (5.3)$$

where $P_{grid}(h)$ represents the power consumption from the grid to charge an EV in one hour (in [kW]), E_{grid} stands for the energy consumption from the grid during the same hour, in which the EV is plugged-in (in [kWh]), and t is the time step of the simulations (in this project, considered as 1 h). The maximum EV load is considered as 6.6 kW in this project (as in [33]). The power consumption from the grid for each EV can be determined as it follows:

- In the first hour the average load is 6.6 kW
- In the second hour the average load is represented by 3.9 kW

If these values are integrated over a one hour interval, the total energy obtained is equal to the necessary 10.5 kWh for each EV during one day.

5.1.1 Charging availability of electric vehicles

This section focuses on presenting the time intervals in which EVs are at home and available for charging. This is necessary as the integration level of electric vehicles depends on the time at which they are free for charging by the renewable sources. The EVs probability of being home during one average weekday is highlighted in Figure 5.1.

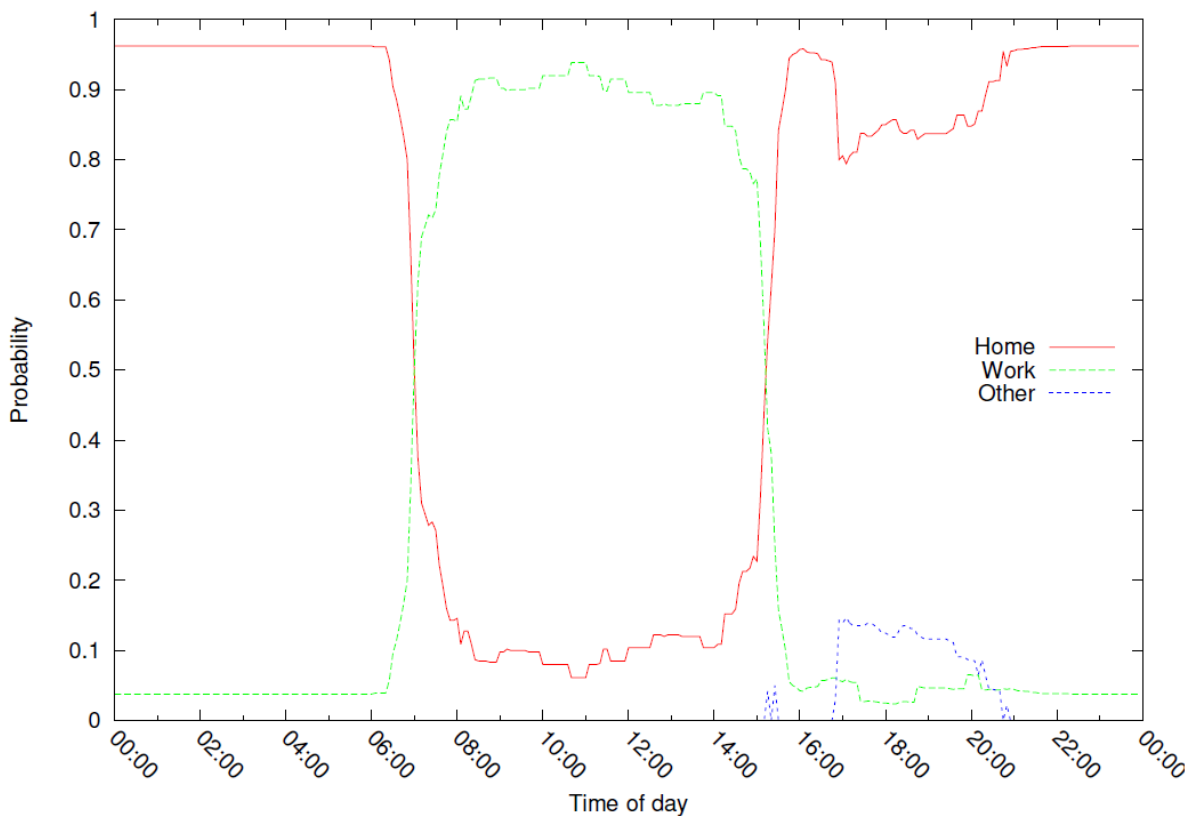


Figure 5.1: Probability plot for EV regarding the availability for charge during an average weekday [13]

By looking at Figure 5.1, it can be seen that the highest probability for the EVs to be at home occurs during 21:00-6:00. During the day time hours, it can be observed that at around 7 a.m., most of the EV shift from a *home* state to a *work* state. In the figure, the 'other' state indicates that the vehicles are engaged into other trips (such as trips to shops for daily supplies, etc.). In the late afternoon, the probability of the vehicles to be home is higher as most of the EVs return home after the workday. The probability curve highlighted presents a huge emphasis on the scenarios investigated in the next sections.

The assumption imposed for all charging strategies investigated is that at the beginning of the week, all EVs present a state of charge (SOC) of 95%. The simulations are performed by taking into consideration that every EV consumes each day 9 kWh for traveling. By considering the charging efficiency and the 'aggregate correction factor', each electric vehicle consumes from the grid a total of 10.5 kWh each day. The aim is that at the end of each charging cycle, every vehicle should reach a SOC of 95%. With this presumption, the different charging strategies are investigated in the following sections.

5.2 Dumb charge strategy for the EVs between 17:00-19:00

In this section, the results of the power flow analysis on the grid are presented, when the all vehicles are charging between 5 pm and 7 pm. The RES are even distributed, having the same penetration level as in Section 4.5, meaning that a total of 1183 PV modules and 45 wind turbines are producing power. By taking into consideration the availability of EVs to charge (Figure 5.1), the EV integration level is estimated as:

$$EV_{pen} = \frac{N_{EV}}{M_{households}} \quad (5.4)$$

where, N_{EV} represents the total number of EVs available for charging (this number is dependent on the probability of EVs to be at home at different intervals of the day) and $M_{households}$ stands for the number of residential homes in the grid (according to Table 4.1, the grid presents 647 homes connected at 13 nodes).

In this project, the electric vehicle penetration limit is determined by investigating the three grid constraints shown in Section 4.4. The simulations are performed by progressively increasing the EV number until one of the conditions (voltage fluctuation limit, power transformer and cable loading) is violated.

In the following subsections, the results of the load flow calculus are highlighted, when the maximum EV penetration is reached. All EVs are charged by using the 'dumb' strategy between 5-7 pm. This represents the base scenario, when EVs start to consume power immediately after they arrive home.

5.2.1 Winter case

In this subsection, the results of the load flow calculus are highlighted with regards to the winter scenario. The results are presented with regards to the voltage fluctuations, transformer and cable loading. For the even distribution of RES (highlighted in Section 4.5), in Figure 4.8a, it can be observed that the lowest voltage occurs at busbar 652. This will be considered as the the weakest node in the distribution grid, hence the simulation results will be presented with regards to it.

The results presented in Figure 5.2, reveal that when the EVs start to charge, the voltage at the weakest bar starts to decrease down to 0.958 p.u. during the first charging cycle of the week. This is expected as the EVs represent active power loads ranging from 6.6 to 3.9 kW. Regarding the infeed power from the system, during the charging hours it can be seen that the power exchange increases with approximately 0.6 MW, during 5 to 6 pm and 0.375 MW during 6 to 7 pm, each day of the week. This represents the average power used for charging the EV fleet during the time interval.

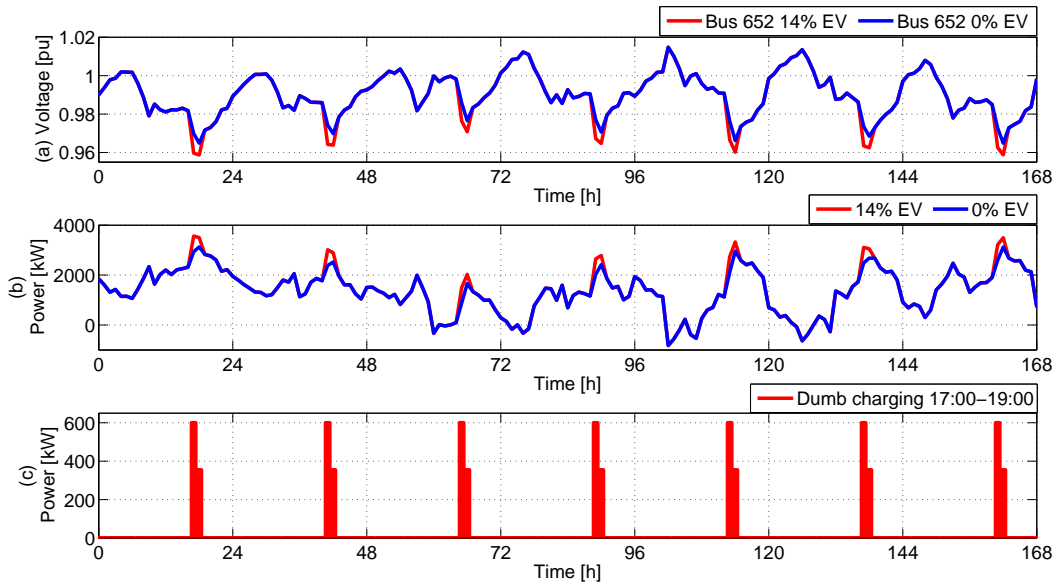


Figure 5.2: Results for the power flow analysis during the January case, with regards to the voltage fluctuations at the weakest busbar (a), the infeed power from the system (b) and the power consumed during the dumb charge (c)

The results of the power flow calculus, with regards to distribution transformer and the most congested cable loading are highlighted in Figure 5.3.

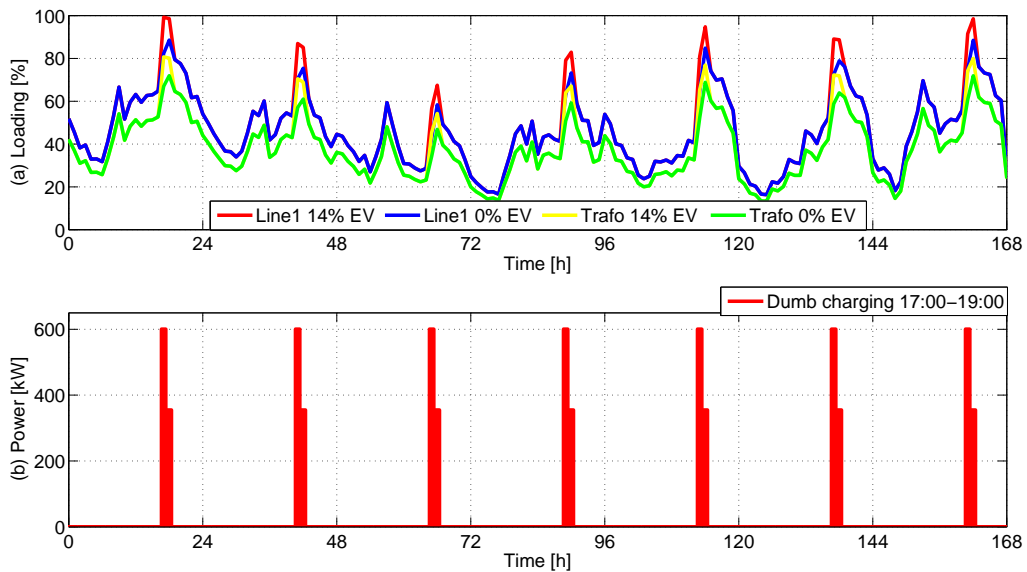


Figure 5.3: Results for the power flow analysis during the January case, with regards to the transformer and cable loadings (a) and the power consumed during the dumb charge (b)

By looking at Figure 5.3, it can be seen that once the EVs start to charge, both loading factors are rising. This comes as a result of the load increase by the integration of electric vehicles. During the week interval, the transformer loading does not exceed the limit, although the EV charging takes place during the peak-load hours. The cable limit is reached during the first day of the week, in the high-load hours. By reaching the operational limit of the cable system, the maximum EV penetration level is determined for the January case. This represents an integration factor of 14% for the electric vehicles. This means that at each busbar, 14% out of the households are able to plug-in an electric vehicle for charging.

5.2.2 Summer case

Regarding the summer scenario, the power flow investigation is performed by looking at the same grid parameters as in Section 5.2.1. The RES present the same even distribution and penetration level as in Section 4.5. In Figure 5.4, it can be observed that during the charging hours of the EVs the voltage at the most weakest bus is decreasing, due to the high load from the electric vehicles. The lowest voltage value reaches 0.978 pu in the fourth day of the week. If looking at the infeed power, it can be seen that in the midday hours, when no EVs are plugged-in, there is an excess power generation from the renewables. Depending on the RES generation, once the vehicles start to charge the renewables are able to cover part of the load demand (from EVs and households); for all charging intervals, the power comes from both the renewable sources and from the external grid.

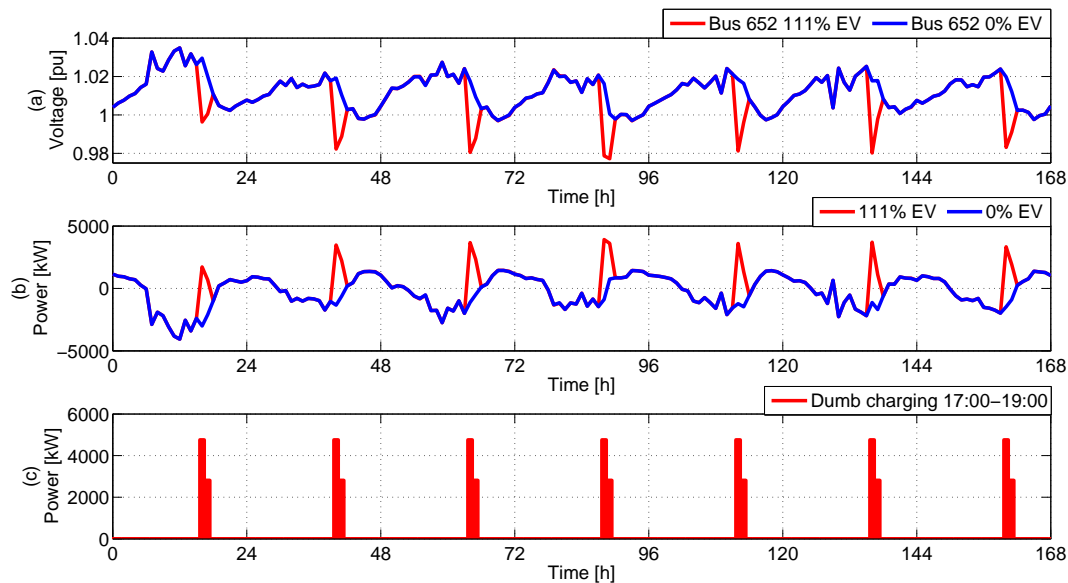


Figure 5.4: Results for the power flow analysis during the July case, with regards to the voltage fluctuations at the weakest busbar (a), the infeed power from the system (b) and the power consumed during the dumb charge (c)

The transformer and cable loading factors, presented in Figure 5.5, show that both of these factors are increasing once the EVs start to charge. The transformer does not reach the limit during the whole week. The maximum transformer loading occurs during the midday hours of the first day (when the renewable generation is maximum) and in the first hour of the charging cycle in the fourth day. The maximum loading is represented by 82%. Regarding the cable loading, it can be seen that in the first day the cable reaches its limit due to the excess renewable production. In the fourth day of the week, due to the integration of the electric vehicles, the cable loading reaches 99.89%. This represents the condition for which the maximum EV penetration level is determined for the summer scenario.

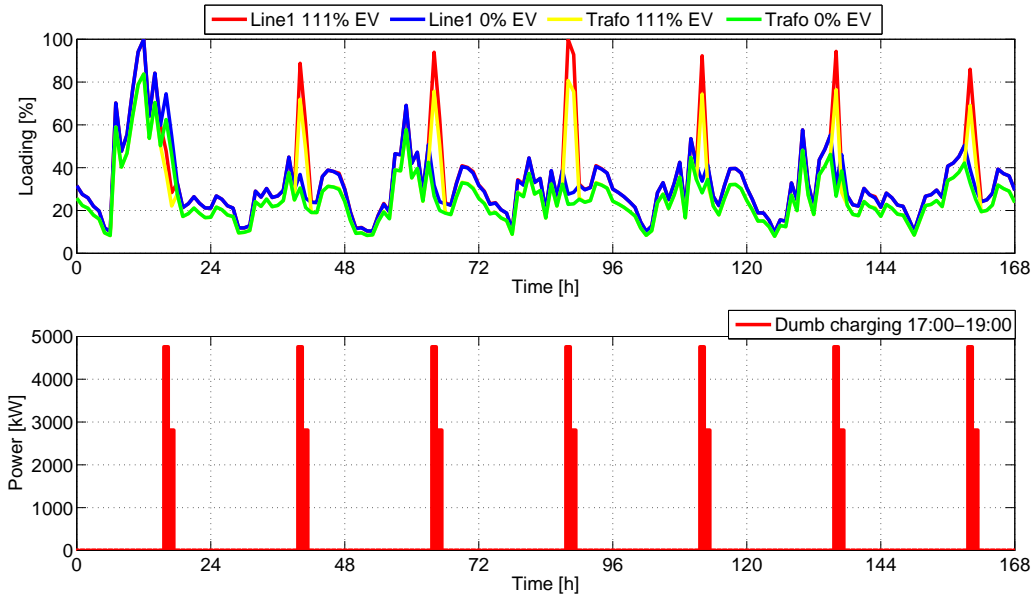


Figure 5.5: Results for the power flow analysis during the July case, with regards to the transformer and cable loadings (above) and the power consumed during the dumb charge (bellow)

5.2.3 Section summary

In this section, the results for the 'dumb charge' strategy for EVs (between 5-7 p.m.) has been presented. Based from the results obtained it can be seen that the worst EV penetration level occurs in the winter case, when it reaches 14%. This represents the base case for the EV charging strategies. The following sections will focus on presenting the results of the simulations for different charging strategies of the electric vehicles.

5.3 EV night charge between 00:00-2:00

In the following section, the results of the load flow simulations performed when the electric vehicles charge at night during 0-2 am are presented. When plugged-in, the load for each vehicle represents 6.6 kW in the first hour of and 3.9 kW in the second hour.

5.3.1 Winter scenario

In this scenario the distribution network is analyzed when the EVs charge during the night. In Figure 5.6 an overview of the grid operation is given, with regards to the voltage fluctuations infeed power and load demand of the electric vehicles.

In plot a) it can be observed that the voltage profile at the weakest bus remains unchanged during the hours in which there is no load from the EVs. It can be observed that during the time interval in which they charge the voltage is decreasing down to 0.962 p.u. This low value is due to the lack of renewable generation in this interval, hence all load is covered by the external grid. Also by looking at plot b) it can be seen that the infeed power increases during the charging hours, reaching a maximum of 3.7 MW during hour 96 of the week. Plot c) highlights that the maximum demand for charging reaches 1.7 MW in the first hour of charging, and 1.05 MW in the second hour for each day.

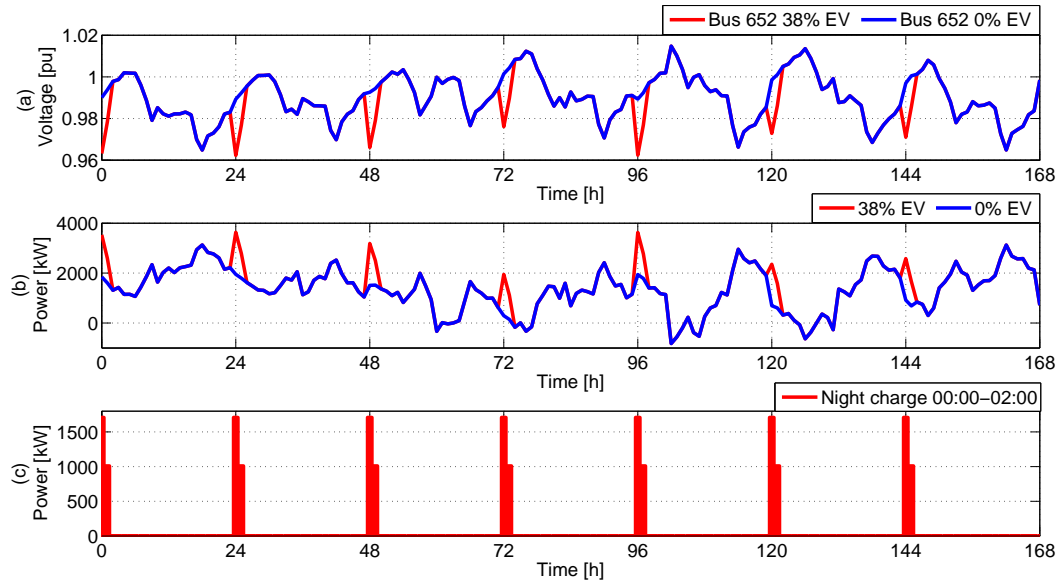


Figure 5.6: Results for the power flow analysis during the January case, with regards to the voltage fluctuations at the weakest busbar (a), the infeed power from the system (b) and the power consumed during the night charge (c)

In Figure 5.7, plot a) presents the fluctuation of the loading factors for the transformer and the most congested cable system (Line 1). It can be seen that during the period when the vehicles are plugged-in for charging, the cable loading is increasing. The maximum value reaches 99.5% in the second day and 99.65% in the fifth day of the week. By reaching the current limits of cable in these time intervals, the maximum EV integration level is determined for this particular scenario. As shown in the figure, the allowable number of electric vehicles that are able to plug-in by using this charging strategy is 38%, due to the limitations of the cable system.

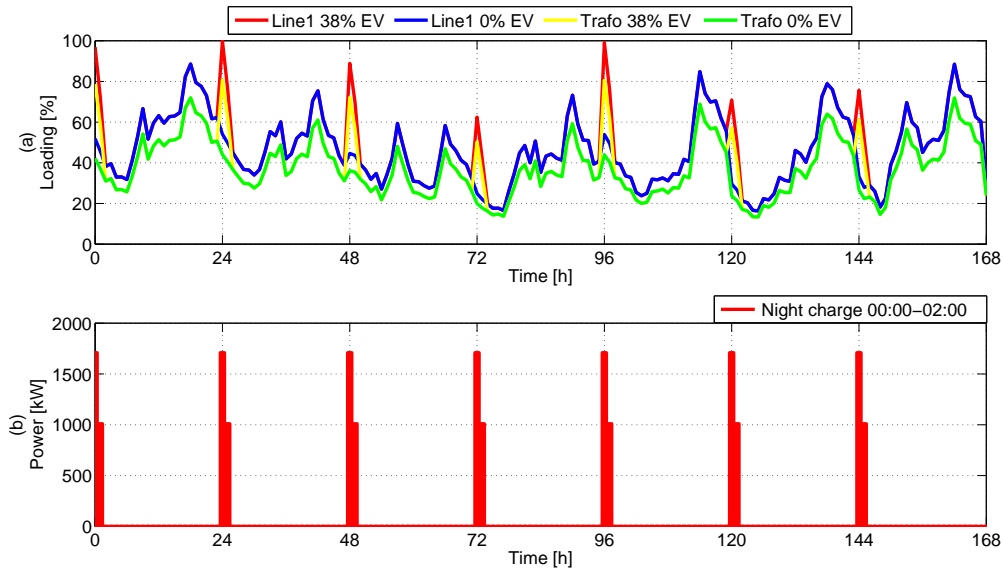


Figure 5.7: Results for the power flow analysis during the January case, with regards to the transformer and cable loadings (a) and the power consumed among night charge (b)

5.3.2 Summer scenario

The summer case analysis with regards to the voltage profile at the weakest node is presented in Figure 5.8, plot a). It can be seen that the voltage is decreasing during the hours in which

the vehicles are plugged-in, down to approximately 0.98 p.u. in the first hour of the charging. This is typical, as the EVs represent a high active load. Plot b) highlights the power exchange with the external grid, when EVs are connected and not. During the charging hours, the power demand reaches a maximum of 4 MW. This high power is due to the low generation of the renewable sources in the charging hours. Plot c) reveals that the power consumed for charging the EV fleet represents 2.74 MW in the first hour and 1.62 MW in the second hour of charging.

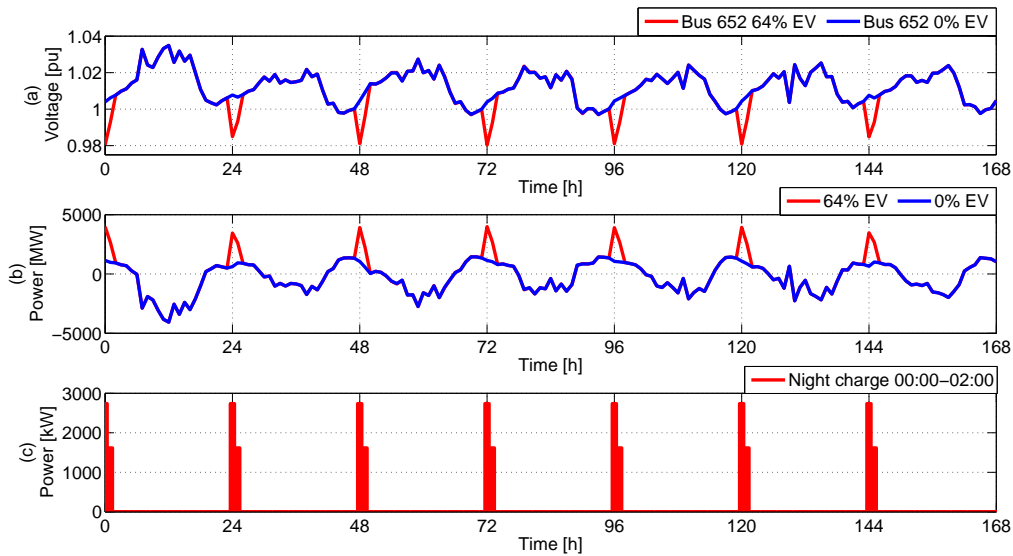


Figure 5.8: Results for the power flow analysis during the July case - voltage fluctuations at the weakest bar (a), the infeed power from the system (b) and the power consumed for the night charge (c)

The loading factors for the transformer and the most congested cable system in the grid are highlighted in Figure 5.9. It can be observed that for the whole week, the transformer is not overloaded as the maximum loading represents 84%. The cable system in this case is the one that gives the highest number of EV that can be charged, as it can be seen that if 64% of the houses plug their EVs for recharging, the cable limit is reached during hours 72,96 and 120.

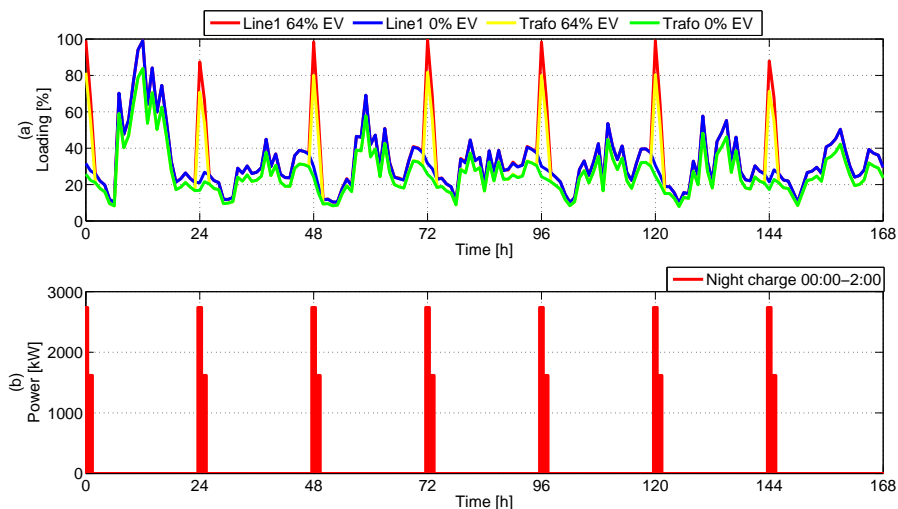


Figure 5.9: Results for the power flow analysis for the July case, with in regard with the transformer and cable loadings (a) and the power consumed during night charge (b)

5.3.3 Section summary

The night charge of the EVs between 00:00 and 02:00 indicate that for the winter case, 38% of the households are able to charge their vehicles, without violating any condition of the normal operation of the grid. Regarding the summer scenario, the number of EVs can be increased up to 64%, until the cable limit is reached. For this night charge strategy, the maximum EV integration is considered to be during the January case, when it reaches 38%.

5.4 EV night charge during 02:00-04:00

In the following, the power flow analysis on the grid is being highlighted, when the EVs charge from 2 to 4 am, by using the same charging profile for each vehicle, as in Sections 5.2 and 5.3.

5.4.1 Winter scenario

The power flow analysis is being presented in this subsection, when the EVs charge in a regular week in January. From Figure 5.10, plot a) it can be seen that when the EV fleet are being plugged-in, the voltage at the far away node is decreasing down to 0.965 p.u. Simultaneously, the power demand from the grid (represented in plot (b)) starts to raise among the charging time, reaching a maximum of 3.71 MW in the second night charging cycle. It can be seen that the infeed power fluctuates according to the renewable generation and the household consumption. By charging the vehicles in the off-peak hours, it can be observed that among each charging cycle, shown in plot (c), (for the whole number of vehicles), the load overcomes the demand in the peak-load hours.

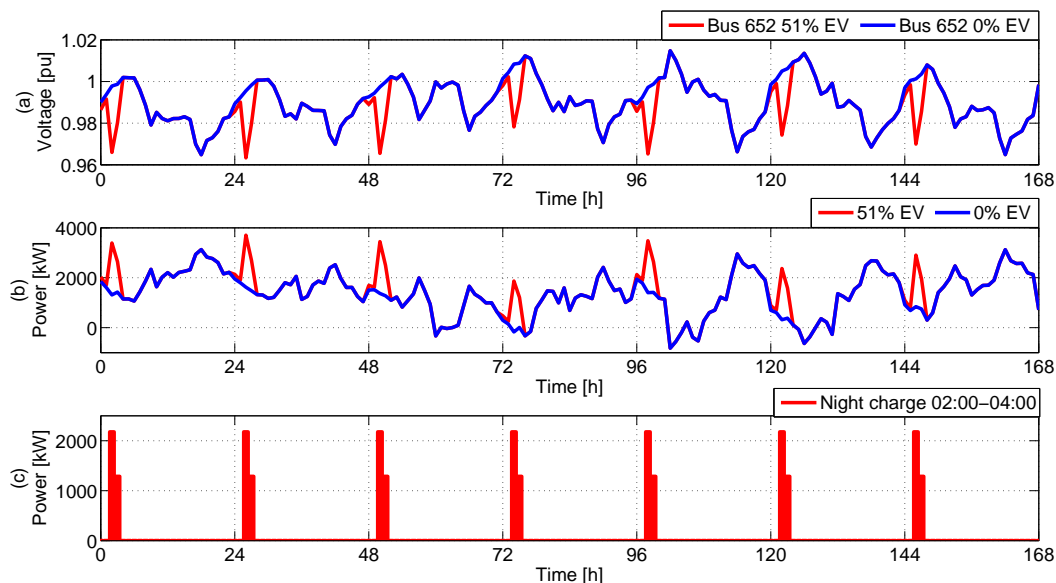


Figure 5.10: Results for the load flow analysis among the January case, with regards to the voltage fluctuations at the weakest busbar (a), the infeed power from the external grid (b) and the power consumed during the night charge (c)

The loading factors, represented in Figure 5.11, show that during the non-charge hours, both the transformer and cable loading remain unchanged. It can be seen that while the vehicles start to charge, the loading are high, due to the integration of EV load. The transformer reaches the highest loading in the second day of the week (82%). It can be seen that the power flow via the transformer is varying with the load consumption by the EVs. Regarding the most congested

cable system in the grid, the loading reaches the limit (99.97%), in the first charging hour of the second day of the week. By reaching the cable current limit, the maximum EV penetration level is determined for this case. In this scenario, 51% of the houses can plug-in an electric vehicle and charge it between 02:00 and 04:00.

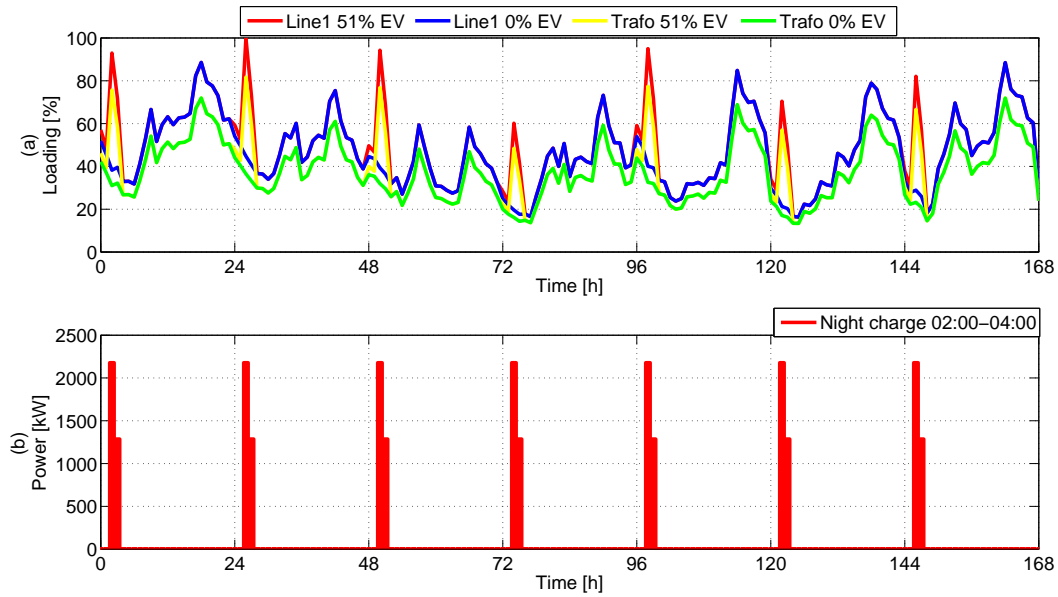


Figure 5.11: Results for the load flow analysis during the January case, with regards to the transformer and cable loadings (a) and the power consumed among night charge (b)

5.4.2 Summer case

In the following subsection, the results of the power flow analysis, when the EVs are plugged-in between 2-4 am are being highlighted for the summer case.

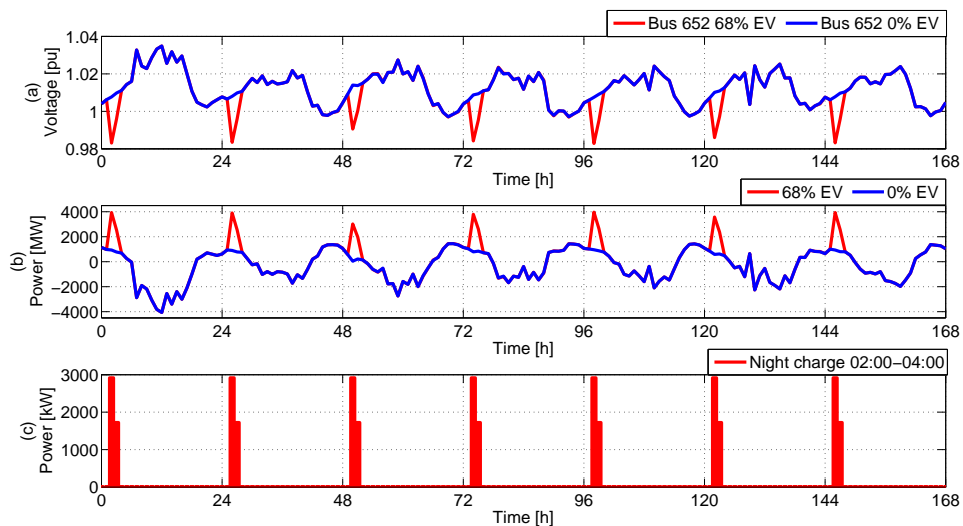


Figure 5.12: Results for the load flow analysis during the July case, with regards to the voltage fluctuations at the weakest busbar (a), the infeed power from the system (b) and the power consumed during the night charge (c)

The results of with regards to the summer scenario are shown in the following subsection. From Figure 5.12 - plot a), it can be observed that the voltage fluctuation at the weakest bar is

decreasing down to 0.982 p.u., while the vehicles are plugged-in for charging. Also by looking at plot b), the power demand from the system can be observed. Among the charging hours, it reaches a maximum of 4 MW. By looking at plot c) it can be seen that the EVs demand approximately 3 and 1.8 MW in the first and second hour of charging.

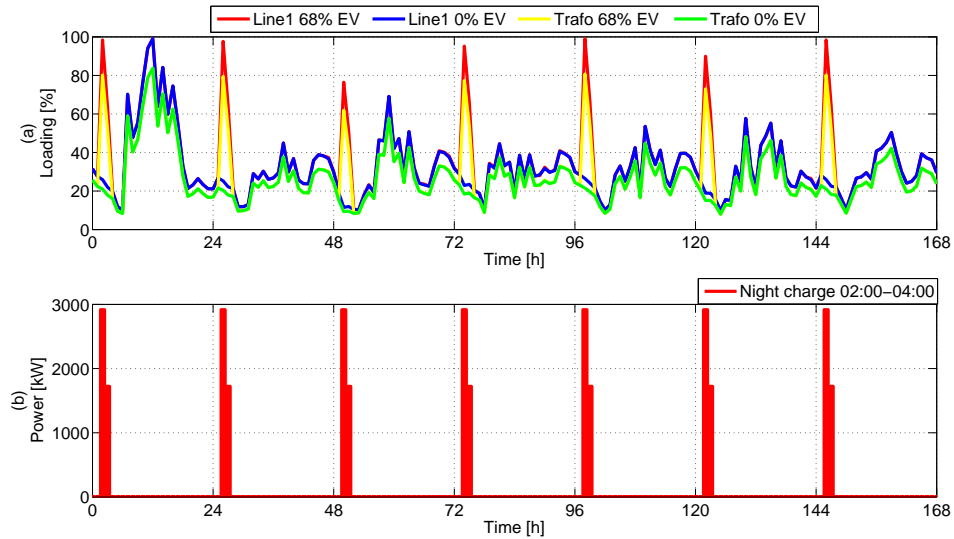


Figure 5.13: Results for the load flow analysis during the July case, with regards to the transformer and cable loadings (a) and the power consumed among night charge (b)

The loadings highlighted in Figure 5.13 reveal that during the summer case, the maximum transformer loading level reaches 84%, but this value is reached in hour 13, due to the high generation of RES. From plot a) it can be seen that, during the charging hours of the EVs, the transformer is loaded from 62 to 81%. This is dependent on the renewable generation. It can be observed that the cable system of Line 1, reaches the admissible limit in days one, five and seven (99.9%). By achieving the cable operational limit, the maximum level of electric vehicles that can be integrated into the grid is determined. The EV penetration quota stands for 68% for this scenario, meaning that 442 out of the 647 households are able to plug-in an electric vehicle.s

5.4.3 Section summary

For the case when the electric vehicles charge between 02:00 and 04:00 the allowable limit of integration is given by the cable admissible limit, for both scenarios. From the two cases, the maximum penetration level for EVs is given by the winter scenario, when it reaches 51%. Also in both cases, the transformer loading and voltage fluctuations are within the grid limits.

5.5 EV morning charge between 04:00-06:00

The following section aims to highlight the results on the grid parameters, when the electric vehicles charging occurs in the morning hours (4-6 am). Also, each of the EV is charged by consuming the same amount of active power as is Sections 5.2, 5.3 and 5.4.

5.5.1 Winter case

By applying the morning charge strategy in January, it can be seen that the voltage at the weakest bus is reduced down to 0.963 p.u., as shown in plot a), in Figure 5.14. Compared to the other charging strategies, the only difference represents the hour in which the voltage reaches the minimum. The power exchange with the external grid - plot b), shows that during the charging

hours, the maximum load demand raises up to 3.7 MW, out of which 2.3 MW represents the maximum EV load.

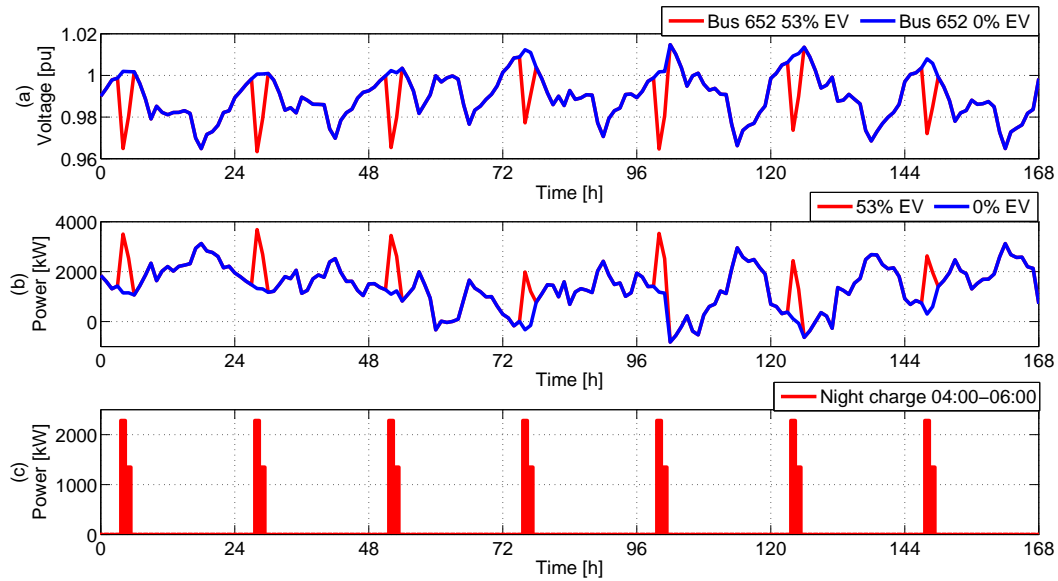


Figure 5.14: Results for the load flow analysis during the January case, with regards to the voltage fluctuations at the weakest busbar (a), the infeed power from the system (b) and the power consumed during the night charge (c)

Regarding the transformer loading, presented in Figure 5.15, it can be observed that during the morning hours the factor is high due to the charging of EVs. During the week, the transformer loading does not exceed 81%. The loading factors are comparable during the peak-load hours of the day, and the hours in which the vehicles are plugged-in. The most congested cable system (Line 1), reaches the limit in the second day of the week. This condition grants the maximum EV penetration level for this scenario. The simulation reveals that in the winter, in average 53% of the households can plug their electric vehicles for charging in the morning, without violating the grid operation conditions.

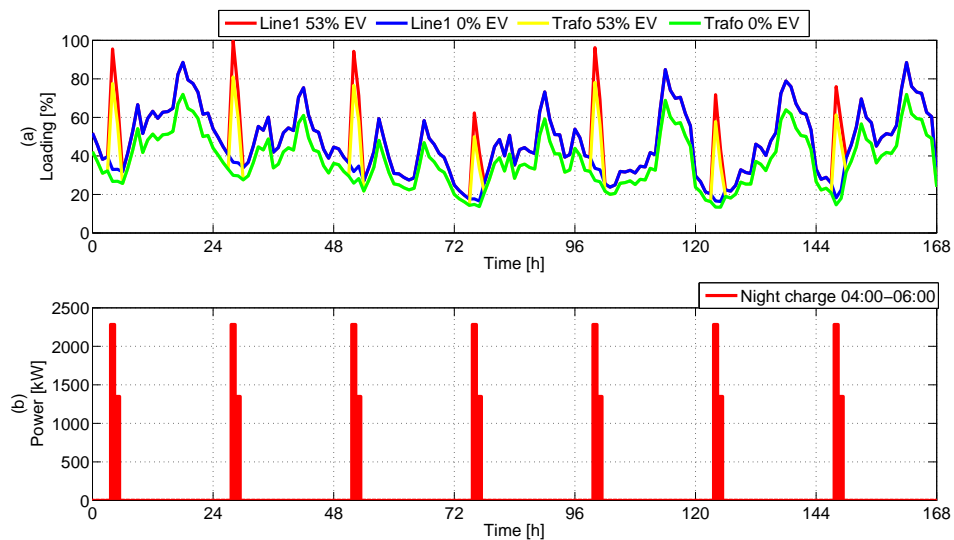


Figure 5.15: Results for the load flow analysis during the January case, with regards to the transformer and cable loadings (a) and the power consumed among night charge (b)

5.5.2 Summer scenario

The power flow analysis, with regards to the July case, is being presented in the following. In Figure 5.16, the voltage fluctuations at bus 652 - plot (a), goes down to 0.984 p.u.(due to the load of the EVs in the morning hours). The voltage at the farthest away bus decreases synchronously with the power increase from the external grid, shown in plot b). During the morning charge of the EVs, the peak load reaches approximately 4 MW, out of which 3.12 MW represents the peak power consumption for charging the vehicles.

The transformer and cable loading factors are represented in Figure 5.17 for the summer scenario. By looking at the transformer loading profile in plot a), it can be observed that during the whole week, when the vehicles are plugged-in for charging, the power flow through the transformer is within the admissible limits. The maximum value reaches 84% in hour 13. This high loading is due to the excess power generation from the renewables in the first day of the week. It can be seen that during the morning charging of the EVs, the loading of the transformer varies between 64 and 82%. Regarding the most congested cable system in the distribution grid - Line 1, it can be observed that there are five spikes. Four of them occur during the morning hours (when EVs are plugged in) and one appears in the hour in which the renewable generation is at its maximum. The cable reaches the limit during the morning of the last day of the week, when EVs are plugged in for charging. In this case, the cable loading stands for 99.8%, hence the maximum EV penetration level is determined as being 73%. By using this charging strategy in the summer scenario, a total number of 346 electric vehicles are able to be plugged-in. If comparing plot a) and b), it can be observed that, the loading factors increase together with the load demand of the electric vehicles.

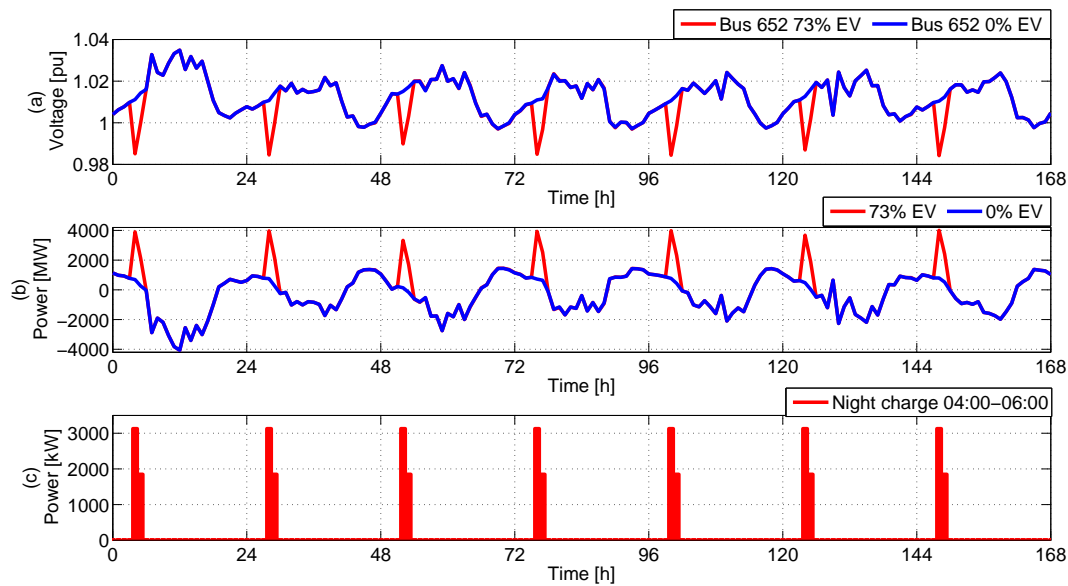


Figure 5.16: Results for the load flow analysis during the January case, with regards to the voltage fluctuations at the weakest busbar (a), the infeed power from the system (b) and the power consumed during the night charge (c)

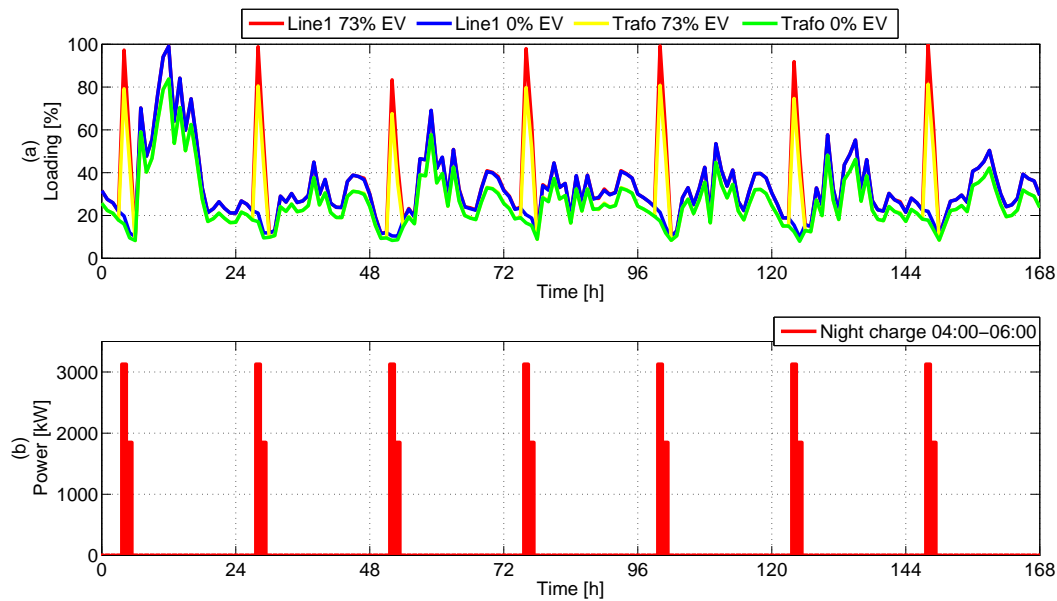


Figure 5.17: Results for the load flow analysis during the January case, with regards to the transformer and cable loadings (a) and the total power consumed among the morning charge (b)

5.5.3 Section summary

By charging the vehicles in the morning hours (4 to 6 am), the electric vehicle integration limit is determined when reaching the ratted current for Line 1. From the two cases investigated in this section, the maximum EV penetration is given by the winter scenario, when it represents 53%. It has been shown that for both cases, the other grid parameters, such as voltage fluctuations and the transformer loading, are within the admissible limits.

5.6 Distributed charging of EVs between 00:00 to 06:00

The following section aims to highlight the results obtained, when the electric vehicles are charged in a distributed manner, between 0-6 am. This charging strategy requires to divide the charging intervals as it follows:

- First charging interval - from 00:00 to 02:00, in which the EV charging takes place at nodes 611, 632, 633 and 634.
- Second charging interval - from 02:00 to 04:00, in which the vehicles connected an buses 645, 646, 650 and 652 are plugged-in for charging.
- Third charging interval - from 04:00 to 06:00, in which the EV charging occurs at busbars 671, 675, 680, 684 and 692.

All of the electric vehicles charge by following the same pattern as in Sections 5.2, 5.3, 5.4 and 5.5, in which the load for the first hour of charging is 6.6 kW and during the second hour represents 3.9 kW.

5.6.1 Winter case

In the following, the results for the distributed charging of EVs are presented, with regards to the winter scenario. In Figure 5.18, the voltage profile for the weakest buses is highlighted together with the infeed active power from the external grid. Plot a) highlights the voltage fluctuations

at the weakest node (611) for the first charging interval. The minimum voltage value in this case stands for 0.954 p.u. Plot b) represents the voltage variation at the weakest node (652) for the second group. In this case, the voltage drops down to 0.954 p.u. In plot c), the voltage change at node 680 (third charging group) shows that the minimum value goes down to 0.954 p.u. If comparing the three voltage profiles with the infeed active power in plot d), it can be seen that the voltages fluctuate simultaneously with the power increase from the system.

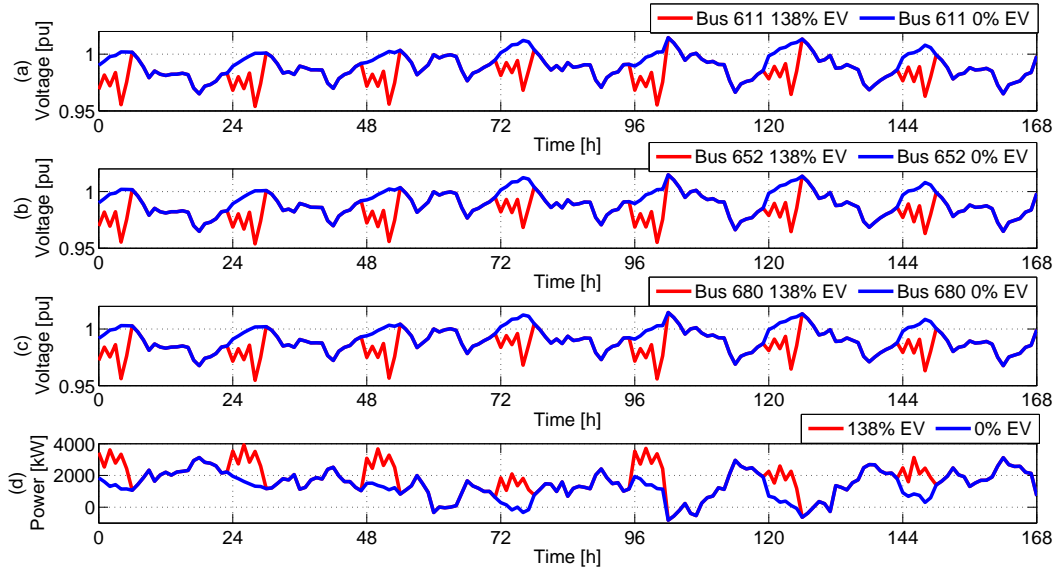


Figure 5.18: Results of the load flow analysis for the January case, with regards to the voltage fluctuations at the weakest busbars (a), (b), (c) and the infeed power form the system (d)

The maximum load rises up to 3.95 MW, according to plot d), during the charging interval of the vehicles. Once the EVs are plugged-in, the high charging load affects the voltage at the nodes, whom are decreasing. In this case during the first charging interval 232 EVs are able to be plugged-in, 340 vehicles can be connected during the second interval and 318 EVs can be charged in the third interval.

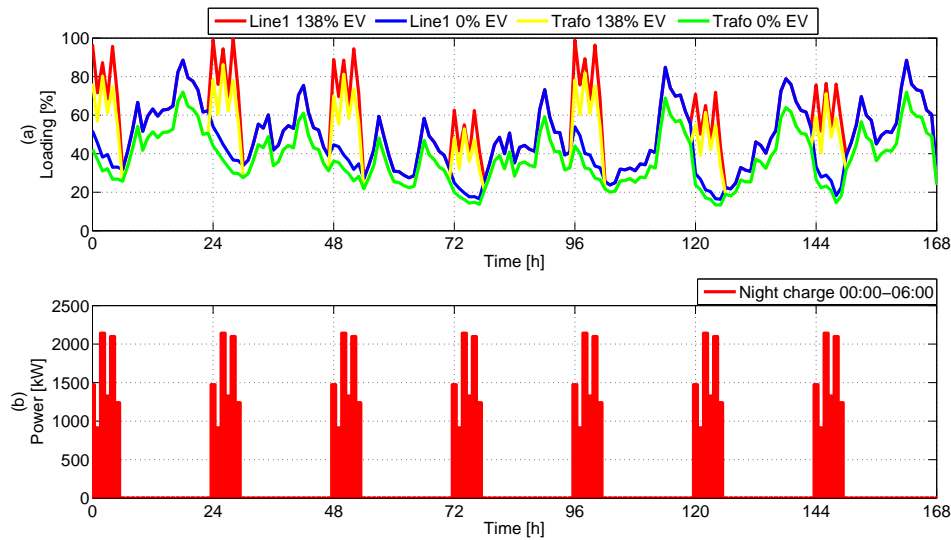


Figure 5.19: Results of the power flow analysis for the January case, for the transformer and cable loadings (a) and the power demand for EV charging (b)

In Figure 5.19, the loading factors for the winter scenario are presented. The loading of the distribution transformer is kept below the admissible limit during the whole week. From plot a) and b), it can be seen that once the EVs are connected at the busbars, the transformer loading is increasing. During the charging hours, the loading reaches a maximum of 86%, comparable with the loading in the peak-load hours. The cable system of Line 1, is the most congested in the grid. It can be seen that during the second day of charging, the current limit is reached (99.9%), thus one of the grid constraints is disregarded. This gives the maximum EV penetration level for the winter scenario. This level is determined as it follows:

$$EV_{pen} = \frac{N_{EV1} + N_{EV2} + N_{EV3}}{M_{households}} \quad (5.5)$$

where, N_{EV1} , N_{EV2} and N_{EV3} represent the maximum number of EVs that can be plugged-in during the first, second and third charging interval and $M_{households}$ stands for the total number of residential homes.

For the winter scenario, the electric vehicle integration limit is determined by using Equation 5.5:

$$EV_{pen} = \frac{232 + 340 + 318}{647} = 138\% \quad (5.6)$$

5.6.2 Summer case

The results of the power flow analysis, with regards to the voltage variation at the weakest nodes and the power exchange with the external grid are shown in Figure 5.20. From plots a), b) and c) it can be observed that, the voltages are decreasing when the EVs are plugged-in for charging. During each charging cycle, the voltage goes down to less than 0.98 p.u., in the third charging interval. This is due to the high load demand by both the vehicles and the residential consumption during the night. By looking at all four plots in the figure, it can be observed that once the EVs start to charge, the power demand increases, rising up to approximately 3.95 MW. In the night, the renewable generation is low, thus most of the power required for charging is provided by the grid.

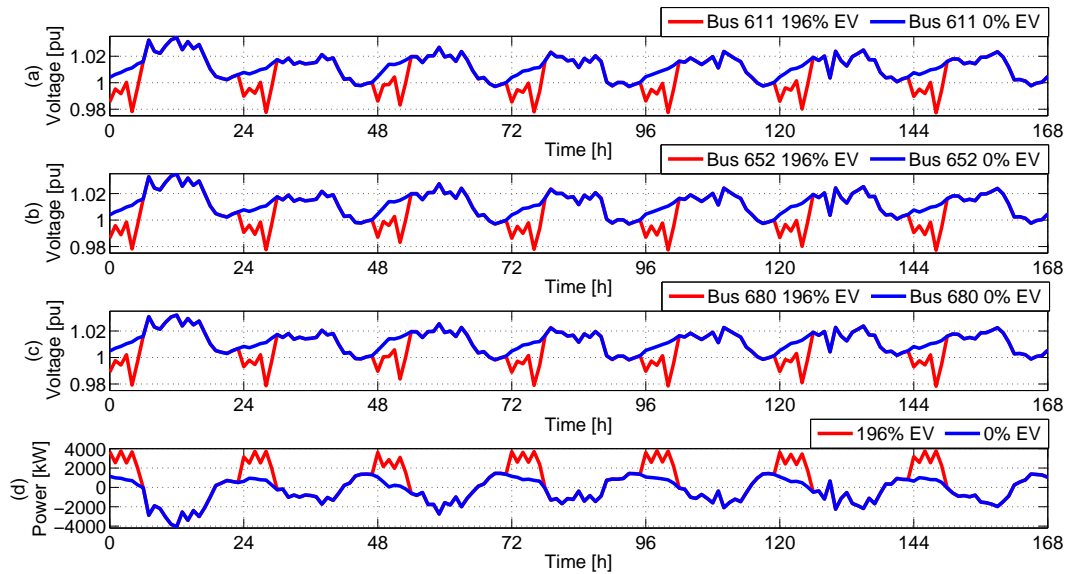


Figure 5.20: Results of the load flow analysis for the July case, with regards to the voltage fluctuations at the weakest busbars (a), (b), (c) and the infeed power from the system (d)

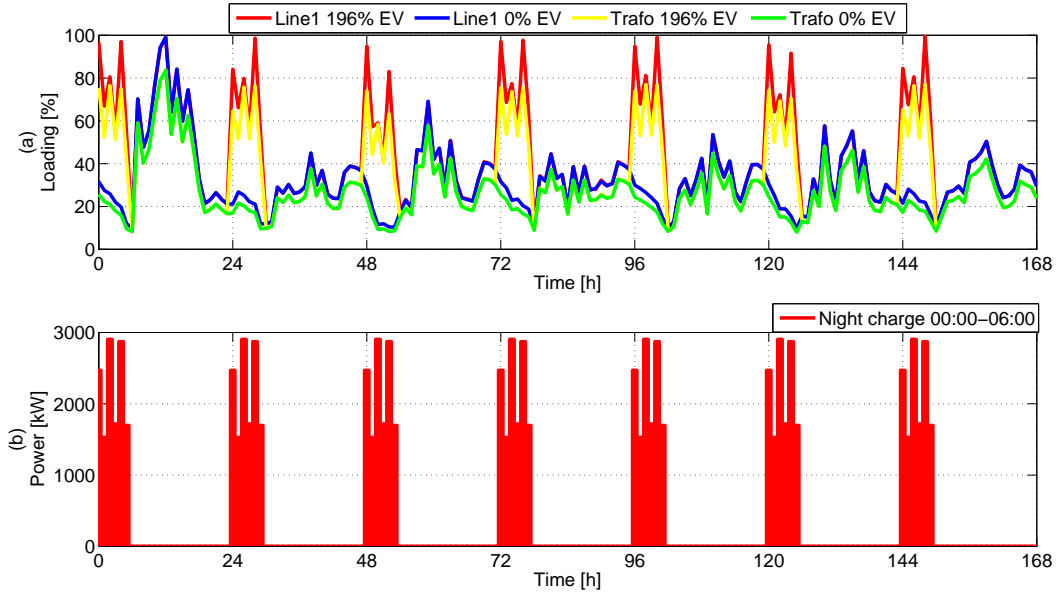


Figure 5.21: Results of the power flow analysis for the July case, for the transformer and cable loadings (a) and the power demand for EV charging (b)

In Figure 5.21, the transformer and cable loadings are shown in comparison with the load demand of the EVs. The distribution transformer is operating under normal conditions for the whole week in July. It can be seen that during the charging hours, the loading ranges between 45 and 83%. Regarding the cable loading factor, it can be seen that during the time in which the vehicles are connected for charging, the loading varies from 50% up to the limit. During the last day of the week the loading of Line 1 reaches 99.9%, hence the grid operation limit is reached. This leads to the determination of the maximum EV integration for the summer scenario. This is done by applying Equation 5.5:

$$EV_{pen} = \frac{392 + 440 + 435}{647} = 196\% \quad (5.7)$$

It can be observed that the power demand for the EV charging varies from approximately 1.6 MW up to 2.92 MW, as seen in plot d).

5.6.3 Section summary

If the distributed charging strategy is applied from 0 to 6 am, it can be seen that the EV integration level increases significantly for both winter and summer scenario. In both cases, the integration limit for the electric vehicles is given by the cable loading factor. For this charging strategy, the maximum penetration level with regards to the electric vehicles is given by the winter scenario, when it reaches 138%. The results presented show that for this amount of EV load, the voltage fluctuations and transformer loading factor are maintained within the admissible limits of the distribution grid.

5.7 Summary of charging strategies

In the following, the most important results from all charging strategies investigated in this chapter are presented. This is necessary in order to assess the overall impact on the distribution grid. The results are presented in Table 5.1.

Table 5.1: Overview of results for different charging strategies

Case	EV_{pen} [%]	PV_{pen} [%]	WT_{pen} [%]	V_{max} [pu]	V_{min} [pu]	$Cable_{lf}$ [%]
I	14	172	39.4	1.035	0.958	99.91
II	38	172	39.4	1.035	0.962	99.65
III	51	172	39.4	1.035	0.963	99.97
IV	53	172	39.4	1.035	0.963	99.81
V	138	172	39.4	1.034	0.954	99.9

where *I*, represents the 'dumb charge' strategy from 17:00-19:00, *II* stands for the night charge between 0-2 am, *III* is the night charge from 2 to 4 am, *IV* represents the morning charge from 4:00-6:00 and *V* is the distributed night charge from 0-6 am.

If looking at Table 5.1, it can be observed that the distributed night charging of the EVs presents the highest penetration level. In this case, the grid is able to support up to 890 vehicles that are connected for charging. This high integration level is due to the fact that the vehicles use power during the off-peak load hours, and the fact that the load is distributed into three charging intervals. If this strategy is applied, the voltage at the weakest bus, varies between 0.954 to 1.035 p.u., which is close to the voltage fluctuations limit of 0.95-1.05 p.u. It can be observed that for all strategies, the EV integration level is given by the current limit of the distribution cables.

As explained, it is considered that the renewable sources are evenly distributed in the grid (if spread in the grid, the distribution power losses are lowered, as the generation sites are located close to the consumers, represented by the households and electric vehicles), having the same penetration levels as in Section 4.5. The estimation of wind power generation and PV production per household can be determined if dividing the total installed power to the number of households. This is done by using Equation 5.8 and Equation 5.9:

$$WT_{household} = \frac{WT_{total}}{N_{households}} = \frac{2250}{647} = 3.47[kW]/household \quad (5.8)$$

where, WT_{total} represents the total installed wind capacity in the grid (45 wind turbines having a nominal power output of 50 [kW]) and $N_{households}$ represents the total number of houses in the grid.

$$PV_{household} = \frac{PV_{total}}{N_{households}} = \frac{6270}{647} = 9.7[kW]/household \quad (5.9)$$

where, PV_{total} stands for the total installed PV generation capacity in the grid (1183 modules of 5.3 [kWp]) and $N_{households}$ represents the total number of residential homes.

By taking into consideration the numbers presented above, for this particular distribution grid, the maximum allowable wind power production, photovoltaic generation and electric vehicle charging per household has been determined. This is done by taking into consideration also the grid operation parameters (voltage fluctuations, transformer and cable loading).

Conclusions and Future work 6

6.1 Conclusions

The aim of this master thesis was to determine the maximum allowable integration of wind and solar power production and EV charging per household on a typical distribution grid. The initial focus has been placed on the validation of the IEEE 13 bus distribution system, in order to obtain a benchmark model of a typical distribution system. For this test model, steady-state power flow simulations have been performed in DIgSILENT PowerFactory software. After the validation of the model in PowerFactory, the load flow analysis has been implemented on an hourly time step, during a one week interval for two distinct cases: one week in January - when the residential consumption is at its highest; and one week in July - when the household load is lowest. In this project, the house loads have been modeled as aggregated loads, having a power factor of 0.9.

Based on the wind speed and solar irradiation profiles, the generation profiles for a 50 kW WT and a 5.3 kWp PV module has been determined for further use in the power flow analysis. The renewable sources have been modeled as aggregates, producing power at a constant power factor of 1. The maximum renewable integration level has been determined by using a 'trial and error' strategy, in which three grid parameters have been investigated (maximum voltage fluctuations, transformer and distribution cable loading factors). Three distinct cases have been analyzed with regards to the placement of the renewable sources, for both January and July scenarios. From the cases investigated, the even distribution of renewable sources has been selected; the main reason for this is represented by the fact that the generation sites are located close to the consumers (households and EVs), hence the distribution power losses are limited.

In the steady-state power flow study, the electric vehicles have been modeled as aggregate loads. From the available data, the daily energy consumption for the EV fleet has been determined. Five different charging strategies have been implemented, in order to determine the allowable EV integration. It has been shown that during the peak-load hours, the maximum integration level of EVs reaches 14%. If the vehicles are plugged-in for charging during the off-peak load hours, the penetration level can reach up to 53%. If using the distributed charging strategy in the night hours, the maximum EV penetration level rises up to 138%.

The voltage fluctuations for both summer and winter scenarios are maintained within the admissible limits for all the cases investigated. During the summer, when the renewable generation is high (especially due to the PV systems), the voltage rises up to 1.035 p.u. In the winter scenario, when EVs are plugged in for charging, the minimum voltage goes down to 0.954 p.u. For all the cases investigated, the distribution transformer is not overloaded for neither hour of the week.

It has been shown that the maximum penetration level for both electric vehicles and renewable sources is reached, simultaneously with the current limit of the most congested cable system (Line 1) in the grid. For the distribution grid investigated in this project, this is the main grid parameter which determines the maximum allowable renewable production and electric vehicle

charging.

As the final conclusion of this project, it can be stated that the allowable wind power production, PV generation and EV charging per household for a typical distribution grid has been determined, by considering the two distinct cases - summer and winter scenarios. In both cases, the power flow analysis has been performed by investigating the grid parameters. It has been highlighted that if the vehicles are charged during the night hours, the integration level increases significantly, as the distribution grid is less congested. This master thesis aims to present a possible solution to determine the allowable RES and EV integration levels in distribution grids.

6.2 Future Work

In this final section, several aspects are presented which could be expanded as future work:

- Due to the rapid fluctuations of the renewable sources, the power flow analysis can be implemented with a smaller time step for the simulations. By doing so, the generation profiles of the renewable sources are expected to be more accurate, hence a more detailed investigation can be performed.
- As shown in the steady-state simulations, the voltage fluctuations do not exceed the 0.95-1.05 p.u. grid limitation. Although the minimum value stands for 0.954 p.u. when EVs are plugged-in, an investigation regarding the reactive power dispatch of the wind turbines should be implemented.
- In this project, the power flow calculus has been performed by taking into consideration only the electrical consumption of each household. In the future, it is expected that the households will have an electric heating system. An analysis should be performed by considering also the electric heat consumption of a typical household (which in some cases can be up to four times higher than the electrical demand).
- As shown in the simulations, during the summer case, the renewable generation exceeds the residential consumption (due to the PV systems) in most of the days. The economical aspect should be evaluated, as in this case most of the households act as 'prosumers', injecting active power into the grid. An economical calculus should be performed in order to determine the financial earnings for each house in regards with this aspect.
- Additional charging strategies of the EVs should be investigated. Intelligent charging of the vehicles should be implemented, in which the vehicles are charging only when the renewable generation exceeds the residential demand, by considering also the charging availability of the electric vehicles.

Bibliography

- [1] The European Wind Energy Association, “Wind in power - 2014 European Statistics,” Feb. 2015.
- [2] The Danish Energy Agency, “Energy Statistics 2013 - Data, Tables, Statistics and maps,” Mar. 2014.
- [3] ———, “The Danish Climate Policy Plan,” Aug. 2013. [Online]. Available: http://www.ens.dk/sites/ens.dk/files/policy/danish-climate-energy-policy/danishclimatepolicyplan_uk.pdf
- [4] A. R. Dalmau and D. M. Perez, “Application of Power to Gas (P2G) Systems in Danish Electric Electric Distribution Networks,” May 2015.
- [5] Energinet.dk and The Danish Energy Association, “Smart Grid in Denmark,” Sep. 2014. [Online]. Available: <http://www.energinet.dk/SiteCollectionDocuments/Engelske%20dokumenter/Forskning/Smart%20Grid%20in%20Denmark.pdf>
- [6] K. Hadegaard, H. Ravn, N. Juul and P. Meiboom, “Effects of electric vehicles on power systems in Northern Europe,” *Elsevier*, vol. 48, pp. 356–368, May 2012.
- [7] J. R. Pillai, P. Thorgersen, J. Moller and B. Bak-Jensen, “Integration of Electric Vehicles in Low Voltage Danish Distribution Grids,” 2012 IEEE Power and Energy Society General Meeting, Jul. 2012.
- [8] P. Lico, M. Marinelli, K. Knezovic and S. Grillo, “Phase Balancing by Means of Electric Vehicles Single-Phase Connection Shifting in a Low Voltage Danish Grid,” Power Engineering Conference (UPEC), 2015 50th International Universities, Sep. 2015.
- [9] J. R. Pillai and B. Bak-Jensen, “Impacts of Electric Vehicle Loads on Power Distribution Systems,” 2010 IEEE Vehicle Power and Propulsion Conference, Sep. 2010.
- [10] B. Gohla-Newdecker, U. Wagner and T. Hamacher, “Analysis of Renewable Energy Grid Integration by Range Extension Technologies of BEVs,” Clean Electrical Power (ICCEP), 2013 International Conference, pp. 155–162, Jun. 2013.
- [11] IEEE Power and Energy Society, “Distribution Test Feeders - 13 bus distribution system.” [Online]. Available: <http://ewh.ieee.org/soc/pes/dsacom/testfeeders/>
- [12] Weatherbase, “Weather profile accros the globe,” Jan. 2016. [Online]. Available: <http://http://www.weatherbase.com/weather/weatherall.php3?s=8160&units=&cityname=Copenhagen%2C+Capital+Region%2C+Denmark&set=metric>
- [13] A. B. Pedersen, A. Aabrandt and B. Poulsen, “Generating Geospatially Realistic Driving Patterns Derived From Clustering Anakysis of Real EV Driving Data,” 2014 IEEE Innovative Smart Grid Technologies - Asia (ISGT ASIA), pp. 686–691, May 2014.
- [14] J.C. Smith, A. De Broe, A. Estanquero and G. Duclos, “Wind Energy - The facts. Grid Integration - Part II,” Feb. 2010. [Online]. Available: <http://http://www.wind-energy-the-facts.org/images/chapter2.pdf>

- [15] Danish Ministry of Climate, Energy and Building, "Smart Grid Strategy - The intelligent energy system of the future," May 2013.
- [16] Dansk Elbil Alliance, "Bestand af elbiler i Danmark," Dec. 2015. [Online]. Available: http://www.danskelbilalliance.dk/Statistik/Bestand_modeller.aspx
- [17] Energinet.dk, "Electricity facilities," The Danish electricity grid, Oct. 2014. [Online]. Available: <http://energinet.dk/EN/ANLAEG-OG-PROJEKTER/Generelt-om-elanlaeg/Sider/default.aspx>
- [18] The Danish Energy Association, "Danish Electricity Supply '09," Apr. 2009.
- [19] Copper Development Association, "Voltage Disturbances," Standard EN 50160 - Voltage Characteristics in Public Distribution Systems, Jul. 2004.
- [20] K. Hansen, B.V. Mathiesen and D. Connolly, "Technology and implementaion of electric vehicles and plug in hybrid electric vehicles," Dec. 2011.
- [21] IEEE Power and Energy Society, "IEEE Recommended Practice for Monitoring Electric Power Quality," IEEE Std. 1159-2009, Jun. 2009.
- [22] H. Saadat, Power System Analysis. New York, NY: The MC-Grah Hill Companies, 1999.
- [23] A. R. Bergen and V. Vittal, Power System Analysis. New Jersey, NJ: Prentice Hall In., 2000.
- [24] R. T. Bhimaresetti and A. Kumar, "A New Contribution to Distribution Load Flow Analysis for Radial and Mesh Distribution Systems," Computational Intelligence and Communication Networks (CICN), 2014 International Conference, pp. 1229–1236, Nov. 2014.
- [25] J. R-Pillai, "Steady state analysis of power systems - course notes," Jun. 2015.
- [26] S. Mandava, V. Ramesh and P. Karthikeyan, "A Simiple Load Flow Method for Radial Distribution System," Advances in Electrical Engineering (ICAEE), 2014 International Conference, pp. 1–6, Jan. 2014.
- [27] DIgSILENT GmbH, "DIgSIlent PowerFactory 15 - User Manual," Gomaringen, Germany, Oct. 2013.
- [28] R. A. Kordkheili, B. Bak-Jensen, J. R-Pillai and P. Mahat , "Determining Maximum Photovoltaic Penetration in a Distribution Grid considering Grid Operation Limits," 2014 IEEE PES General Meeting - Conference and Exposition, Jul. 2014.
- [29] F. M. Andersen, H. V. Larsen and R.B. Gaadrestrup, "Long term forecasting of hourly electricity consumption in local areas in Denmark," ELSEVIER - Applied Energy, vol. 86, pp. 147–162, May 2013.
- [30] N. A. Masood, R. Yan and T. K. Saha, "Estimation of Maximum Wind Power Penetration Level to Maintain an Adequate Frequency Response in a Power System," 8th International Conference on Electrical and Computer Engineering (ICECE 2014), pp. 587–590, Dec. 2014.

- [31] Q. Wu, A.H. Nielsen, J. Ostergaard, S.T. Cha, F. Marra, Y. Chen and C. Traeholt, "Driving Pattern Analysis for Electric Vehicle (EV) Grid Integration Study," 2010 IEEE PES Innovative Smart Grid Technologies Conference Europe (ISGT Europe), pp. 1–6, Oct. 2010.
- [32] C. Jin, X. Sheng and P. Ghosh, "Energy efficient Algorithms for Electric Vehicle Charging with Intermittent Renewable Energy Sources," 2013 IEEE Power and Energy Society General Meeting, pp. 1–5, Jul. 2013.
- [33] H. Zhao and A. Burke, "An Intelligent Solar Powered Battery Buffered EV Charging Station with Solar Electricity Forecasting and EV Charging Load Projection Functions," Electric Vehicle Conference (IEVC), 2014 IEEE International, pp. 1–7, Dec. 2014.

